Technische Universität München

Friedrich-Schiedel Institut für Neurowissenschaften

Ultra-fast two-photon microscopy for in vivo brain imaging

Ulrich Leischner

Vollständiger Abdruck der von der Fakultät für Medizin der Technischen Universität München zur Erlangung des akademischen Grades eines

Doctor of Philosophy (Ph.D.)

genehmigten Dissertation.

Vorsitzender: Univ.- Prof. Dr. Thomas Misgeld

Prüfer der Dissertation:

1. Univ.- Prof. Dr. Arthur Konnerth

2. Univ.- Prof. Dr. Dieter Braun
   Ludwig-Maximilians-Universität München

Die Dissertation wurde am 24.2.2011 bei der Technischen Universität München eingereicht und durch die Fakultät für Medizin am 4.3.2011 angenommen.

Table of Contents

Chapter 1: Introduction

Optical imaging is a good method for investigation of physiological signals in medical research, such as the changes in calcium concentration in cells, because these signals can be detected simultaneously throughout the whole image. For example, when we acquire images with video-rate of a group of cells, loaded with an indicator dye for monitoring the intracellular calcium concentration, we can measure calcium changes inside the different cells at the same time. Calcium is needed for a lot of biological processes inside the cell, and a sudden rise in the calcium concentration in a cell indicates the activation of a cell. The calcium then triggers a lot of secondary chemical reactions. Changes of the membrane potential of nerve cells are also often accompanied by calcium entry into the cell, and therefore the changes of the calcium-concentration are indicators of a wide range of cell activity. By monitoring such a signal in a group of cells, we can distinguish between more active and passive cells, and observe the patterns of the activity in a group of nerve cells in the brain.

These physiological signals are also of interest on a smaller scale, like a small section of a dendritic branch of a nerve cell in the brain. A nerve cell in the brain is connected to thousands of other cells by synapses on spines. These spines are of a very characteristic shape, mushroom like extrusions from the dendritic branch. It is unknown how strong these connections are, and what kind of activity pattern they form in the intact brain. When we are able to resolve the calcium signal in such a spine, we can deduce the connection and transmission strength between two cells, and compare the response of a cell to different input pattern. Such measurements can investigate the mechanisms of the integration of different inputs to a single cell, and reveal the properties of input from other cells on the scale of a single cell. A lot of details of the network connections and the transmission properties are still unknown, mainly because the cellular networks in the brain are highly complex with thousands of connections, and measurements on an intact brain are very difficult. However, a lot of network malfunctions cause mental diseases like Alzheimer's dementia or schizophrenia, and details of the underlying network alterations are largely unknown. Optical measurements are an excellent tool for investigation of the normal network functions like the spatial organization of input to a cell, and to compare the overall response of a cell to different stimulation pattern. In another step, optical methods have the potential to detect alterations of the network functions in mental diseases.

Although optical imaging is a good method for investigation of network connections in brain cells, the measurements on an intact brain are very difficult, because brain tissue is highly opaque and is not suited for optical imaging in deeper layers. Without a specialized technique, we can only acquire images from the brain surface. The opaqueness of brain tissue is caused by the highly non-homogeneous composition of substances in the brain. Most components of brain cells are transparent, like lipids, proteins or water, but the non-homogeneous mixture with many membranes embedded by water generates a lot of light-scattering bounding surfaces. Scattering causes the photons to change their direction, and after one scattering process, we can no longer determine the origin of the photon, and use it for an image projection. Such direct widefield projection imaging is only suited for images from the surface. The resolution of the images rapidly degrades when we want to acquire images in deeper layers of brain tissue. Confocal microscopy (Minsky, 1961) was the first technique to increase the imaging depth. This technique illuminates only one point, and removes all scattered photons not coming from that point. This increases the imaging depth in biological tissue

up to the ‘mean free path’ of a photon between two scattering events. In practice this ‘mean free path’ is about 40µm (Ntziachristos, 2010), and this can still be considered as the surface region.

The invention of two-photon (2p) microscopy was a major improvement in this respect (Denk et al., 1990). The 2p excitation technique generates fluorescence just at one point by using a focused high-power pulsed laser. Only highest photon densities allow for a simultaneous excitation of a fluorophore with two photons at the same time, and these high photon densities are only present at the focus spot of a laser beam. As fluorescence excitation can only occur at the focus spot, the fluorescence emission can only originate from this location as well. This technique does not need an optical projection technique for image formation, but gathers all photons coming from the sample and directs them to the photo detector. We can get 2D images by scanning the object. As scattering processes in the detection pathway do not degrade image quality, this technique allows for the image acquisition much deeper than the ‘mean free distance’ between two scattering processes, like it is the limit of confocal microscopy. With the 2p technique, it is possible to image up to a depth of 1mm, which means a 25-fold increase in imaging depth.

This technique needs a movement of the focus spot to scan the sample in 2D or 3D to get the raster image information. Moving a spot of focused light through the image plane is mainly done by revolving mirrors, but revolving a mirror is time consuming, as a change of the orientation angle of a mirror requires an acceleration and deceleration. The mirrors are the speed-limiting component of a scanning microscope, and most microscopes are limited to an image speed of about 10 images per second. Therefore, investigations with 2p microscopy are limited to slow processes, as we can not observe fast processes with such a slow detection technique.

There is an alternative device for beam deflection: acousto-optical deflectors (AOD). These devices can deflect a beam at different angles by changes of the diffraction pattern of a grating. The grating is generated by an acoustic wave in a transparent crystal, and this grating can be changed as fast as we can change the acoustic frequency. These devices are inertia free, and therefore they can perform a line-scan with a 10-fold frequency increase compared to a revolving mirror.

The subject of this PhD thesis is the design and construction of a high-speed 2p imaging microscope by using AODs for beam deflection. The beam deflection in AODs is done by changes of the diffraction pattern of an optical grating. This is a different physical principle than a light reflection on a flat mirror, and hence such a beam deflection is accompanied by different optical artifacts, requiring different compensation mechanisms. I will analyze the different artifacts, how they can be compensated, and will present an apparatus that can acquire images of high quality with more than 1000 images per second. In the end I will present some measurements realized with the newly developed apparatus, and demonstrate the capabilities and the image quality of this new microscope.

As two-photon imaging is a central technique, I will first give a detailed introduction of the 2p imaging technique in the first part of this thesis, and I will describe the current status of the technical developments.

The general layout of a two-photon scanning microscope

We can modify a standard commercial microscope and use it as a 2p microscope by simply exchanging some filters, mounting a photomultiplier (PMT) at the right position and attach the scanning optics for the two-photon laser. A normal brightfield microscope needs a homogeneous illumination, and good optics for capturing the photons and projecting them to the camera chip. A 2p-microscope needs such optics in the opposite way: good optics for a precise illumination, and a possibility to capture all photons emitted from the sample. Therefore we can just use the detection pathway for illumination, and the illumination-pathway for detection. This requires mounting the PMT to the place where we previously attached the light fiber for the illumination light (figure 1). This allows for the detection of all photons coming from the surface of the sample. The other pathway for image detection can be used for a precise illumination. To do this, we need to project a focused spot of the 2p-laser at a location called the 'image plane'. The 'image plane' denotes the location of the CCD chip, where the sharp image from the sample is projected. The camera chip is normally placed at this location. But as we do not detect the image with a camera, we can simply dismount the camera and mount the scanning device to perform the image scan at the image plane. In this way we use the detection pathway in the other way: When we project a spot of light at the location of the image plane, the light is guided through the optical lenses of the microscope downwards to the sample, and illuminates one sharp point there.

Altogether, to modify a microscope to use it for 2p-imaging, we need some minor optical modifications. We must dismount the camera, and attach a scanning device that projects a spot of light at the position of the camera chip. We then just need to exchange some filters and mount the PMT. I present the general layout of such an apparatus in figure 1. In the later sections I will explain some details of the scanning device, and how to achieve high-speed scanning with good results.

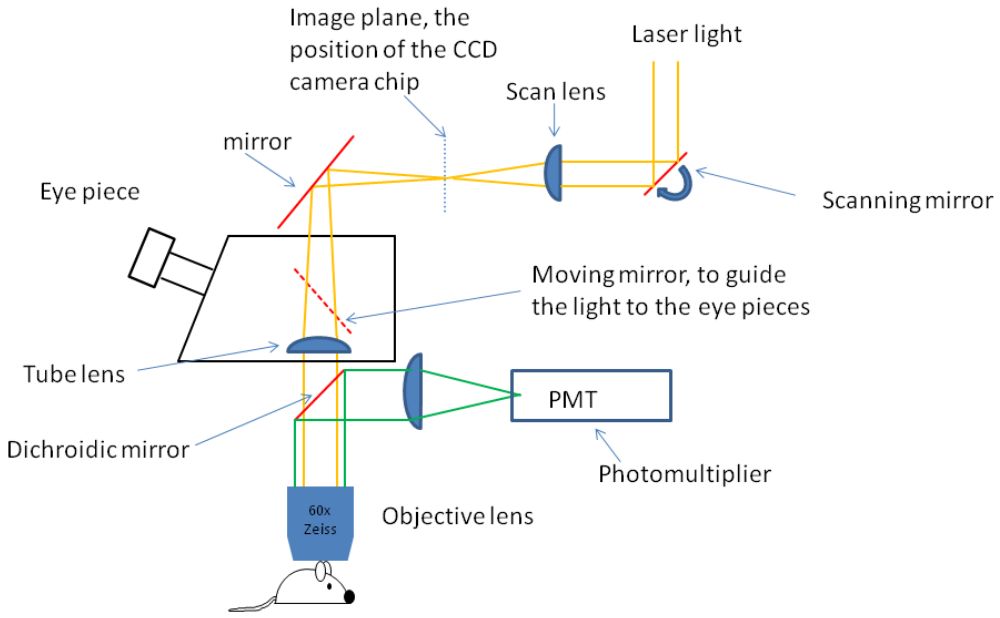

Figure 1, modification of a brightfield microscope for 2p scanning microscopy: The detection pathway (green lines) served previously as illumination pathway, and the imaging pathway (yellow line) now serves as illumination pathway. This way, we can precisely illuminate the sample, but not detect the precise position of the generated fluorescence. But as we know the position of the focus spot, we do not need the information of the origin of the fluorescent light. Therefore, we can just detect all photons coming from the sample, irrespective of how many times the photons have been scattered. We gain the 2d image information by scanning the sample. In this work, I have developed a fast scanning system that allows for scanning at frequencies of more than 1000 images per second.

I used most of the optical components from standard commercial products. My main work was the development of a fast scanning system. Furthermore, we only had to make some minor modifications like replacing the illumination light source with a photomultiplier, changing the dichroic mirror (fluorescence brightfield GFP imaging: reflection 460-500nm, transmission 510-600nm; new filter for two-photon imaging: transmission 750-900nm, reflection 500-700nm), and mounting the scanning system to a position where it can illuminate the image plane.

A simple scanning unit with galvanometric mirrors

As this work mainly focuses on the development of a fast scanning system, I will first explain the principle of the easiest scanning system. The most simple device is based on revolving galvanometric mirrors. In addition to the revolving mirror we just need a lens to build a scanner. A lens is focusing a collimated (non-focused, ideally parallel) laser beam to a spot of light in focal distance from the lens, the position of the image plane. The approaching angle defines the position of the focus spot. The revolving mirrors are used to control the incident angle (fig. 2).

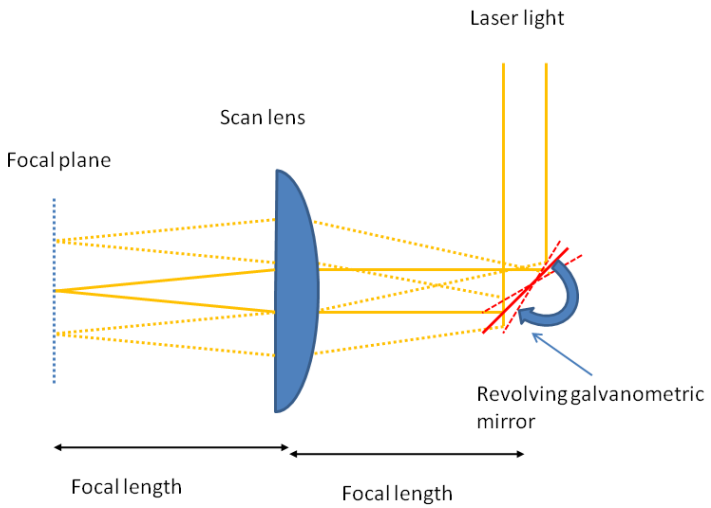

Figure 2, scan principle using a revolving mirror: A collimated laser beam creates a focus spot at focal length from the lens. The position of the focal spot in the focal plane changes when we change the angle of incidence of the laser beam. This works best when the revolving mirror is placed in a distance equal to the focal length from the scan lens. This one-dimensional scanning principle can be easily extended for two dimensional scanning by the use of a second galvanometric mirror for the other axis, placed close to the other revolving mirror.

When the collimated laser beam is approaching the mirror in a different angle, the focus spot is located at a different position in the focal plane. We can control the angle of incidence very precisely by using revolving galvanometric mirrors. This thus allows for a precise control of the position of the focal spot in the image plane. This one-dimensional scanning principle can be extended to two dimensions by an additional mirror placed very close to the other galvanometric mirror, and with a rotation axis perpendicular to the other direction.

The use of acousto-optical deflectors as scanning units

To explain the advantages and disadvantages of acousto-optical deflectors as scanning units, I will first explain the advantages and disadvantages of the standard rotating moving mirror types, the galvanometric mirrors and resonance mirrors.

Galvanometric mirrors:

Revolving galvanometric mirrors adjust their position precisely according to a given voltage signal. They try to follow the command signal as fast as possible. We can control the scanning pattern very precisely in this way. When we want to acquire two-dimensional image data, we perform a fast line-scan with the one mirror and a slow line-scan with the other mirror. To scan such a line-scan pattern, we change the command voltage constantly and so change the angle with constant velocity, jump back to the initial position and continue the scan again with continuous velocity. Such a line-scan mode uses a command-signal with the shape of a saw-tooth. As the scan velocity is homogeneous,

the pixel size is the same throughout the image, and image distortions are at a low level only at the image borders when the mirror jumps back. The disadvantage is that this scanning mode is very slow, also depending on the mirror size and its inertia. For large mirrors (diameter of about 15mm) we can scan about 200 lines per second in this mode (also dependent on the amplitude). The smallest and fastest galvanometric mirrors can scan a line in this mode with a frequency of up to 2000 lines per second. When the images should be of acceptable size, e.g. consist of more than 100 lines, we would end up with about 10-20 images per second. This is a relatively low image frequency.

Resonance mirrors:

The next faster mirror type are resonant mirrors. They oscillate in their resonance frequency. Such a frequency can be about one magnitude higher, about 10 000 to 18 000 lines per second. The scan velocity varies with a sinusoidal function, and the scanning pattern is bidirectional. The object is not scanned with constant velocity, hence the edges of the image are a bit distorted. Another disadvantage of resonant mirrors is the change of position with a sinus-function. They move at resonance frequency, hence constantly accelerate and decelerate. As they permanently change their revolving speed, the pixel sizes are also changing and the images look a bit distorted. Additionally, they remain at the turning points for quite a while. This can be problematic with the use of a two-photon laser, as these lasers are normally high power lasers and always generate photo damage. We burn the sample when the focused laser spot remains on one position for a longer time at the turning points. To avoid this, the laser light must be modulated with high speed and turned off at the turning position where it would stay for a long time. This is usually done by a Pockels-cell, an optical element that allows for the fast modulation of the intensity of the laser beam.

By using resonance mirrors, the scanning speeds can be increased by about one magnitude, a factor of about 10. This allows for image frequencies of up to several hundreds of images per second.

Acousto-optical deflectors (AODs):

A relatively new option for scanning is the use of acousto-optical deflectors. They do not steer the beam by revolving a mirror, but make use of a different physical principle. They modify the diffraction pattern of an optical grating. A classical optical grating consists of a light absorbing material with a number of non-absorbing and transparent holes. These holes are normally of a certain predefined geometrical shape. In the case of a classical grating, the holes are line-shaped, parallel orientated and equally distanced. When the grating is illuminated from one side, the light can only pass the grating through the holes. On the other side the propagation of light is now defined by the principle of Huygens: The principle of Huygens predicates that light propagates as if every point in the wave front emits a spherical wave. The overall diffraction pattern results in the overlay of all the spherical waves. After an optical grating, the diffraction pattern is predefined by the positive and negative interferences of the spherical waves (figure 3)

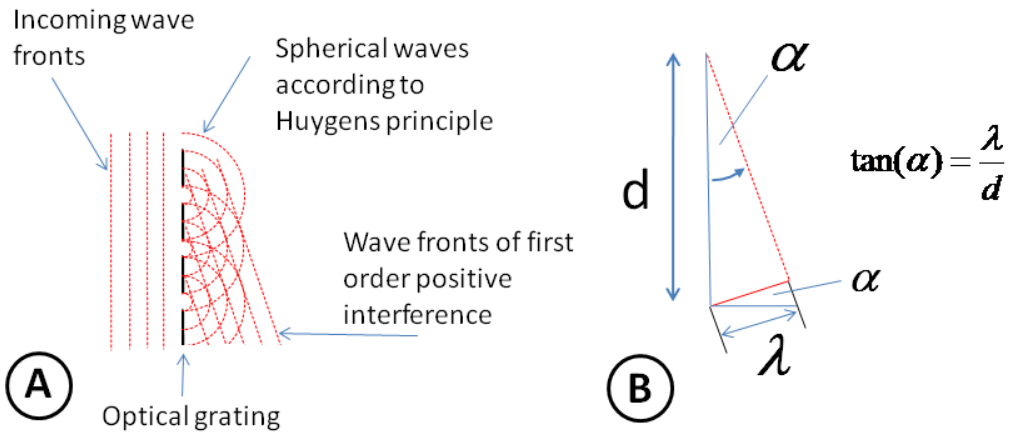

Figure 3, diffraction principle of light at a grating: A: The incoming wave fronts are parallel. After the holes of the grating, the light propagates as spherical waves according to the principle of Huygens. Positive interference occurs in a certain angle, and parallel wave-fronts leave the grating in this direction. B: geometry for the angle for positive interference: Positive interference occurs in an angle, where the spherical waves interfere positively. The first positive interference is in an angle where one maximum interferes with the next wave front from the adjacent grating hole. This angle is predefined by the formula $\tan(\alpha)=\lambda/d$, d being the grating constant (the distances between the holes), λ the wave length of the light and α the deflection angle.

This is the basic principle of a classical optical grating (Gottlieb et al., 1983). This principle is also applicable to acoustic waves traveling through a transparent crystal. An acoustic wave in a transparent crystal generates compressed and non-compressed parts of the crystal, in equal distance and traveling in one direction. Such a compression results in a different refractive index, resulting in different phase-shifts when light is passing the crystal. This homogeneous, periodic pattern of differences of the refractive index produces the same diffraction pattern as an optical grating, as if the grating consists of equally spaced slits. We can now change the grating constant very easily by simply changing the acoustic frequency. This then results in a different diffraction pattern behind the grating, and the first order maximum is deflected in a different angle. We can use this change of deflection angle as a scanner, like a revolving mirror. These changes can be very fast, and changes in the beam deflection angle are faster than a moving mirror. We can change the diffraction pattern as fast as we can change the acoustic wave in the crystal.

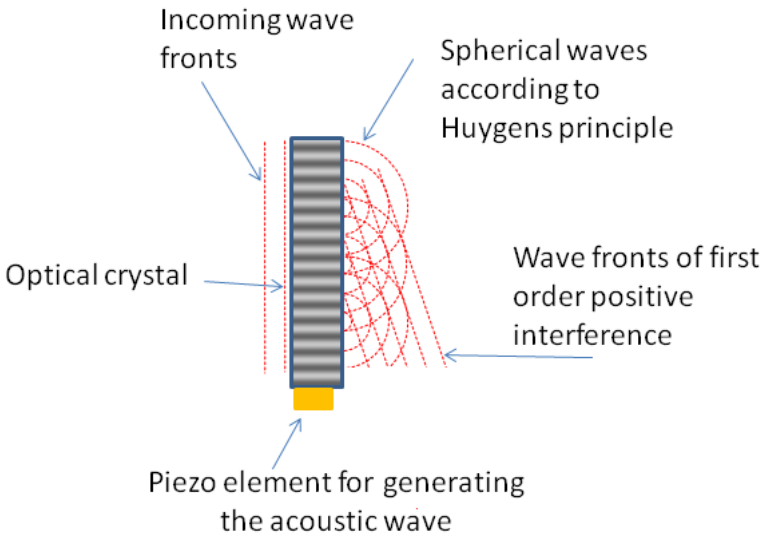

Figure 4: Principle of an acousto-optical deflector: The grating is now created by an acoustic wave in a transparent crystal. By generating acoustic waves of different wave length, we can modulate the grating constant, and hence the diffraction pattern after the grating. These devices do not have any moving parts, hence a change of the diffraction pattern can be done very fast. We can switch the angle of first order interference as fast as we can change the acoustic wave in the crystal. The limiting constant is now the velocity of the acoustic wave in the crystal.

Although the increased speed is a main advantage of an acousto-optical deflector, there are a number of disadvantages. These disadvantages are mainly due to the fact that we use a different physical principle for beam deflection, not a simple reflection on a flat surface. The deflection angle is now also dependent on the wave-length of the light, described by the formula $\tan(\alpha)=\lambda/d$. This can cause problems when we use laser light with a broader spectrum, and not light of only one sharp wavelength. Different colors are deflected in different angles. This specially applies for 2p-lasers, as they need short pulses and hence (due to the Heisenberg-uncertainty principle) are characterized by a relatively broad spectrum. AODs work quite fine with monochromatic light, but when the light is composed of different wave length, an effect called chromatic dispersion occurs. Chromatic dispersion means that different wavelengths of the laser beam propagate in different directions. This effect worsens the beam quality and results in a deterioration of the image quality.

The second disadvantage of an AOD is the relatively small scanning angle. The deflection angle is dependent on the grating constant ($\tan(\alpha)=\lambda/d$), and hence on the acoustic velocity and the acoustic frequency ($d=v/f$, d: grating constant, v: acoustic velocity in the crystal, f: acoustic frequency), $\Delta \tan(\alpha)=\Delta(\lambda/d) = \Delta f\lambda/v$. The slower the acoustic velocity, the larger the scanning angle. Hence vendors try to use crystals with an acoustic velocity as slow as possible. The other possibility would be a large change of the acoustic frequency. The larger the acoustic frequency range, the larger the scanning angle. But this effect is limited by the material of the crystal. The acoustic frequency can not

be changed over some magnitudes, and is normally between 70MHz and 200 MHz, resulting in possible scanning angels of about 4°. Galvanic mirrors are normally able to rotate about 40°.

Special properties of AODs

I will now explain some general properties of AODs, and the limitations resulting from the different beam deflection principle.

The fly back time

The speed-limiting parameter of an AOD is the acoustic velocity of the crystal. We can not scan faster than the time that is needed for the acoustic wave to pass through the laser beam. The acoustic velocity TeO_2 is 660 m/s, and the diameter of the laser beam is at least 2 mm, hence the acoustic wave needs t=x/v = 2mm/660 m/s = 3 µs. In the line-scan mode, this defines the time that is needed to jump from one end of the line back to the starting point of the line. This is the limit for line-scans. We can not scan a line faster than the time needed to jump back. This time constant can be increased by using a different crystal with a higher acoustic velocity, or by a smaller diameter of the laser beam. I will discuss both options now.

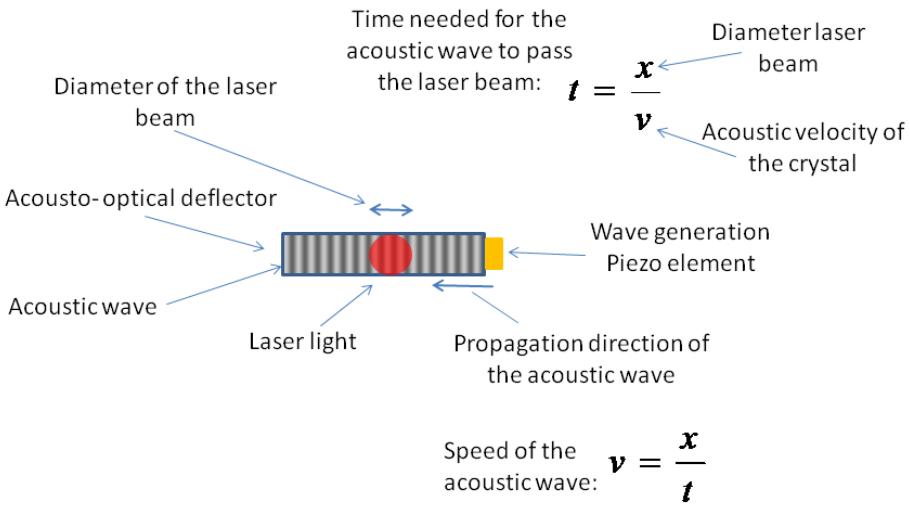

Figure 5, The fly back time as general limit for the line scan frequency of AODs: The acoustic wave propagates with the acoustic speed through the crystal. In the line-scan mode, we sweep constantly through the acoustic frequencies, and then jump back to the initial frequency. The time for jumping back is called the 'fly-back time'. With a 2mm diameter of the laser beam, the acoustic wave needs t=x/v = 2mm/ 660m/s = 3 µs to pass through the laser beam. This is the time that is needed to jump back to the beginning of the line-scan and is a fundamental limit for the line-scan frequency. In practice we use about 10 µs for a line scan, 7 µs for a constant scan and 3 µs for jumping back. During fly-back we acquire 60 pixels (50ns pixel dwell time). These pixels can not be used for image analysis. This mode results in line-scan frequency of 100kHz, about 10 times faster than a resonance scanning mirror.

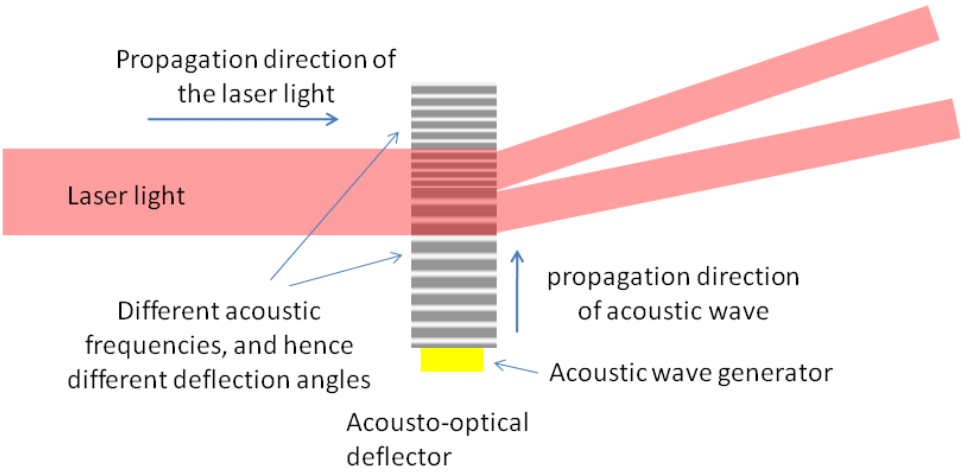

Figure 6, The fly back time as general limit of line-scan frequency for acousto-optical deflectors: We change the acoustic frequency continuously, hence change the deflection angle continuously and scan the object. When we reach one end, and restart from the beginning again, a sudden change of the acoustic frequency results in a deflection of the laser beam in two different directions. The time that is needed to change the acoustic wave from one frequency to another is called the fly-back time. It is dependent on the acoustic speed of the crystal and the beam diameter. It takes about 3µs for a 2mm beam in a TeO_2 crystal. During this time the beam is deflected in two different angles, and the acquired pixels show an overlay of both image locations. This part of the image can not be used for analysis of the physiological data.

As derived before, an increase in the acoustic velocity of the crystal would result in a decrease of the fly-back time, but also in a decrease of the scanning angle. This results in a trade-off between scanning angle (and hence the corresponding field of view) and the scanning speed.

The number of resolvable points of an AOD

One possibility to increase the scanning speed is a decrease of the fly back time by reducing the beam diameter. A smaller beam diameter of the laser beam results in a shorter time that is needed for the acoustic wave to travel through the laser beam. But this also decreases the image quality and is not an option. I will shortly explain the relationship.

A decrease of the laser beam diameter is not an option because this would results in a loss of resolution and a loss of the number of resolvable points. The explanation is as following: The intrinsic divergence of a beam is given by the formula $\Delta\theta = \lambda/d$, (with d being the diameter of the laser beam and λ the wave length of the laser light (Brimrose, 2011)). This formula predicts the natural broadening of the beam diameter. This relation is the same as how the numerical aperture predefines the resolution, but this is the other extreme end. When we focus light to a small spot, the used focusing angle determines how small the focus spot can be. The larger the focusing angle is, the smaller is the focus spot. The intrinsic divergence describes the relation between smallest beam diameter and the broadening of the beam: When we have a relatively small beam diameter, we

have a relatively large broadening of the beam and hence a large diverging angle. When we want a relatively constant beam diameter of the laser beam for some distance, we need a relatively large beam waist.

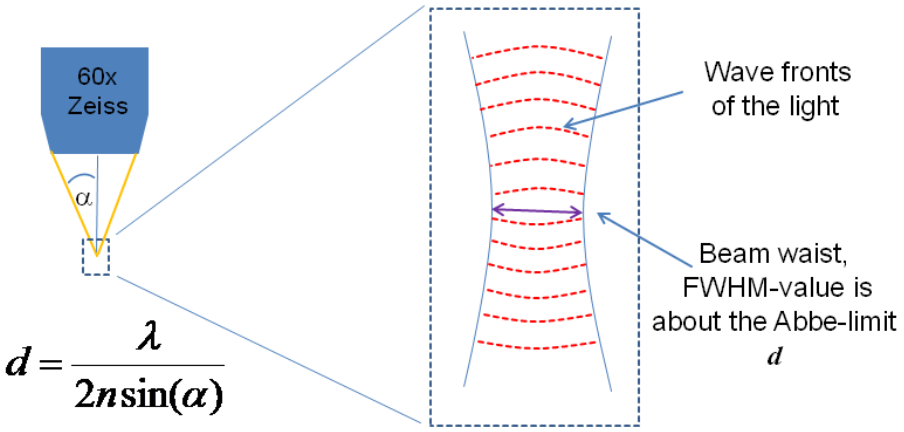

Figure 7, the intrinsic divergence of light. In general, a laser beam is divergent (as long as it does not have an infinite diameter). How much it diverges is dependent of its diameter or the beam waist. The relation is the same as how the numerical aperture describes the resolution $\Delta x = \frac{\lambda}{2\,sin(\alpha)}$*, in this case using the Abbe-criterion. This formula describes the relation how small laser light can be focused by a lens. I can write this formula in a different way:* $2\,\alpha \cong 2\,sin(\alpha) = \frac{\lambda}{\Delta x}$*. This formula now describes the intrinsic divergence (=opening angle), predicted by the beam diameter and the wave length. The beam waist is about the same like the Abbe-distance (15% difference). The smaller the focus spot or the beam waist, the larger the diverging angle.*

For normal beam diameters like 1-4 mm, the intrinsic divergence is very small and in the range of mrad. The intrinsic divergence, defined as $\Delta\theta = \lambda/d$, is normally below 1 mrad (milliradian), and for normal applications this can be ignored. The typical scanning angle of AODs is about 20-100 mrad. Although there is a difference of 2 magnitudes, this can still become problematic. The task is to resolve a number of distinct points. In optical imaging we want to have an image size of at least 100 to 1000 points, hence the scanning angle must be 2-3 magnitudes larger than the intrinsic divergence. Although the intrinsic divergence of a laser beam of 2mm beam width is very small, it needs to be 2-3 magnitudes smaller than the scanning angle, to get a deflection precision that is sufficient to distinguish between 100-1000 different points. This prohibits the use of very small beam diameter, or the use of a focusing optics that makes extreme small beam diameters at the AOD. (The number of resolvable points in the catalogue of AODs is not so critical, as the AOD vendors apply a very strong criterion: They just divide the scan angle by the opening angle (=intrinsic divergence). In optical imaging we normally sample the object with the Nyquist frequency, a value of about Half-Width-Half-Maximum of the light spot. This value is smaller by a factor of about 2. Hence, when an

AOD vendor states that their AOD is suited to distinguish 200 points, the AOD is good enough to record images with about 400 Pixel, according to the Nyquist sampling rate.)

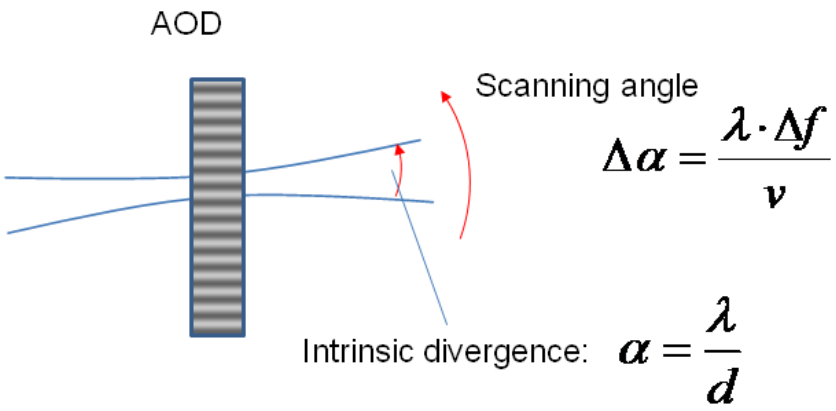

Figure 8, the resolution of an AOD: The resolution is defined by the intrinsic divergence and the scanning angle. The intrinsic divergence predicts the naturally occurring broadening of the laser beam. The larger the beam, the smaller the propagation angle, as explained earlier. This intrinsic divergence broadens the laser beam and hence reduces the number of resolvable points in the predefined scanning angle. This relationship limits the use of small beam diameters. Large AODs and large laser beams have a much higher number of resolvable points, but this results in a large fly-back time. This is again a trade-off between image resolution and speed.

The use of small beam diameters could reduce the fly back time, but this would reduce the number of resolvable points and hence the image quality. The number of resolvable points can be calculated by $N = \Theta/\Delta\theta = \Theta D/\lambda$ (Θ is the absolute scan angle $\Theta = \lambda \frac{\Delta F}{v_a}$, ΔF is the range of the acoustic frequency, and v_a the acoustic velocity of the crystal, $\Delta\theta$ is the intrinsic divergence of the laser beam), hence the larger the beam diameter, the more distinct points can be resolved (Brimrose, 2011). The number of resolvable points is often abbreviated by the so called time-bandwidth product: $N = \Theta/\Delta\theta = \Theta D/\lambda$, $\Theta = \lambda\, \Delta F/v_a = \Delta F/\Delta T$ (ΔT being the fly back time, the time needed for the acoustic wave to pass through the laser beam).

The cylindrical lens effect

When we scan with extreme frequencies, the acoustic wave is not homogeneous in the crystal and the beam is deflected in different angles. I demonstrate this effect in the next figure.

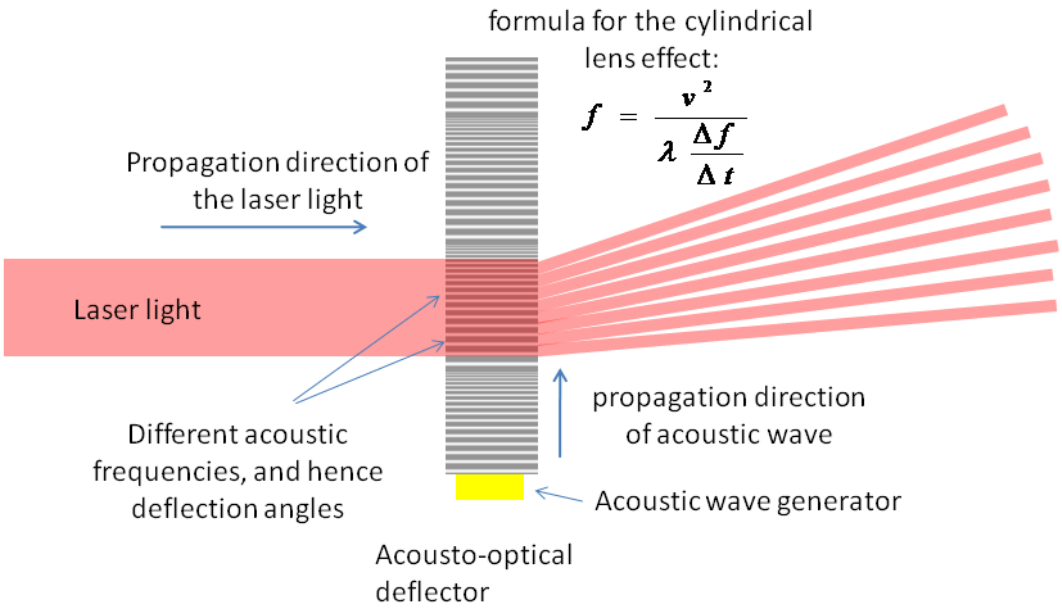

Figure 9: When I sweep through the acoustic frequencies in an extremely short time, the acoustic wave is not homogeneous throughout the laser beam, and different positions of the crystal deflect the laser in different angles. This is called the cylindrical lens effect, as the beam distortions are similar to the effects of a cylindrical lens. This effect can be dramatic for extremely fast scanning sweeps. The focal length of this effect is in the range of 100 mm to 1000mm. We normally work with this effect in the range of 250mm-700mm. I will later explain how I compensate for this effect.

With a linear chirp in the acoustic wave, we have a cylindrical lens effect. The focal length is predefined by the formula $f = v^2/(\lambda\ (\Delta f/\Delta t))$,(v being the acoustic velocity of the crystal, $\Delta f/\Delta t$ the change in the acoustic frequency per time interval, and λ being the wave length of the laser light) (Gerig and Montague, 1964). The focal length of this effect can be positive or negative (depending whether Δf is positive or negative), hence we can control whether we focus the laser beam or broaden it. Hence this effect can be like a convex- or a concave cylindrical lens. This corresponds to the direction of the sweep, whether we scan from a high frequency to a low frequency or vice versa. I will later explain how I compensate for this effect.

The chromatic dispersion

We can describe the deflection angle by the formula $\tan(\alpha)=\lambda/d$, hence the deflection angle is dependent on the wavelength of light. AODs were already used in one-photon microscopy, with highly monochromatic laser light. This effect is not present when we use a highly monochromatic laser, and the beam quality is not altered when the laser is passing through the AOD. In two-photon microscopy, we mainly use pulsed lasers with a spectral width of about $\Delta\lambda$ = +- 10nm. With this spectral composition of the laser, the different color components are deflected in different angles, and the beam quality deteriorates behind the AOD, and does not allow for the acquisition of good images.

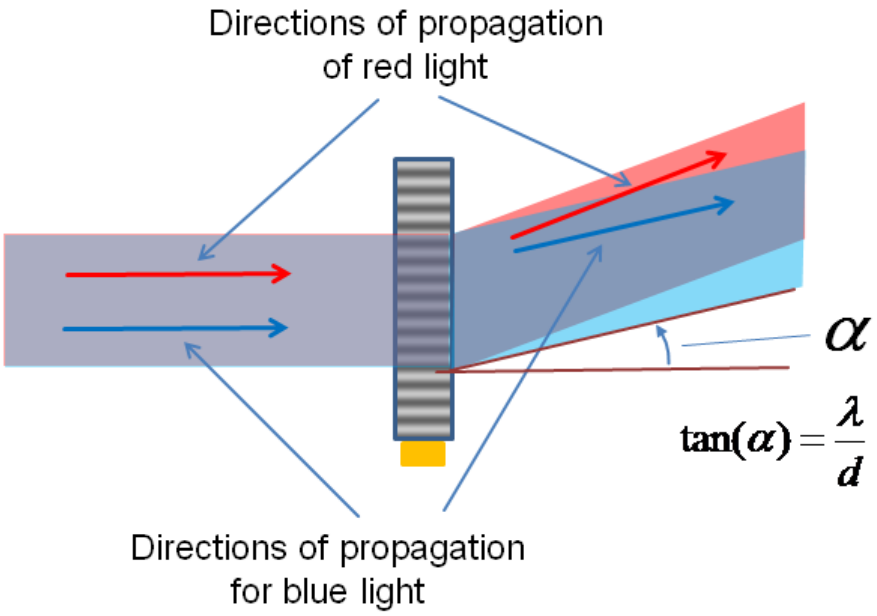

Figure 10, Chromatic dispersion: As the deflection of acousto-optical deflectors uses the principle of an optical grating, the deflection angle is predefined by the formula tan(α)=λ/d, hence different color components of the laser beam are deflected in different angles. We must compensate for this effect when we want to use a standard two-photon laser beam with a spectral width of about Δλ = +- 10nm

Movement artifacts require the acquisition of fast 2d image data

An artifact is very often visible when we image with video frequency: the pulsing blood flow moves the vessels in an oscillating way, and hence the brain tissue nearby is also moving. These movements can be in the range of several micrometers and depend on the heart beat of the animal, hence are in a frequency between 100-500 per minute, also dependent on the anesthetics used and the depth of anesthesia. For the observation of large objects like the somata of pyramidal cells, these movements can be ignored, as these objects are much larger than the movement, and a physiological signal can be derived anyway. But for investigations on physiological signals in smaller compartments of cells like dendrites or spines, an acquisition with no movements or a compensation of this movement artifact is a prerequisite. If there are movements present, we do not know whether a change in fluorescence originates from a physiological signal, or if the object simply moved out of the focus.

The detection of fluorescence signals in small compartments of cells requires a high sensitivity. Many researchers believe that random access scans are an option to increase the sensitivity, as they allow for sampling rates in the range of several kHz. Using AODs, we can indeed increase the sampling rate by some magnitudes(Grewe et al., 2010), but we lose the lateral image information and do not know what we actually scan.We can not check whether the dendrite is still at the place we are currently scanning. Therefore we decided to focus on the fast acquisition of two-dimensional image data at high frame rates. A high scan rate increases the sensitivity by simply acquiring more data, and simultaneously allows for the detection of the location of a cell. In this way we can check if a measurement is corrupted by movement artifacts.

Chapter 2: The current status of acousto-optical scanning systems

Acousto-optical scanners have already been used for a long time in fluorescence microscopy, but mainly for one-photon microscopy and with highly monochromatic laser light(Draaijer and Houpt, 1988; Houpt and Draaijer, 1989). We can ignore the chromatic dispersion when we use highly monochromatic light. The beam quality is not compromised in this case and AOD-scanning with a highly monochromatic laser results in images of good quality. The situation is different when using a pulsed laser for two-photon microscopy. These lasers are characterized by a relatively large spectral width with different wavelength-components (+-10nm). AODs induce a chromatic dispersion when we use such a laser, and this chromatic dispersion needs to be corrected. There are a number of recent publications that aim at a compensation of this chromatic dispersion.

The chromatic compensation by Lechleiter:

The chromatic dispersion denotes the effect that light with different wavelengths exits the AOD with different angles, and hence compromises the beam quality. There are a number of optical elements that generate a chromatic dispersion, e.g. prisms or gratings. The idea of a compensation is quite simple: When one optical element generates a chromatic dispersion, we just insert another optical element that generates the chromatic dispersion in the opposite direction, and hence reverses the chromatic dispersion.

The first approach was done by Lechleiter (Lechleiter et al., 2002)who modified a commercial AOD-based confocal microscope (Odyssey, from Noran Instruments) for the use for 2p-lasers.

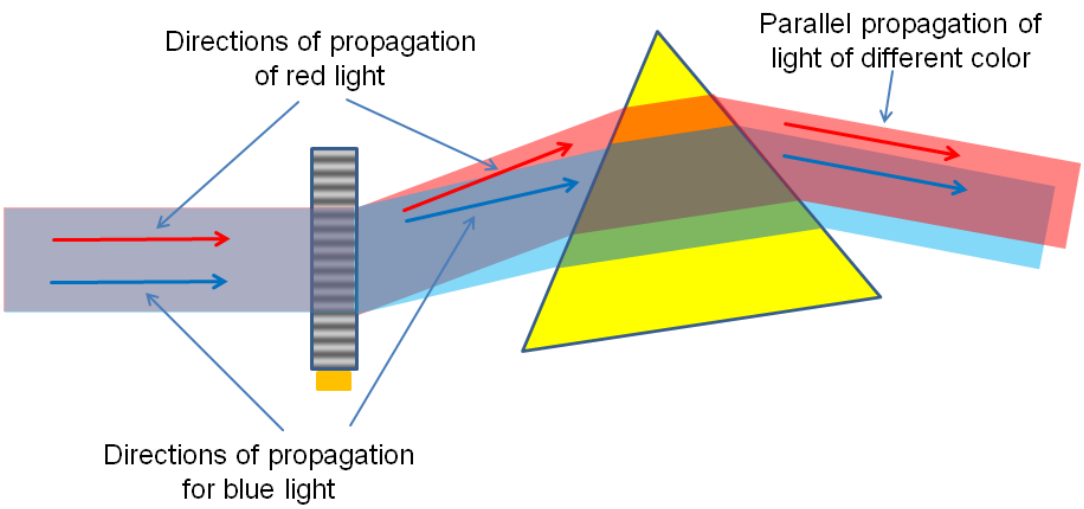

Figure 11: Compensation principle of the chromatic dispersion by Lechleiter (Lechleiter et al., 2002). Behind the AOD, the deflected light is directed on a prism that reverses the chromatic dispersion. As the separation of different color components is dependent on the incidence angle of the laser beam, a perfect compensation is only achieved at one deflection angle. The chromatic dispersion is only partially compensated for lower or higher deflection angles. However, it compensates the dispersion to a large extend and reduces the chromatic dispersion to about 20% of the uncompensated value. This then allows for the acquisition of images of good quality, even at the border of the image.

The research group of Lechleiter inserted an additional prism behind the AOD of a commercially AOD-based scanning system. The slow image scan was done by a galvanic mirror. This modified instrument made quite good images. The disadvantage was the position of the prism. It must be fine-tuned by revolving the prism in a sub-degree range, because the angle of incidence of the light predicts the amount of chromatic dispersion. This turning also changes the absolute output angle of the parallel beams. This results in an unpractical procedure of optimizing the prism angle. The beam was guided to the other parts of the optic by additional mirrors.

The chromatic compensation by Roorda:

The research group of Miesenböck modified the same commercial AOD-based microscope by inserting the prism in front of the AOD (Roorda et al., 2004). They used the same commercial AOD scanning system. The slow second axis was scanned by a galvanometric mirror, as in the apparatus of Lechleiter. They additionally replaced most of the lenses with lenses of different glass types and different anti-reflection coatings to get a higher transmission in the 800 nm wavelength range.

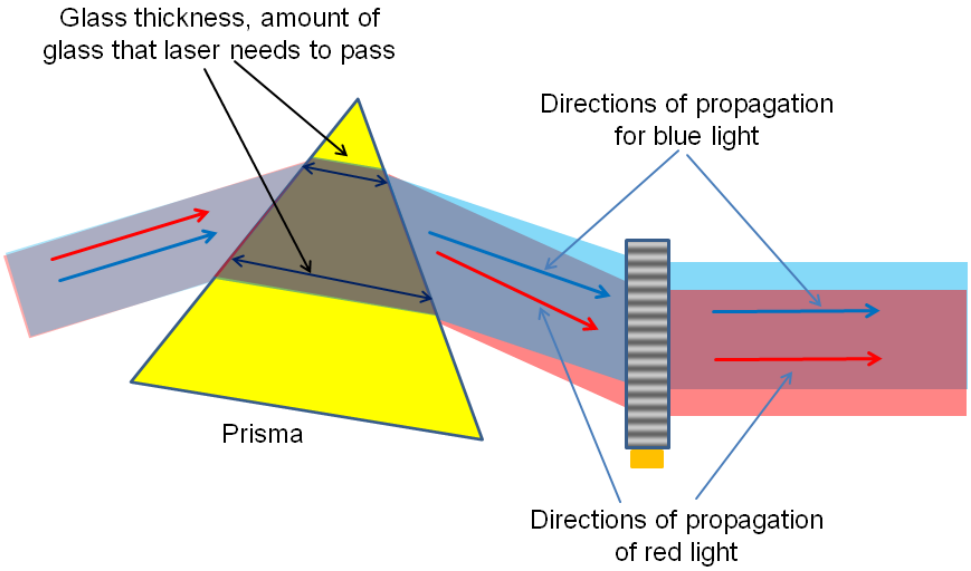

Figure 12, Chromatic compensation by Roorda: They placed the prism in front of the AOD in order to compensate for the chromatic dispersion.

The systematic analysis of the position of the prism

Shaoqun Zeng made a number of publications on AOD based scanning systems(Bi et al., 2006; Lv et al., 2006; Zeng et al., 2007; Zeng et al., 2006). He compared the two possibilities: An AOD followed by a prism (named AOD-prism) or a prism followed by an AOD (named prism-AOD). The performance of the compensation of the chromatic aberration is in general the same. The difference is in the geometric setup. In the AOD-prism configuration, both components contribute to the absolute deflection angle. The AOD deflects the laser light in different angles onto the prism. This influences the absolute deflection angle of the subsequent prism. Due to geometric reasons, the absolute scanning angle of the AOD-prism configuration is only about half of the scanning angle of the prism-AOD configuration. Considering the need of a large field of view in biological research, this strongly recommends the prism-AOD configuration.

There is one additional advantage of this configuration: The distance between the prism and the AOD can be used for so called ‘prechirping’, naming the compensation of the group velocity dispersion (GVD). This names the effect that light with shorter wavelength passes through the glass of the lenses a bit slower than light with a larger wave length. As a pulsed laser consists of different spectral components, this effect broadens the laser pulse and reduces the two-photon effect. This can be compensated by so called ‘prechirpers’, instruments that induce a temporal shift of blue light in advance of red light. These instruments normally consist of a pair of prisms and a mirror. Blue light travels a shorter distance and hence it runs in advance to the red light after the prechirper. This compensates the naturally occurring GVD, induced by the glass of the optical elements. When we use a prism to compensate for the chromatic dispersion, different color components travel a different light path and light-distance, and hence the chromatic compensation itself already generates a prechirp (a compensation of the group-velocity dispersion). To compensate for the natural occurring GVD, the AOD and the Prism must have a distance of about 35 cm (Zeng et al., 2006).

In the AOD-prism configuration, the AOD and the prism must be placed very close, as they are both active deflection elements and they should be placed in focal distance from the scan lens (figure 2). Hence the AOD-prism configuration does not allow for a GVD compensation. The additional GVD-compensation was a minor issue for us, as we normally always included an additional prechirping instrument, placed right after the laser.

The compensation by using an AOD instead of a prism

We can also use an AOD instead of a prism to compensate for the chromatic dispersion. This was first done by Salomé in the lab of Dieudonné (Salome et al., 2006).

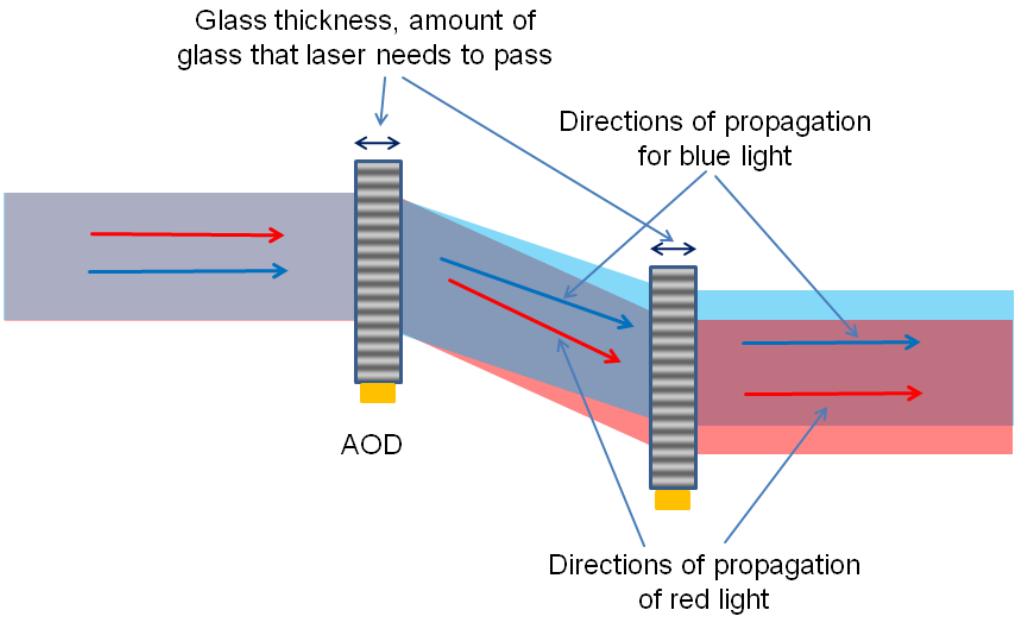

Figure 13, Compensation of the chromatic dispersion by using an AOD instead of a prism

The disadvantage of using an AOD instead of a prism is the price. AOD cost about 2000-5000 Euros, a prism about 100 Euros. But there is one major advantage: the distance of the crystal (in our case TeO_2 ,the material of the AOD) is homogeneous. When laser light is passing a piece of glass, the glass generates a group-velocity dispersion, as the speed of light is slower for blue than for red laser light. The red parts of the laser pulse run in advance of the blue parts of the laser pulse. This is called GVD and we must compensate for this. If we do not compensate for it, the pulse is broadened and the two-photon efficiency declines. By compensating for the chromatic dispersion with a prism, we create an inhomogeneous GVD throughout the laser beam (fig 13). We can not compensate for this effect with a standard prechirper. Therefore, an AOD as compensation for chromatic dispersion is a better solution than a prism, although it is much more expensive.

Systems without chromatic compensation

The minimum duration of a laser pulse and the minimum spectral width are limited by the Heisenberg uncertainty principle. When we have a short laser pulse, the spectral bandwidth of the pulse is necessarily quite large. Lasers with a pulse width of about 80fs are normally used for two-photon imaging, as they compress the pulse energy in a short pulse and increase the two-photon effect. These lasers have a spectral width of about +-10nm. There are lasers available with a long pulse (~1ps) and a smaller spectral width (+-1nm). These lasers are quite monochromatic, hence the chromatic dispersion is less severe and need not be compensated. As these lasers have a broader pulse, the two-photon efficiency is decreased, and hence the images are characterized by a lower signal-to-noise ratio. However, such scanning systems are an option for an easy construction of an AOD-based scanner, as they do not need a chromatic compensation.

I know of two such systems. One was published by Otsu (Otsu et al., 2008) in the lab of Dieudonné, and the other one was build here in our lab, mainly by Yuri Kovalchuk. I measured the performance of all available systems and compared them. The image quality of a system using an AOD scanner and a highly monochromatic pulsed laser (800nm +- 1nm, pulse width ~1ps) was about 50% worse than a resonance scanner system. The measuring parameters were standardized (same illumination power under the objective lens, same fluorescence brightness of the sample, same amplification of the PMT). The penetration depth of a system with a long pulse was highly reduced. We could image in about 100-150 µm depth in biological tissue. Such an instrument can be used for 2p imaging in slices (Otsu et al., 2008). For in-vivo observations, they are only suited for recordings very close to the surface. We were not able to investigate deeper layers of the intact brain with such a scanning system.

Random access scans

One way of increasing the sensitivity of two-photon measurements is the random-access scan mode. In this mode, we first record a two-dimensional image and select some positions of interest. These positions then should be recorded with high frequency by jumping with the laser beam from one location to the next. Mirrors are not suited for this, as they need quite a long time for acceleration and deceleration and hence are not suited to jump between different positions. AODs are inertia free, and the jumping time equals the fly back time, about 3µs. I will demonstrate the possible potential now with a short example. As a jump will take about 3µs (as long as the fly-back time), we could jump to a new position and then record the fluorescence for another 7 µs. In such a mode we could record the fluorescence signal from 10 positions with a temporal precision of 10kHz (Grewe and Helmchen, 2009; Grewe et al., 2010; Otsu et al., 2008; Reddy and Saggau, 2005; Salome et al., 2006). This would be a big increase in temporal resolution, and in theory this approach should provide an excellent signal after application of noise-reduction filters.

The data from in-vivo imaging are often compromised by movements of the tissue. These movements normally originate from the pulsing blood flow, moving the tissue near blood vessels in an oscillatory manner. We must also check if these movements compromise the measurement or not. Therefore we must acquire real image data with a high frequency. The movements are with the frequency of the heart beat, up to 400 times per minute. The image acquisition rate must be faster than 20 images/second to resolve these movements. We do not see these movements when we scan

in a random access scan mode, and hence do not know if the measurement is corrupted by moving tissue or not.

Another disadvantage of the random access scan mode is possible photodamage. Two-photon lasers deliver a lot of energy into the tissue. When we place the focus spot of the laser on one certain position and wait for some time, we will probably damage the cell. We always try to preserve the sample as much as possible and reduce the illumination power to a value as low as possible. Additionally, without two-dimensional image information we do not know if the photo-damage takes place. Photodamage can look very dramatic, as we describe it as 'The cell explodes'. This describes a rupture of the membrane and a mixing of intracellular and extracellular solution. These fresh mixtures are highly fluorescent, and we see a high fluorescent content around the cell. Images from such a cell resemble an exploding or burning cell. We can not detect this kind of photo-damage when we just scan in a point-scanning mode.

Chapter 3: The work of my PhD thesis: The layout and assembly of a custom built two-photon scanning microscope.

Commercial two-photon microscopes all suffer from a relatively low temporal resolution (2-10 images per second). A custom build two-photon microscope in our lab, based on resonant mirrors, is optimized to acquire images with the speed of video rate (32 images/second), but it can also acquire images with up to 200 images per second. This is quite fast compared to commercial systems. However, that microscope uses a frame-grabber to acquire the data. The frame-grabber is optimized for images with video rate, and a change of this configuration to higher image frequencies is quite difficult. Therefore, we first had to exchange the electronics for data acquisition in order to explore the effects and characteristics of a high acquisition rate.

Software development for a fast scanning system.

A previous custom-built two-photon microscope in this lab used a frame-grabber for data acquisition. There are some advantages for using a normal frame-grabber electronics: The bandwidth is optimized for the used sampling frequency, and the software from the vendor is well developed for standard applications. But there are some disadvantages: A frame-grabber is optimized to acquire movie data for human observers. A human observer needs about 25-30 images per second to have the impression of a fluent and live display, hence the frame grabber is optimized for image frequencies of about 30Hz. The configuration of the frame-grabber is complicated when we want to acquire the images with higher speed. Next, the eye of a human observer can distinguish between about 150 grey values, hence there is no need to acquire the images for video data with a higher precision. A frame grabber normally acquires the image in 8 bit precision (256 grey values) with three color channels, for red, green and blue. This is quite fine for a human observer. These parameters are also in an acceptable range for the acquisition of images in two-photon microscopy. The digitizing range was fixed for 0-1V in the frame grabbers, hence we must amplify the signal in a way that it fits between 0-1 V. If the electronic signal from the photomultiplier exceeds this range, the detector is in saturation and can not detect the precise value. Finally, a frame-grabber is optimized to provide a life image. The philosophy is as follows: It is not a big problem when one frame is missed or one is recorded twice, as long as the live data stream is not interrupted. The image data is moved into the memory, and the frames are grabbed with a regular frequency (the memory is read out). If the computer is busy for a short time (due to activity of antivirus software or other programs), the frame grabber will miss the actual image and continues with the next image. This is not a big problem for shooting movies, but for precise measurements this can be problematic. We mainly want to record a continuous stream of data and save it to disc, because we normally analyze the data off-line. We do not want to have some data twice or a missed image. As we normally analyze the data later, we do not really need a live display, but a precise and continuous track of recorded images.

All the mentioned disadvantages of frame grabbers can be avoided by replacing the frame grabber with a high precision digitizer. The disadvantage is that I now have to start programming all imaging routines from the scratch, and can no longer use the given image acquisition routines from the frame-grabber vendor. However, we decided to do so, as we could sample with higher speed (shorter pixel dwell time, hence more pixels per second) and precision (more grey values). Additionally, it is easier to configure the image acquisition for other image dimensions and higher frame rates.

I decided to buy all data acquisition devices from National Instruments, as they also develop the software LabView, a very powerful and flexible environment for programming measurement

routines. Software development is very fast using this computer language. We bought the card NI PXIe 5122 for digitizing the signal from the fluorescence detector. This digitizer has a sampling range from -10 to 10 Volt, a sampling frequency up to 100MHz, a sensitivity of up to 12µV and 14 bit precision, corresponding to 16 384 grey values. This allows for a flexible configuration. The general limitation for the sampling speed is at 82MHz, the pulsing frequency of the two-photon laser. If we run the digitizer with 82MHz, we would illuminate each pixel with one laser pulse. We can not go beyond that speed. We found that 82MHz is already too much, as there are not enough fluorescence photons coming from the sample, and the data is too noisy. 20MHz is a good compromise between imaging speed and data fidelity. If we sample too fast, the data is too noisy and the data analysis becomes problematic.

The data acquisition must be synchronized with the command signal for the galvanometric mirrors and the AOD. The company National Instruments specializes in instruments for measurements and provides a lot of devices for such applications. I generated the command signal for the AODs or galvanic mirrors with arbitrary waveform generators (model NI PXI 5412). The digitizers and the waveform generator are mounted in an external chassis. The chassis also contains a master clock, allowing for the synchronization of all the devices mounted in the chassis. With this, I can sample the fluorescence signal with high speed, and the control signal for the movements of the mirror and the AODs is always in synchrony with the digitizer.

The design of a fast scanning system with a compensation of the non-homogeneous grating of the AOD

There were already some experiments with high imaging speed with another AOD-based 2p microscope with a frame-grabber electronic for data acquisition. The overall effect was a deterioration of the image quality with a higher frame rate. However, it was quite difficult to investigate the image deterioration and modify the frame-rate systematically, as frame grabbers are quite difficult to configure. With the new software I can now make a systematic investigation of image quality and imaging speed.

The cylindrical lens effect as origin of image distortions and their compensation

I started a systematic variation of image rate (frames per second) and image quality of an AOD-based system (figure 14,15). I used pollen grains to investigate the image quality. Pollen grain preparations (mixed pollen grains from Carolina Biological Supply Company) are the objects of choice for investigations of the image quality, because I can easily determine the resolution of the microscope by looking at the spiny protrusions at the surface of the pollen grain. This can be clearly seen in the following figures.

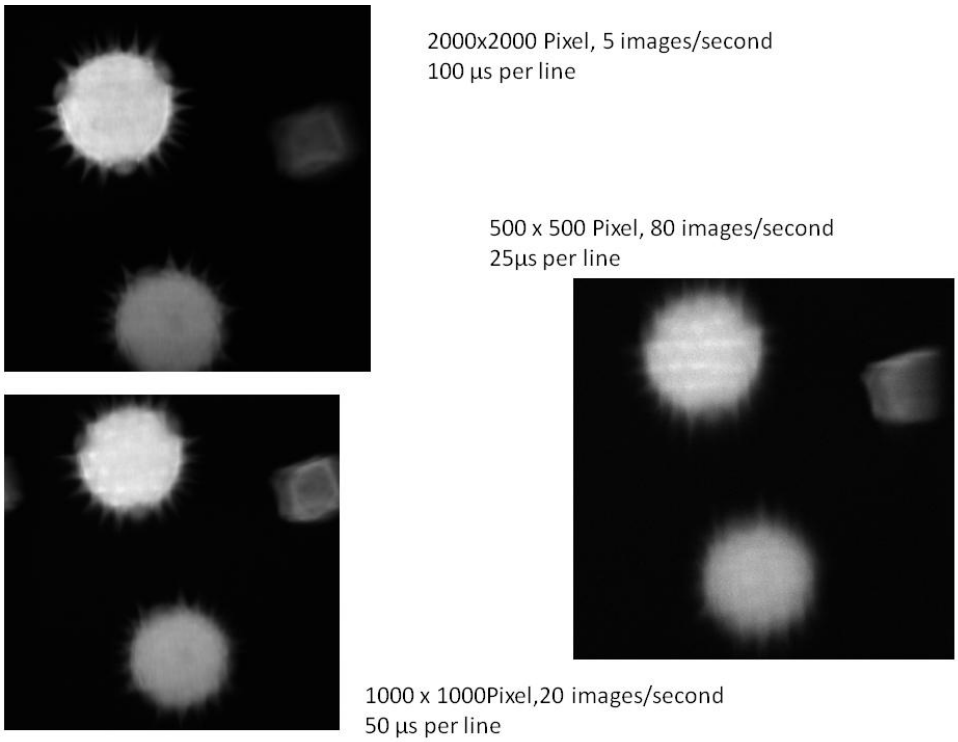

Figure 14, the effects of increased image frequency on image quality. The increased line frequency results in a cylindrical lens effect in the AOD, and hence a distortion of the laser beam and a worse image quality. Image quality is only acceptable with up to 20Hz without a compensation of the cylindrical lens effect.(images were resized)

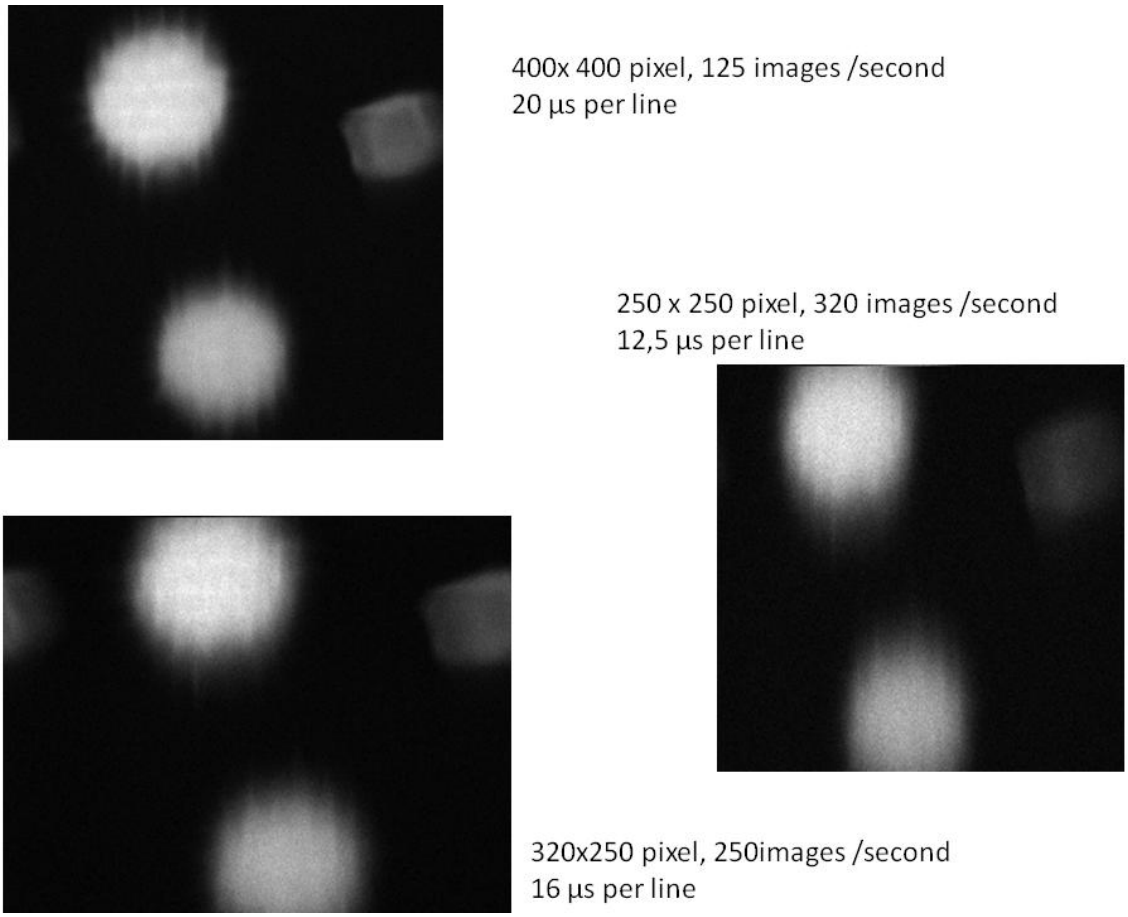

Figure 15, image quality for imaging high frame rates. Increasing the frame rate also increases the cylindrical lens effect, hence disturbs the beam quality, and this affects the image quality. Image rates above 100 Hz result in a poor image quality. I gain images of good quality only up to video rate. We can also reach this frequency by the use of resonant mirrors. As AODs also introduce chromatic dispersion and have a much smaller scanning angle, AODs are at first not advantageous compared to resonant mirrors.

The image quality deteriorates with an increased line-scan frequency. Image quality is only acceptable with frame rates of 20-30 Hz. We can also achieve this frequency by using a resonant mirror scanning system. Hence, there are at first no big advantages for the use of AODs.

I made a numerical simulation of this effect. I was interested in the quality of the cylindrical lens effect, whether there are typical lens artifacts, like barrel distortion or image field curvature. The result is given in figure 16.

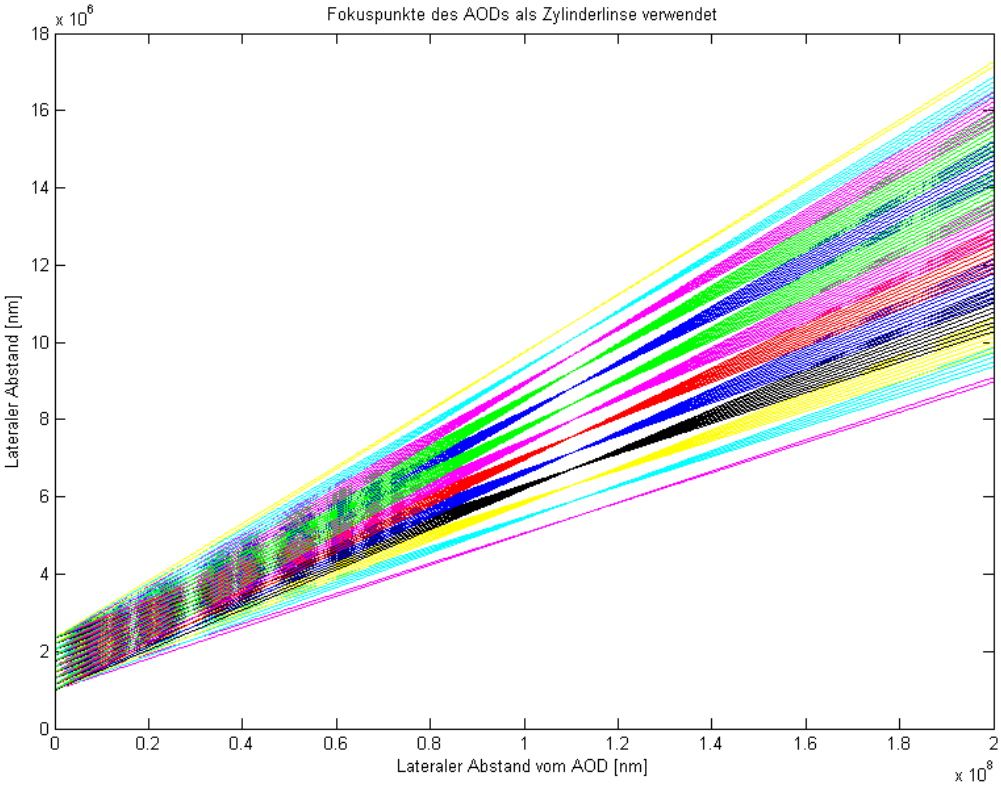

Figure 16, numerical simulation of the cylindrical lens effect of an AOD at different time-points during fast frequency sweeping. Different colors represent the deflection at a different time point. The focus spot is at the predicted distance, and it is quite sharp, hence the analogy with a cylindrical lens is a good description of this effect. I could not detect artifacts like a 'barrel distortion' or an 'image field curvature'.

My first approach to compensate for this effect was the introduction of special optical elements in front of the AOD. The idea is analogous to the compensation of the chromatic dispersion: If the light exits the AOD with different angles, we can compensate for this by irradiating the AOD with different angles. When the incident angles correspond to the angles caused by the cylindrical lens effect, the beam should be collimated after the AOD. I visualized my first compensation optics in figure 17.

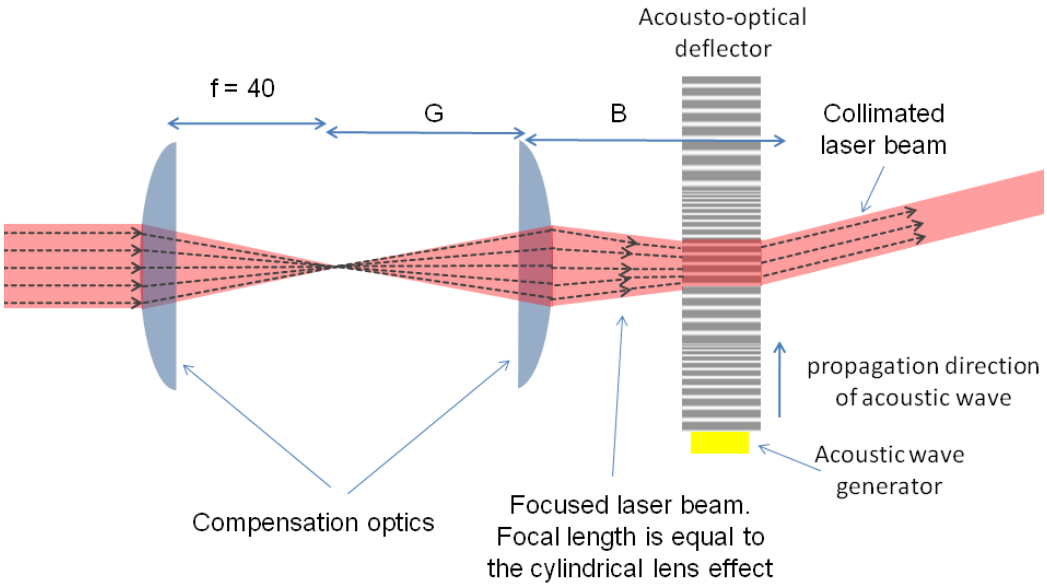

Figure 17, the first layout of my compensation optics for the cylindrical lens effect. I insert two cylindrical lenses into the laser beam to allow for a continuous variation of the focusing range B. The focal length B can be changed by changing the distance between the two lenses, according to the lens formula 1/B+1/G=1/f (G: distance from the second lens to the focal spot form the lens on the left). When the focal length is equal to the focal length of the cylindrical lens effect, the optical elements compensate for the cylindrical lens effect, and the laser beam is collimated after the AOD.

Two cylindrical lenses are placed in about focal distance. The distance between the two lenses can be finely adjusted. I can calculate the focal length B by the lens formula 1/B + 1/G = 1/f, (B: Bildweite, equal to the focal length of the correction optics; G: Gegenstandsweite, distance of the focus spot from the lens; f: focal length of the lens). This formula predicts the distance of a sharp image from the lens. As I have a focal point, I can calculate the distance B where the light is focused again. I can vary the focal length B continuously by moving the first lens.

I inserted this compensation optics in front of the AOD. Then I ran the 2p microscope in continuous mode and adjusted the distance between the two lenses to the optimum image quality. This was done on an AOD-based system with a frame-grabber based acquisition electronics and a highly monochromatic laser ($\lambda = 800$ nm, $\Delta\lambda$-+1nm), hence a chromatic compensation was not needed.

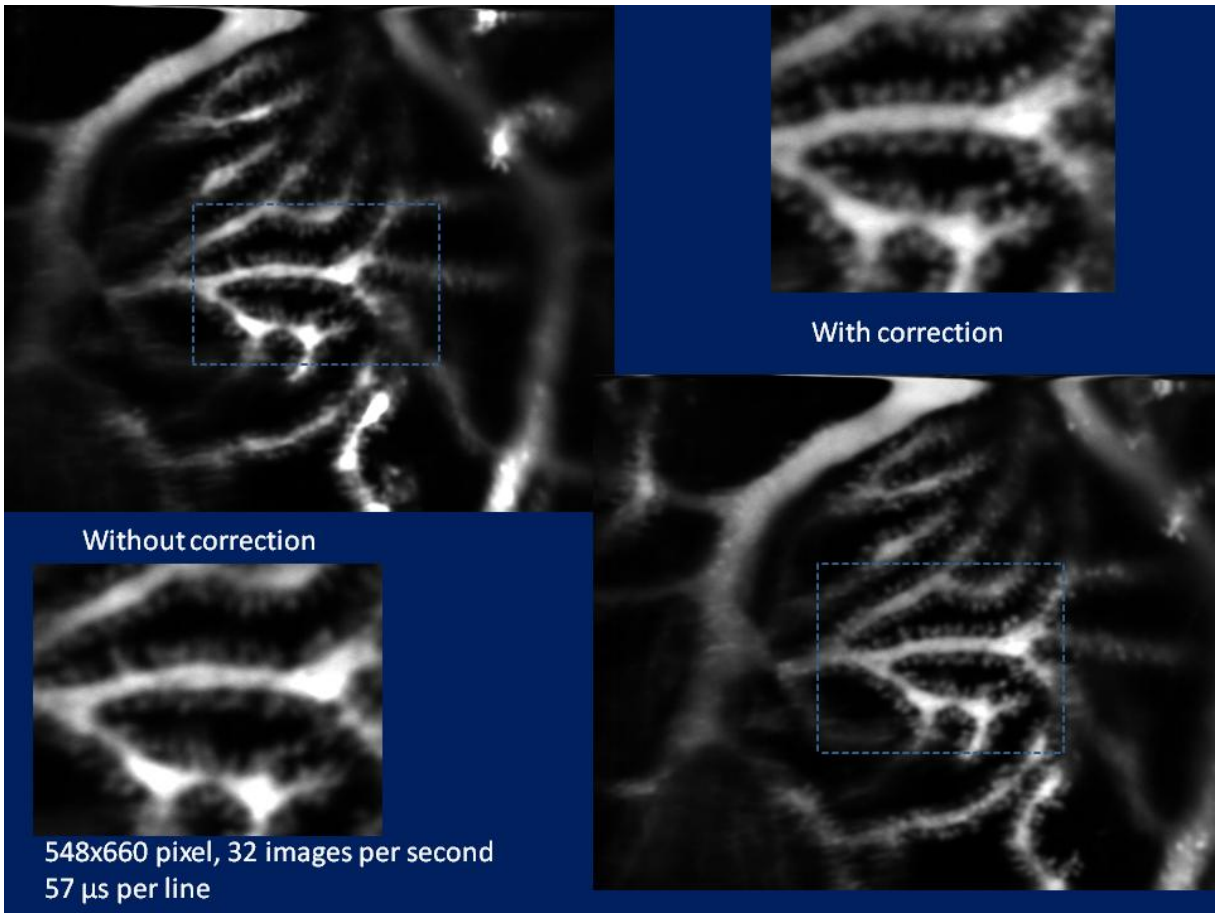

Figure 18, The effect of the compensation optics on image quality: I placed the compensation optics in front of the AOD, as close to the AOD as possible. The imaging system was running in a continuous data acquisition mode and I adjusted the distance between the two compensation lenses. I fixed the lenses at the position of optimum image quality. The distance between the two lenses was about 83 mm (the focal length of both cylindrical lenses was f=40 mm), corresponding to a focal length of 580mm of the compensation optics. The calculated value of the cylindrical length effect was about 600mm. This was the first proof that the cylindrical lens effect is responsible for the image deterioration at higher image frequencies, and that we can increase image quality by compensating for it.

The best position and assembly of the compensation optics for the cylindrical lens effect

I showed a method of compensating for the cylindrical lens effect in the last chapter for a system with a highly monochromatic laser, where a compensation of the chromatic dispersion is not necessary. Such a laser is, in general, not suited for two-photon imaging, because the two-photon effect is reduced by the long pulse duration. We now want to implement the cylindrical lens compensation together with a chromatic compensation, that would allow for the use of a pulsed laser with short pulses (~100 fs).

The first disadvantage of this compensation pattern became apparent very fast: AODs are optimized for a light incident angle equal to the Bragg-angle. This angle minimizes reflections, and allows for high transmission rates. If we irradiate the AOD with a different incidence angle, the deflection

efficiency becomes low. Most of the light passes the crystal of the AOD, and only a very small proportion is deflected to the maximum of first order, and used for scanning the sample. With a compensation scheme like that displayed in figure 17, we can not compensate higher values of the cylindrical lens effect. It works for values of 600mm, where the image deterioration starts being visible. When we would irradiate the AOD with higher incidence angle, we would dramatically reduce the efficiency of the AOD. When we need to compensate values of about 300mm, the AODs become very inefficient, due to the different incidence angles of the focused laser beam.

Another problem would arise when I combine this compensation scheme together with a compensation of the chromatic dispersion as shown in fig. 13. When the element for chromatic compensation (a prism or AOD) is placed in front of the scanning AOD, different wavelengths of the laser beam approach the scanning AOD in different angles. When I insert a lens system into the chromatically dispersed laser beam, this would also change the propagation angles of the different wavelengths. I could place the prism for chromatic compensation behind the AOD, but this has other disadvantages (Bi et al., 2006). Therefore I prefer to place the chromatic compensation in front of (upstream) the AOD.

The next question is the type of compensation optics. I could build it in the Gallilei- or Keppler-configuration. The one configuration uses a concave-convex lens system, while the other uses a convex-convex lens system. The type of compensation affects the chromatic compensation. The Galileo configuration would change the absolute value of the chromatic dispersion (in mrad/nm), while the Keppler-configuration would additionally change the sign, as the beam is inverted with this configuration. I visualize this in the following figure.

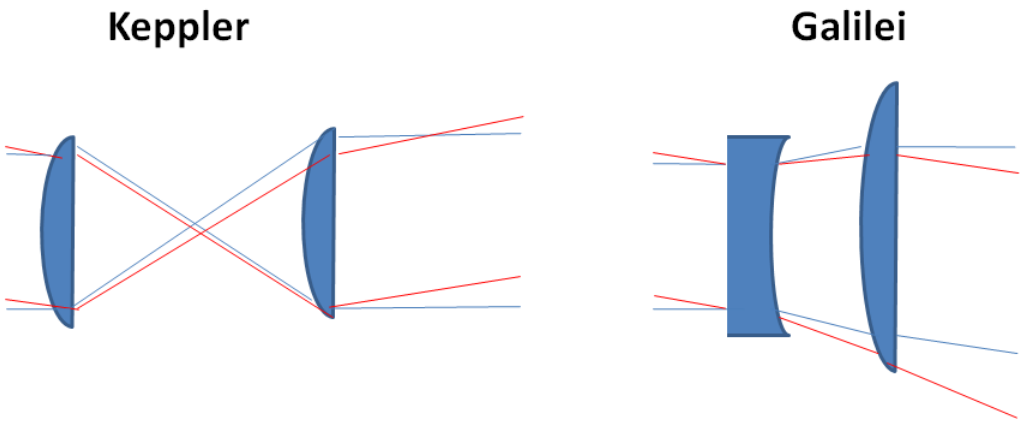

Figure 19: compensation pattern for the cylindrical lens effect according to Keppler- and Galilei-configuration. The absolute value of the chromatic dispersion changes in both cases. The Keppler configuration additionally inverts the compensation, hence switching the sign of the chromatic dispersion.

When we make the chromatic compensation in front (upstream) of the scanning AOD, it is not a good idea to insert the cylindrical lens compensation also there, in the chromatic dispersed beam. This would influence the chromatic compensation, caused by the compensating prism (figure 12) or AOD

(figure 13). There is no chromatic dispersion behind (downstream) the AOD, hence this is a better place for the compensation optics. In this position, the beam is moving according to the scanning behavior, and is not static. The change of the angle of incidence complicates the compensation layout. It must work with different incident angles, and it must be quite compact, as it must fit between the AOD and the scan lens (figure 2). I used scan lenses between 45mm and 75mm, hence the compensation layout must be shorter. I can not insert a compensation optics of several lenses as shown in figure 17 behind (downstream) the AOD.

Adjusting the distance between the lenses to the cylindrical lens effect is very useful for a given scanning frequency and amplitude, but I can also modify the cylindrical lens effect, and match it to a given compensation lens. In this case I would only need one compensation lens. A single lens is quite compact and can be inserted behind the AOD without any problems. The cylindrical lens effect is predefined by $f = v^2/(\lambda\ (\Delta f/\Delta t))$ *(Brimrose, 2011; Gerig and Montague, 1964).* I could also modify Δf *or* Δt in order to match the cylindrical lens effect to a given value of a compensation lens. Modifying Δt is unpractical, as this also modifies the line scan frequency, and I would end with odd numbers for frame rates. Modifying Δf is a good option. This parameter determines the range of the acoustic frequency that is being swept through for one line scan. This corresponds to the scanning angle, and hence the field of view. In this way I adapt the image size to a given compensation value for the used cylindrical lens. I can no longer use an arbitrary zooming factor and field of view. When I insert one certain lens, I compensate only for one fixed value of the cylindrical lens effect. I display the layout of this compensation scheme in figure 20.

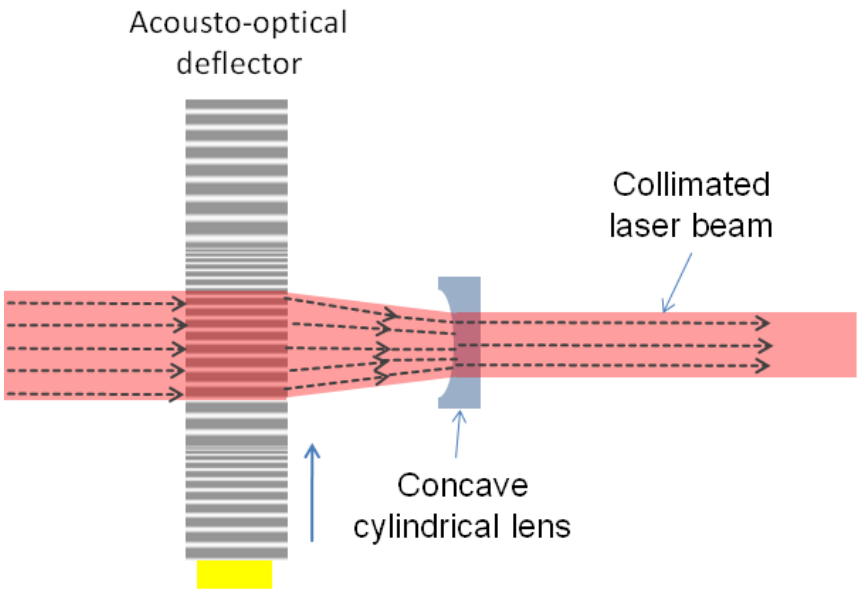

Figure 20, compensation of the cylindrical lens effect by placing one cylindrical lens behind the AOD. The cylindrical lens effect is dependent on the change of the acoustic frequency per time $\Delta f/\Delta t$, and hence the scanning angle per time. By selecting the focal length of the cylindrical lens for compensation, we compensate for one cylindrical lens parameter, hence I can only run the two-photon microscope with a predefined field of view and a fixed linescan-frequency. If we use other parameters, the compensation is no longer perfect. Different line-scan frequencies or image sizes would require a change of the cylindrical lens. We use a filter wheel later for an easy change of the cylindrical lenses in the final version of the apparatus.

With one lens I can only compensate for one value of the cylindrical lens effect. However, this proved to be the only practical way for a compensation of this effect. Complicated optics can not be inserted downstream the AOD, as there is not enough space between the AOD and the scan lens. Additionally, the deflected beam is changing the incidence angle. A beam should pass a lens always in the center of the lens. If the beam is passing the lens at the border, a lens artifact called 'spherical aberration' occurs. The lens must be placed close to the AOD. In this case, the deflected beam is always passing through the center of the lens, and spherical aberration effects (due to the changing emergent angle) are minimized.

I analyzed the optimum position and the layout of the correction optics for the cylindrical lens compensation, but there is still one question to be solved: should I use a convex or a concave cylindrical lens? The cylindrical lens effect can be focusing or expanding, according to the scanning direction. The focal length is determined by $f = v^2/(\lambda\ (\Delta f/\Delta t))$. Δf can be positive or negative, depending on whether we scan from a high frequency to a low one or in the opposite direction, or in other words, from the left to the right or vice versa. Scanning in the other direction would produce a concave cylindrical lens effect, requiring a convex lens for compensation. This relationship is displayed in figure 21.

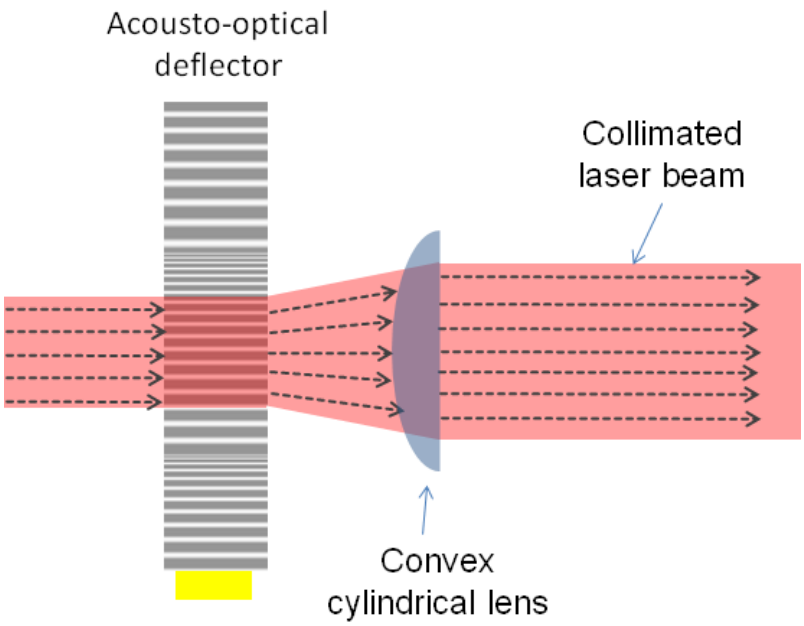

Figure 21: Layout of a convex lens for compensating the cylindrical lens effect. The lens should be placed as close to the AOD as possible, because the beam should pass the lens at the center, to minimize a lens artifact called spherical aberration. As the beam is not static and is changing its emerging angle, the beam would not always pass the lens at the center when the lens is placed at a further distance. Typical image distortions would be more severe. A convex lens results in a larger beam diameter after the AOD. This has some optical advantages (see text and next figure).

When I use a convex cylindrical lens for compensation instead of a concave cylindrical lens, the beam diameter after the lens is a bit larger. A larger beam diameter is beneficial for image quality, as it allows for focusing to a smaller spot. I will display this in figure 22.

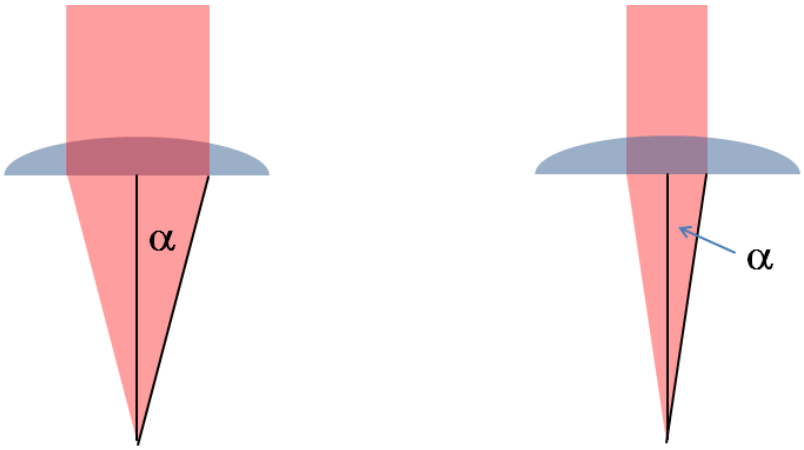

Figure 22, large beam diameter versus small beam diameter: The beam diameter predefines the focus angle α, and hence the numerical aperture (defined by sin(α) in air). The diameter of the focus spot is predefined by the formula λ/(2 sin(α)). With a larger beam diameter, the angle α is larger and hence the focus spot is smaller.

A large beam diameter allows for a higher numerical aperture (for a given focal lens), resulting in a smaller focus spot in the image plane. The smaller the focus spot in the image plane is, the better the image quality. Therefore, a larger beam provides better images and a convex lens is better for compensating the cylindrical lens effect. I could also decrease the size of the focus spot by taking a lens with a shorter focal length, but this also decreases the scanning angle, hence the field of view.

Theoretical prediction of the beam distortions caused by the chirped grating of the AOD

The chirped grating in the fast-operating AOD results in a cylindrical lens effect. This results in a non-collimated and in one direction divergent beam. A divergent beam normally results in a different distance of the focal point. I illustrate this relationship in the following figure.

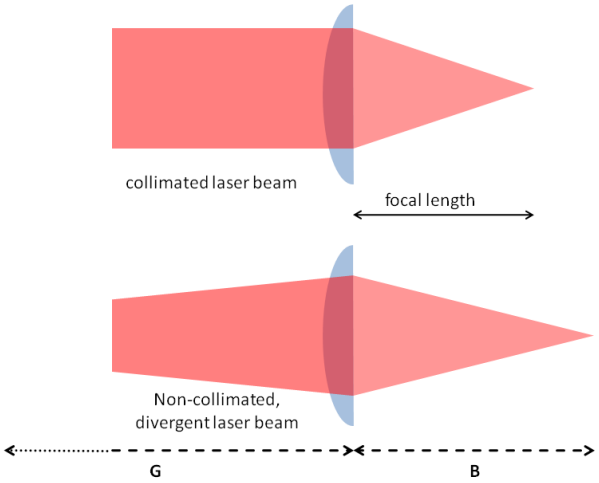

Figure 23, the effects of a non-collimated, divergent laser beam on the focusing properties of a lens. The beam is still focused, but the focus spot is located at a different distance from the lens. This new distance is predefined by the lens formula $\frac{1}{B}+\frac{1}{G}=\frac{1}{f}$. *(B denotes the image distance (Bildweite), G the object distance (Gegenstandsweite), and f the focal length of the cylindrical lens.) A collimated laser beam is one extreme case. The object distance G is infinity, hence 1/G is zero, and therefore the image distance B is equal to the focal length f.*

The chirped grating of the AOD generates a divergence, but only in one direction, like a cylindrical lens. I tried to correct this distortion with a suitable lens, but the effects of a non-ideal compensation are also of interest. I would have a divergence in only one direction. The cylindrical lens effect is predicted by the formula $f=\frac{v^2}{\lambda\frac{df}{dt}}$, *v* denotes the acoustic speed in the crystal, *df/dt* the change of acoustic frequency in the given time interval *dt*, and λ the wavelength of the light. The compensation-optics is normally not perfect, because some parameters vary a bit and can not be measured precisely, e.g. the acoustic speed in the TeO_2 crystal varies between different companies and is dependent on the crystal growth procedure. The company AA Optoelectronics uses crystals with an acoustic speed of 611m/s, and CTI Inc uses crystals with 820m/s. Additionally, the frequency generators vary their frequency dependent on their temperature. I measured the acoustic speeds of the crystals once (by measuring the frequency with a high-bandwidth oscilloscope, and the angle between first- and zero order maximum), but some uncertainties remain. The question arises, what happens when the cylindrical lens effect is not compensated for perfectly.

I think a non-perfect compensation would result in two different focus points, one according to the divergence in x-direction, and the other with the non-divergent, collimated beam in y-direction. I demonstrate this in the following figure.

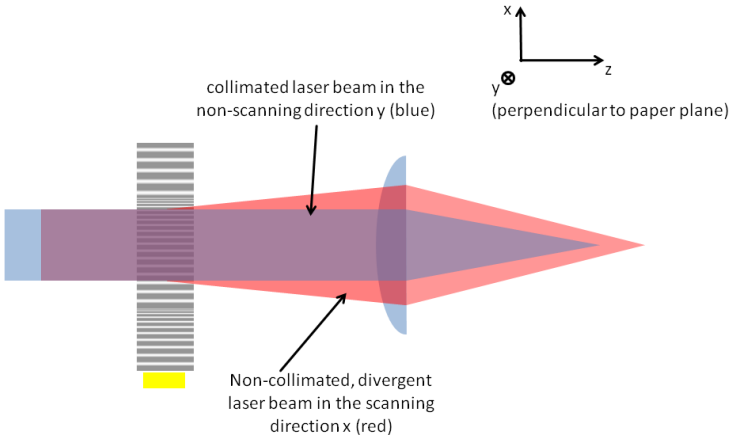

Figure 24. We operate the AOD with an extreme scanning speed, hence we have a chirped acoustic grating with a cylindrical lens effect, resulting in a divergence of the beam. A divergence results in a different focal distance. As the divergence is just in one direction (X), the beam is still collimated in the other direction (Y). This results in two focal distances, and in practice in an elongated focus spot(Vucinic and Sejnowski, 2007). Here we investigate the precise shape of such a deformed focus spot.

A shift of the focus point in the depth direction was already observed by my colleagues Bruno Pichler and Yuri Kovalchuk. They observed a change of the focal plane at an experimental AOD-scanning setup, dependent on whether they perform the line-scan from left to right or vice versa. Changing the scanning direction results in a change of the sign of the denominator in the formula of the cylindrical lens, hence we changed from a concave cylindrical lens to a convex one. This results in a shift of the focus point in the depth-direction. This effect was already used by Vucinic (Vucinic and Sejnowski, 2007) to perform a three-dimensional scanning. He varied the scan speed, hence the divergence and therefore the depth of the focal plane in the tissue. However, he could not demonstrate a measurement of a physiological signal using this trick. Peter Saggau used this effect also for three-dimensional scanning (Reddy et al., 2008). He used two AODs for each scanning direction. In this way he is also able to control the dispersion during the scanning, hence he can predefine the depth of recording. However, I think a setup with 4 AODs is too complicated for practical use and daily measurements.

I previously calculated the shape of the focus point for a different project, when I worked in the MPI of Psychiatry and contributed to the development of a novel imaging technique. This resulted in a comprehensive analysis of the depth-resolution of lenses (Leischner et al., 2009). I will briefly mention the results here, because that analysis of the shape of the focus point is also of interest for this problem, and the results can be transferred easily.

That imaging method used a normal microscope, but applied a somewhat exotic illumination technique. We illuminated not through the objective lens or by transmission through the condenser lens, but perpendicular to the direction of observation. The advantage of this illumination technique is that only the focus plane is being illuminated, hence we do not bleach other parts of the sample.

There is also an optical advantage for this illumination technique. The depth resolution can be increased in some configurations, especially when we use an objective lens with low depth-resolution. In this case, the depth resolution is predefined by the width of the illumination beam, and can be dramatically enhanced. Altogether, this illumination technique is advantageous for the three-dimensional imaging of large biological samples, with sizes between 1-10 mm. Such samples require the use of an objective lens with large field of view, but such an objective lens is normally characterized by a low numerical aperture and hence a low depth-resolution. With an illumination from the side, the depth-resolution is predefined by the illumination beam. In this case, the resolution can be much better than the depth-resolution of the objective lens. I visualize this illumination technique in the next figure:

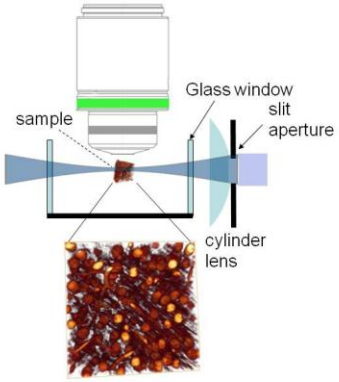

Figure 25. Illumination technique of ultramicroscopy (figure from(Leischner et al., 2010)). We illuminate from the side. The depth-resolution is predefined by the thickness of the illumination beam. Additionally, the depth-resolution of the illumination beam predefines the field of sharp illumination, corresponding to the useful field of view. The depth-resolution of the illumination beam is therefore of interest to predefine the field of view. For these investigations, I made a comprehensive analysis of the shape of the illumination beam, including the development of the beam thickness in depth-direction.

With an illumination from the side, the depth-resolution of the illumination beam predefines the area of a thin illumination beam, and hence the useful field of view. Therefore, I made a comprehensive analysis on the shape of cross-sections of the illumination beam, and concluded values for the depth-resolution with this illumination. The differences between cylindrical lenses and normal lenses are minor, and results can be transferred easily. I will present the results of the shape of the cross-section of the focus spot in the following two figures, a cross-section in the XY- direction (figure 26), and one in the z-direction (figure 27).

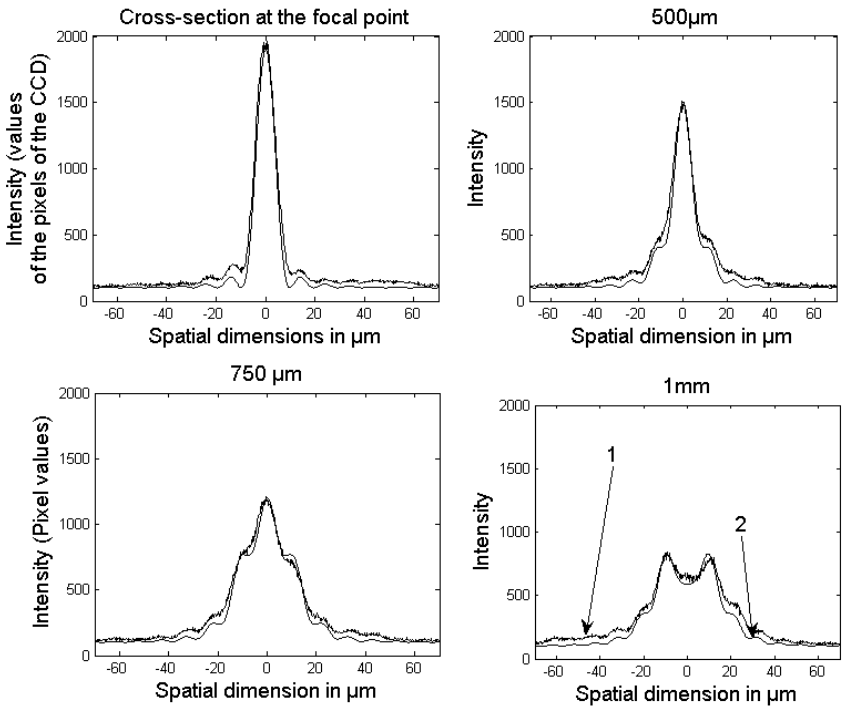

Figure 26: Cross-sections in XY-direction of the light-intensity through the focus spot. At focal distance from the lens, the cross-section corresponds to the well-known pattern of an airy-disc. Besides the focus position, the secondary maxima become larger. (figure from (Leischner et al., 2009)). The line 1 indicates the measured cross-section, and 2 the result from a numerical simulation. Details are given in the publication.

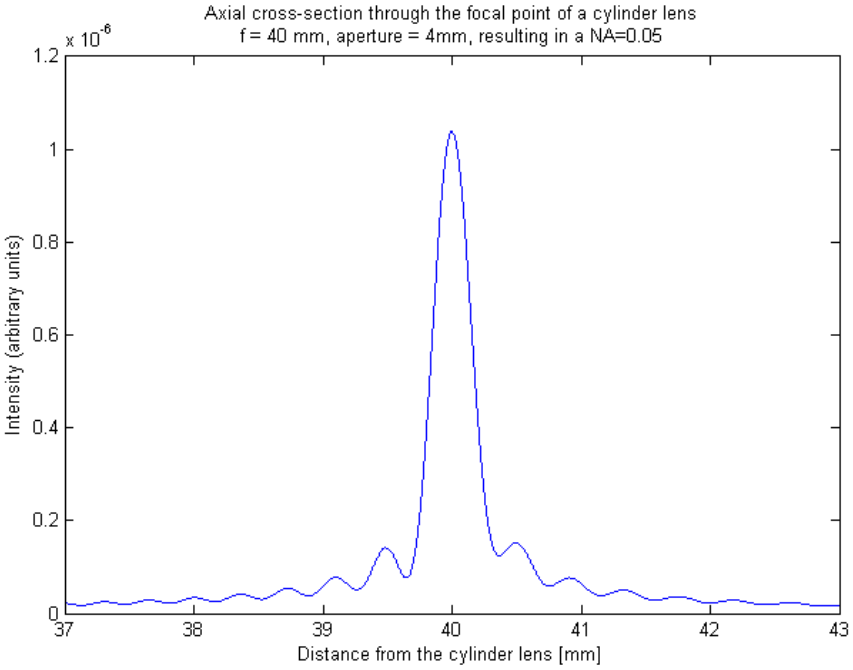

Figure 27: numerical simulation of the intensity-cross-section through the focus spot in axial (depth) direction. The shape is similar to the shape of the cross-section in xy-direction, and is characterized by a main maximum, surrounded by several secondary maxima. We can also apply the resolution criterion of Rayleigh to measure the depth-resolution. This criterion states a resolution value equal to the distance from the maximum to the first minimum.

The last figure displays the cross-section of the intensity in axial (depth-) direction through a focus spot of a cylindrical lens. The shape is similar to a xy-cross-section (an Airy-disk), with secondary maxima on the sides. When we have two focus spots, caused by a different divergence in X- and Y-direction, this should result in an overlay of two such functions with different locations of the main maxima. (To be precise, the square of the multiplicative overlay of the EM-field. Irradiance, also named intensity, is the square of the electrical field. The intensity determines the interaction, not the electrical field. I model different intensity distributions, dependent on different distances of the focus spots, by a multiplicative overlay). I made a numerical simulation of this behavior and display the result in the next figure.

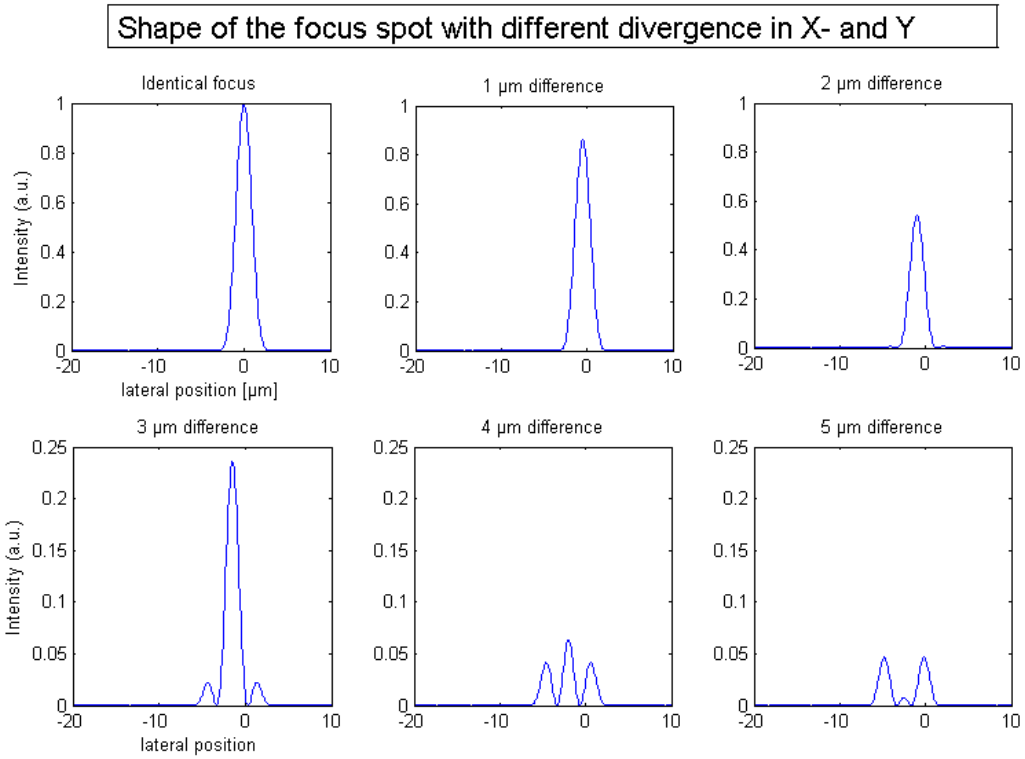

Figure 28: Theoretical simulation of the axial cross-section of the focus spot of a beam with different divergences in X- and Y direction. I simulated the overlay by a multiplication of two axial cross-sections (fig 27), and moved one cross-section by steps of 1µm. The absolute intensity declines, but this is moderate (only one magnitude). This can be easily compensated by an increase of the laser power. The beam shape is still acceptable, when the two focal distances do not differ more than the depth-resolution of the objective lens (in this case 3µm). After this value, the focus spot deteriorates severely.

I modeled the cross-section with a $(\sin(x)/x)^2$ function with a resolution value of $2n\lambda/NA^2$, according to the shape of an axial cross-section through the illumination beam, focused by a normal objective lens (Amos, 1995; Keller, 1995; Leischner et al., 2009). The formula $2n\lambda/NA^2$ predicts the resolution according to the Rayleigh-criterion, hence the distance from the main maximum to the first minimum of the cross-section (figure 27). To calculate the value predicted by the formula $2n\lambda/NA^2$, I used the values of a 40x Nikon objective lens for water immersion (NA 0.8), a lens that is used very often in this lab. This results in an axial resolution of about 3.3 µm. (I might make an error when I simply multiply two such irradiance functions. Maybe this results in the square of the needed function. However, this would only affect the absolute intensity, but this value is normalized. The decline might be less severe, but it has no effect on the lateral location of the secondary maxima. But even when this is an error, the diagram still visualizes the shape of the cross-section, and how much the secondary maxima will contribute to the illumination. However, as 2p effect is quadratic dependent on the illumination intensity, this diagram would then not display the intensity-cross-section, but the 2p-efficiency cross-section)

Figure 28 displays the effect of a different focal distance due to a different dispersion in X- and in Y-direction. When both focal distances are not exactly the same, this is tolerated to some extent, but the amount of misalignment should not exceed the axial resolution. Beyond that value, the shape of the illumination beam severely degrades.

The knowledge of the dispersion is of importance for its compensation. I can control the dispersion in the x-direction very precisely by setting the scanning amplitude $\Delta f/\Delta t$ (the absolute scanning angle) per time. This predicts the cylindrical lens effect of the AOD, and hence the divergence in x-direction. Therefore the divergence in X can be well controlled and corrected.

Measurement of beam distortions, caused by the chirped acoustic grating

I made several approaches to measure and to optimize this cross-section. I wanted to check if the compensation is done at the optimum value, or if I can get a better compensation value. These measurements are also a good check for the overall adjustments of the microscope. If other values are not well adjusted, like the chromatic compensation, there is no optimum visible when I systematically vary the cylindrical lens effect and always use the same compensation lens. In the beginning I did not consider the differences in the acoustic speed of the TeO_2 crystals. With the wrong value for the acoustic speed, I assumed an optimum at a different value, and I could not confirm the optimum. To check if the calculations for the optimum compensation were right, a measurement must prove an optimum alignment.

The first approach was a direct measurement with fluorescent beads of a small size, smaller than the resolution of the microscope. An image of these beads directly displays the shape of the focus spot, and hence the PSF (point spread function). This is not the best way, because 2p imaging is highly bleaching at the focus spot. To perform such a measurement, I have to acquire a 3d stack of fluorescent beads of high quality. This requires a long averaging of each single image from the image z-stack. Because this procedure exposes the sample with 2p-illumination for a long time, the sample is strongly bleached after one recording procedure. This does not allow several measurements with different compensation values to investigate the optimum PSF from several measurements. There is even bleaching during one measurement, and hence an image of a bead does not correspond to the PSF.

In the next approach, I did not acquire a complete z-stack, but only one image for a very short time, to avoid bleaching. I can then modify the scan amplitude, and optimize for the fluorescence signal from the sample. When the fluorescence signal is strongest, the PSF should have the best shape and the 2p-efficiency is the best, and hence the compensation is best. I used pollen grains for this, strong fluorescent objects (Carolina Inc. USA). I could acquire several images of the same sample without a high bleaching. The brightest image should be at the optimum compensation value. However, the results were not comparable with this measurement procedure, because changing the compensation parameter also changes the focal plane. This results in an image of a different focal plane, hence the value is not comparable, because pollen grains have an internal structure and their fluorescence also varies.

Measuring the beam distortions of the focus spot is quite tricky, because the distortions are caused by the fast movements, hence I can not simply point the beam on a frog-device (frequency resolved optical grating) (Trebino et al., 1997). Additionally, we want to know the shape of the focus beam

under the microscope. As the objective lenses have a very low working distance (2mm), it is difficult to point the focus spot onto the detector target.

As bleaching is the major problem in the measurement of the PSF, I was thinking of using a non-bleaching process for such measurements. There is a different non-linear process, closely related to two-photon fluorescence absorption. It is called second-harmonic generation (SHG) (Boyd, 2008; Peterka et al., 2011). This effect makes use of special crystals with different optical properties along the different optical axis. In contrast to 2p-excitation, SHG generates a frequency of half the wavelength, hence it doubles the frequency. This physical process does not involve an excitation of a fluorescent dye, nor requires a relaxation to a meta-stable state. A fluorescence excitation is possibly damaging the fluorescent molecule, as an excitation could completely ionize the molecule. Another photo-damaging process is a dark-state relaxation without emission of a fluorescence photon, as the absorption energy is not radiated in this way, but converted into thermal energy (Min et al., 2009). This non-radiative decay just results in a heating of the dye. Such a heating would additionally contribute to dye damage. As SHG does not involve an excitation, all these damaging processes are absent, and SHG is a non-bleaching process.

SHG is a process of quadratic dependency of the electro-magnetic field. A suitable crystal for the generation of SHG-light is e.g. BBO (Beta Barium-Borate, beta-BaB_2O_4). It is a crystal with a non-inversion symmetric lattice, relatively cheap and not too hydroscopic. Non-hydroscopy is important for practical reasons, as I want to measure the beam shape after focusing with a normally used objective lens. Most of these lenses are built for water immersion, hence the contact medium to the crystal would be water. Such a measurement would be impossible with a hydroscopic crystal.

I then slightly modified the 2p microscope for the measurement, as shown in the next figure.

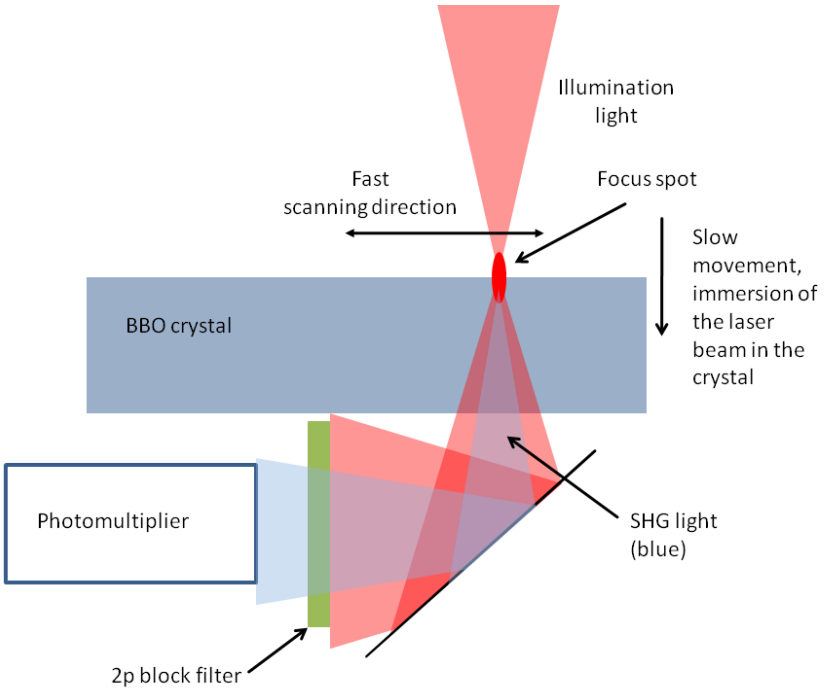

Figure 29. The measurement of the intensity-cross-section of the focus spot in depth-direction. I run the microscope with the high-speed imaging mode (320-1000 images per second) and slowly immerse the focus spot into the BBO crystal. Because the SHG-process is quadratic dependent on the intensity of the electro-magnetic field, only the focus spot contributes to the SHG light. The SHG-light is detected with a photomultiplier, after blocking the illumination light. I run the microscope with the normal programs for image z-stack acquisition. By analyzing the intensity of the image stack, I get an increase of the intensity, dependent on how much of the focus spot is immersed in the crystal. A derivation of this function should result in the beam shape along the z-axis.

I use the standard programs for z-stack acquisition, but place the PMT below the crystal (SHG is not isotropic emitting like fluorescence, but in the direction of the incoming light. Therefore I have to relocate the PMT). I then analyze the z-stacks and plot the intensity versus the location. I present the result in the following diagram.

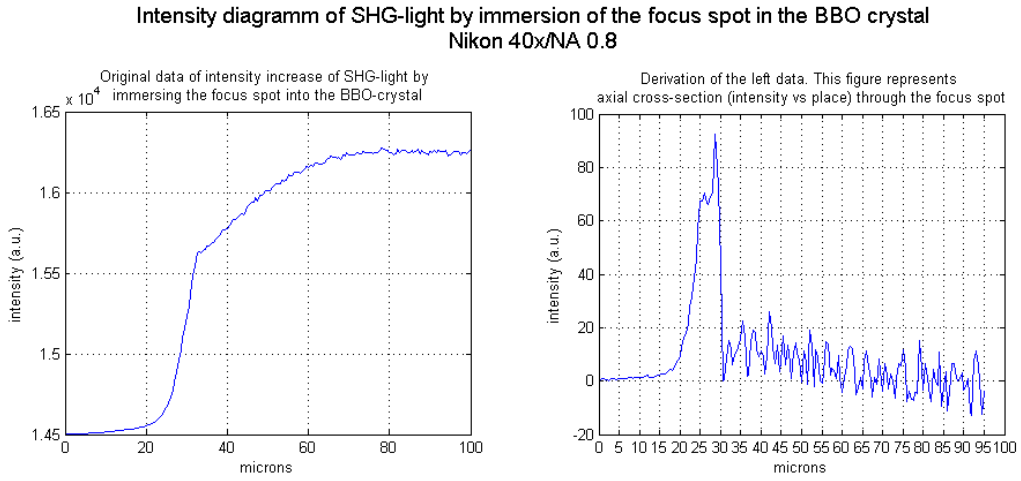

Figure 30: Intensity versus the location of the focus spot during immersion of the spot into the BBO crystal. The SHG intensity increases when the focus spot is immersing into the BBO crystal. The right diagram displays the derivation of the left diagram. Mathematically, this should display the cross-section of the fluorescent spot.

The first data were quite promising, although the trace is quite noisy when the focus spot is moving inside the crystal. The width (full-width-half-maximum, FWHM) is a bit too large. The value should be about 3.3 µm, predicted by the formula $2n\lambda/NA^2$ (Amos, 1995; Keller, 1995; Leischner et al., 2009). The measured value is about 6µm. However, this could be due to the non-optimum compensation of the cylindrical lens effect, resulting in an increase of the depth-resolution or two maxima. The two maxima could be a hint for the non-optimum compensation. Another explanation could be interferences at the surface of the BBO crystal. However, using a different objective lens showed that this measurement procedure is not suited to detect the shape of the focus spot. I will now present a measurement with the Zeiss 63x NA 1.0 objective lens.

Measurement of the axial cross-section of the focus spot by immersion in a BBO crystal.

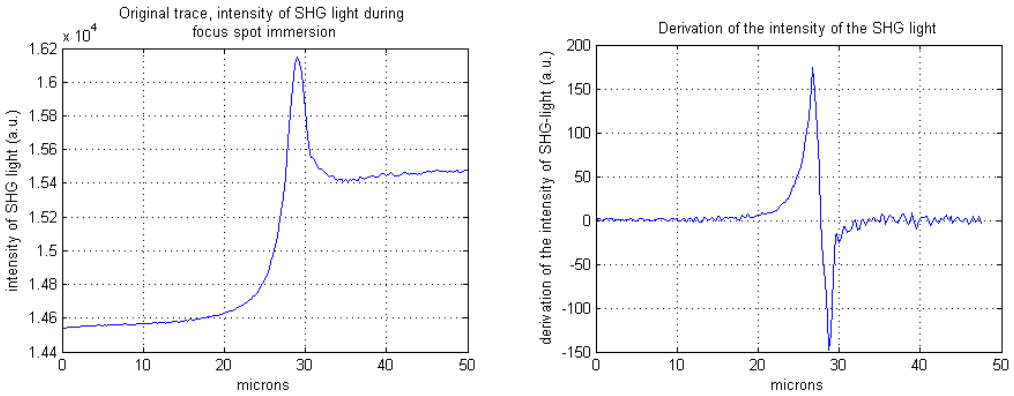

Figure 31. Intensity versus the position of the focus spot during immersion of the focus spot in the BBO crystal, using a Zeiss 63x lens (NA: 1.0). The intensity increases, but then drops again to about 50% of the maximum value. This can be due to interferences, wrong wave-front orientation or other effects like the "walk-off" of the BBO-crystal, or surface-generated SHG. These strange traces just demonstrate that such a measurement procedure is not suited for measurements of the axial component of the point-spread function.

The intensity increases, when the focus spot is immersing into the BBO crystal, but then decreases again, to about 50% of the maximum value. This should not happen when the SHG-effect is only present in the BBO-crystal. Maybe the SHG light has two origins, one from surface-SHG effects and the other from BBO-generated SHG-light. A derivation of this trace does not make sense. There are a number of other drawbacks when I want to use a BBO-crystal for this measurement:

- The generation of SHG-light is preferred in certain angles. This results in a "walk-off" pattern behind the crystal, and some additional interferences.
- The crystal axis of the BBO must be oriented in a precision of one degree to the polarization angle of the illumination light.
- We could get rid of the "walk off" pattern by taking a different SHG crystal. Most of them are temperature-matched, and then easier to handle as they don't show an emission of SHG-light with the walk-off pattern. But most SHG crystals are hydrophilic. This effect is moderate with BBO, but possible complications could arise during long measurements. The objective lenses are optimized for water as contact medium, hence we must drop a bit water on the BBO crystal. With different SHG crystal, this could cause problems, as they might be more hydrophilic.
- The crystal had an antireflection-coating for 800nm, but this coating is optimized for the contact medium air. With water as contact medium, the coating is no longer optimal.
- BBO is not best suited for this measurement, because of the "walk-off" effects. Other crystals do not show this "walk-off" phenomena, but they require a temperature-matching procedure. In that case, the SHG-effect is maximal at a predefined temperature. This requires a heating of the crystal to a predefined temperature. I can not do such a procedure in this biology-oriented lab, as I don't have the equipment for this.

- SHG needs parallel wave fronts of the light. In a focused beam, the wave fronts are parallel at the focal spot in a depth that is equal the confocal parameter. In a well-focused beam, this is a prerequisite for SH-generation. When we have a distorted beam, the wave fronts are no longer parallel at the focus spot. This then would prohibit the SH-generation, and hence I could not measure such a distorted focus spot.

It would be an option to replace the SHG-crystal with a different material that does not generate the bulk SHG-light. In this case I would only get the surface SHG. The other material could be just any transparent material with a high refractive index. SHG needs a non-symmetric medium. This effect also occurs at interfaces between two media (Brevet and Girault, 1996; Shen, 1989), as this is a natural brake in the symmetry of the material. However, I would assume SHG-processes do not occur only at the border, but also on some distance from it, as in the case of 'total internal reflection microscopy'. This is a special technique to illuminate a thin area close to the surface of a glass object holder. The thickness of illumination occurs within a thickness of one wavelength from the border. This would be about 800nm around the surface in our case. As the axial diameter is about 3 µm, I would then have to deconvolve the trace with the contributing surface diameter. I think this will be quite difficult.

I could change to other materials, or use nanocrystals as test objects (Chia-Lung et al., 2009; Hsieh et al., 2009). Or I could change to quantum-dots as test samples (Larson et al., 2003). However, I found a different way for optimizing the 2p-efficiency, and hence determine the optimum compensation parameter. I will explain this in the next section.

The last approach resulted in acceptable results. I combined two methods, measuring the image intensity of pollen grains, and acquired a 3d image stack in a fast way to avoid bleaching. I avoid the problem of the change of the working distance by acquiring complete z-stacks of the pollen grain.

To analyze the 3d-stacks, I marked regions of interest (ROI), computed the average intensity of the ROI of each image, and plotted the intensity versus the slice position. The optimum compensation parameter is the one with the brightest signal amplitude. I can find the optimum scanning amplitude with this method. The intensity-plot of the cross-section is brightest, when the cylindrical compensation lens is about the value of the cylindrical lens effect (with the opposite sign). The maximum is relatively broad. A difference of about 50-100mm of the focal lens does not affect the absolute value of the maximum. The measurement is shown in the next figure.

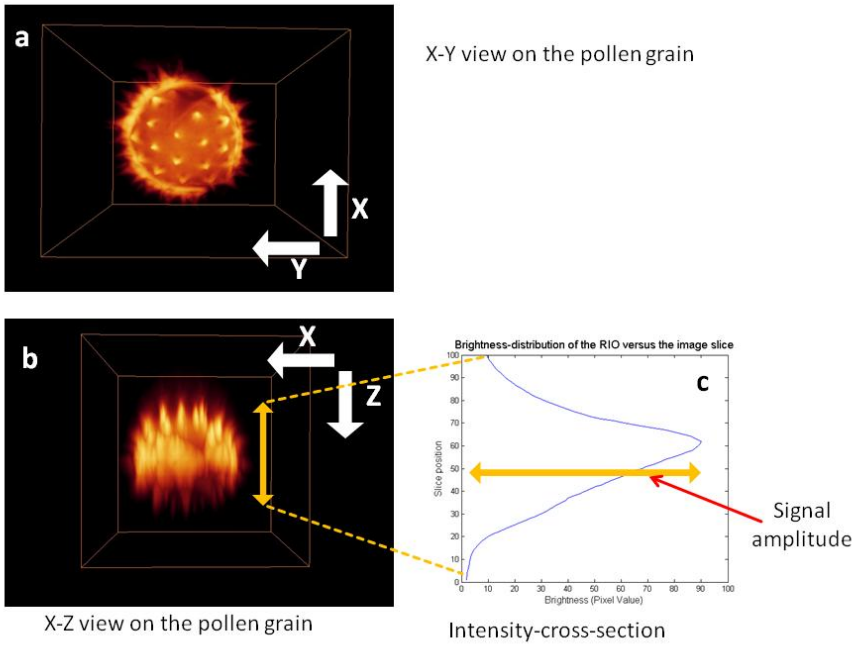

Figure 32: Principle of measurement of the 2p-efficiency with different compensation values. a: X-Y view on an image z-stack of a pollen grain. b: X-Z-view. We analyze the distribution of the brightness of a ROI through the pollen grain and plot it in c (intensity vs. position). From this graph we analyze the signal amplitude. In the next graph I display the signal amplitude for different z-stacks, acquired with different line-scan amplitudes, resulting in different cylindrical lens effects of the AOD.

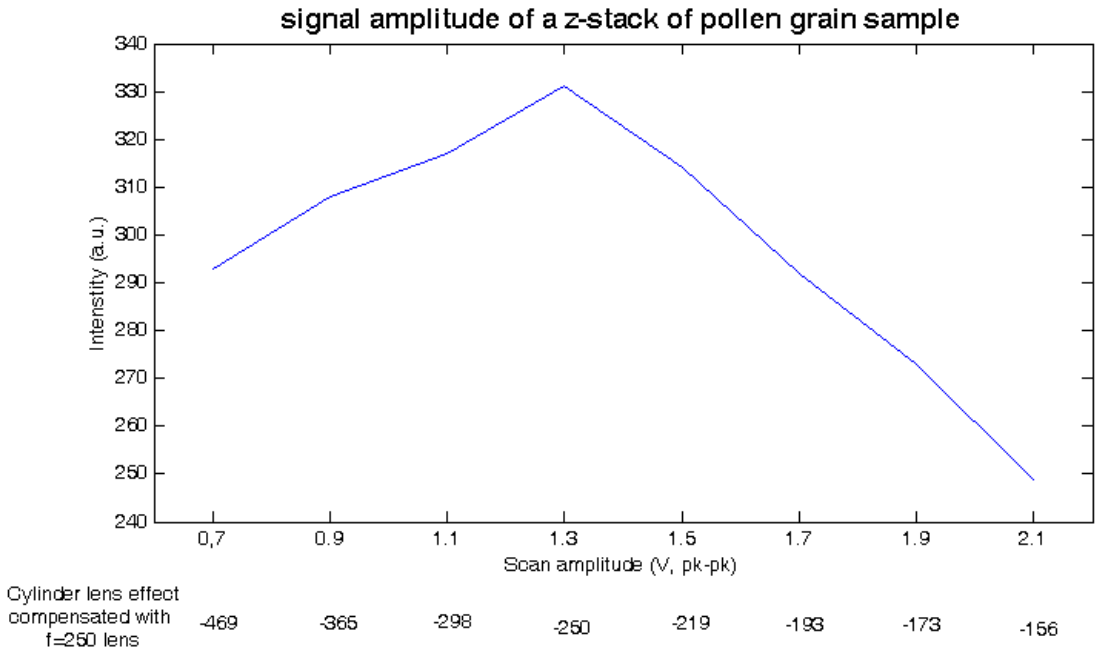

Figure 33: By varying the scan amplitude, hence the value of the focal length of the cylindrical lens effect, we can modify the beam distortion. We compensated the beam distortion with a f=250mm lens. The image is brightest, when the cylindrical lens effect matches with the compensation lens. In this way the beam distortions are best corrected, hence the two-photon efficiency is highest.

The construction of different scanning systems

I build several scanning systems and investigated the different properties, advantages and disadvantages. We did not optimize each system or make a lot of measurements with it, when we saw that a different system was more promising. I will just list all systems in chronological order and discuss the advantages and disadvantages.

The first AOD-based scanning system with two AODs for x- and y scanning and a two-prism correction for the chromatic dispersion

In a first version I built a system with two AODs for scanning in the x- and the y-axis. I compensated the chromatic dispersion with a prism. The chromatic dispersion can be compensated for both AODs with only one prism. In this case, the prism must be oriented in a 45° and give a chromatic dispersion of $\sqrt{2} \cdot chrD$. (chrD being the chromatic dispersion caused by one AOD) (Zeng et al., 2006). This would require an irradiance of the prism with a 3d angle from somewhere diagonally in space. I think such a setup would be quite complicated. I thought it would be easier to adjust the chromatic dispersion for the x- and the y-AOD with two different prisms independently, as this allows for the use of standard components for optical tables and we do not need a custom made prism holder. With a periscope-optics I can easily rotate the beam by 90°, and hence can use identical optical elements for creating the chromatic dispersion in the other direction, to compensate for the chromatic dispersion of the other AOD. This was the fastest way to test this compensation scheme. I demonstrate the resulting image quality in figure 34.

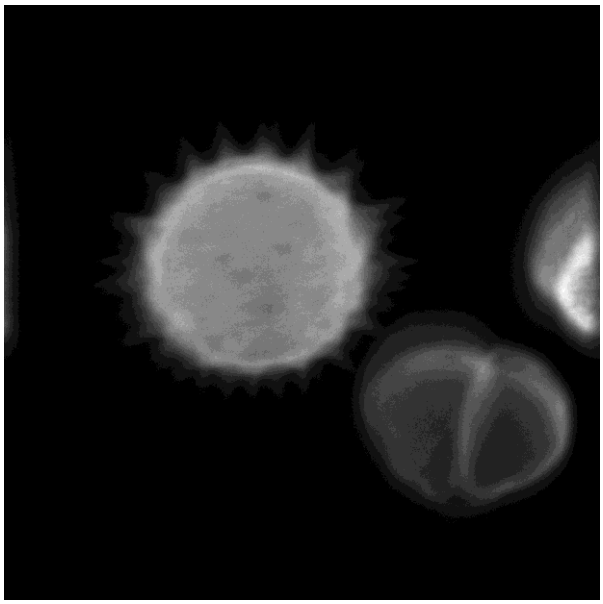

Figure 34, average image(1000 Frames) of a pollen grain, recorded with the two-AOD system. I compensated the chromatic compensation with two prisms, one for each scanning axis. Image dimensions are 1000 x 1000 pixel, acquired with 20 images per second, hence I did not need a cylindrical lens compensation for this image frequency.

The first results were quite fine, hence the calculated dispersion effects of a prism are correct (see appendix, Calculation of the chromatic dispersion of a prism).

In the next step, I wanted to optimize the group velocity dispersion (GVD) by adjusting the prechirper. This can be done by changing the prechirp-value during continuous image acquisition, and monitor the fluorescence brightness. The optimum compensation value is the position of maximum brightness and highest signal amplitude, because there the two-photon effect is best.

During this optimization I did not find a clear optimum. I changed the GVD through a large parameter range, but no optimum was visible. The GVD was non-homogeneous throughout the laser beam, because the light travels through different distances of glass in the prism (figure 13). Therefore I could not compensate the non-homogeneous GVD-value with a standard pre-chirper. This effect is more pronounced with a large laser beam. Beam enlargements are beneficial for imaging quality (figure 22), but they result in a longer fly-back time of the AOD. Additionally, large beams also result in a non-homogeneous GVD when a prism is used for compensating the chromatic dispersion. Therefore, we exchanged the two prisms by one AOD for compensating the chromatic dispersion.

Improvement of the two-AOD scanning system with one AOD for compensating the chromatic dispersion

My first scanning system was using two AODs for scanning in x- and y-direction, and used two prisms to correct the chromatic dispersion of each AOD. I used a Spectra-Physics Mai Tai Deep See laser, equipped with an additional prechirping device that allows for a change the GVD-value very easily. When I modified the GVD-value, I could not optimize it to maximum image brightness. This was a

hint to the non-homogeneous GVD throughout the x-y direction of the laser pulse (the z-direction is the direction of propagation of the laser pulse).

Using an AOD for compensation has a major advantage. AODs are of the same thickness everywhere, hence I would get a homogeneous GVD (Salome et al., 2006), (figure 13). Prisms are very cheap, around 100 Euro. AODs are more expensive, about 2000 - 5000 Euro. I therefore used just one AOD in an orientation of 45°. This creates a chromatic compensation for both axes at the same time.

A scanning system using one AOD for fast line-scanning, and a galvanometric mirror for slow y-scan, together with an AOD for compensating the chromatic dispersion.

It is quite complicated to compensate for the chromatic dispersion by using an AOD with an orientation of 45°. The main difficulty is to align all the AODs, as they have to be irradiated with the Bragg-angle, and the output angle must point to the wanted direction. Additionally, every AOD has a maximum deflection efficiency of about 80%. By using three AODs, we end up having only half of the laser power originally available. Therefore, we want to minimize the use of AODs. Additionally, as we are planning to perform a raster scan and acquire real image data, we do not need the extreme scanning frequencies for the slow axis. It is sufficient for us to reach the kHz range, and scanning with 1000-2000 images per second is enough. This can be achieved with galvanic mirrors. The fastest mirrors can oscillate with up to 2000 Hz in the sawtooth-mode. This makes them suited for our application. Therefore, we decided to build a system with one galvanic mirror for the slow Y-scan, and one AOD for the fast line scan. We compensate for the chromatic dispersion with one identical AOD upstream the scanning AOD. Such a system is able to deliver more light to the probe (as we only use two AODs instead of three), and is easier to align, as I do not need to orient one AOD at 45° orientation, nor do I have to irradiate it from some 3d-solid angle.

Additionally, the compensation of the chromatic dispersion is only possible for one precise deflection angle. When I deflect the beam in a different angle, the compensation is no longer perfect and image distortions will occur. Therefore replacing one AOD by a mirror increases the image quality along the axis that is now controlled by the mirror.

Miesenböck and his lab built a microscope with highest similarity to our instrument (Roorda et al., 2004). For chromatic dispersion they used a prism. We replaced the prism by an AOD (Salome et al., 2006), as an AOD results in a homogeneous GVD throughout the X-Y dimensions of the laser beam. Additionally, we inserted cylindrical lenses to compensate the cylindrical lens effect of the AOD. This allows now for a fast raster scanning. Our apparatus does not allow for a random access scanning procedure, as the cylindrical lens compensation principle requires a constantly moving beam focus.

We requested a galvanic mirror with the highest possible frequency. This allows for scanning frequencies with up to 2000 Hz, even when the mirror is controlled by a saw-tooth signal, a one-directional line-scan pattern. The fly-back time of this fast mirror is in the range of 20-30% of the entire line-scan time, hence the border consists of 10-15 % of the image size on each side. This is acceptable, and the center image is large enough for measurements.

This configuration made images with good image quality, and we could acquire the images with a high speed. Therefore, we started a number of measurements with this configuration.

The advantages of the AODs from CTI Inc., compared to the products from AA-Optoeletronics

The microscope with one mirror for the slow Y-scan and an AOD for the fast X-scan has been used daily for about one year for routine-measurements. I think a configuration with one galvanic mirror for Y-scan, an AOD for the fast line-scan, and an AOD for the chromatic compensation is the best configuration. Additionally, the AODs from Crystal Technology Inc. (CTI) have several advantages, compared to AODs from the company AA-Optoelectronics.

Firstly, CTI Inc. uses different types of TeO_2 crystals for their AODs. They have a slightly higher acoustic velocity (820m/s vs 620 m/s from AA Optoelectronics). This results in a lower fly-back time, hence these AODs are about 30% faster. Additionally, they only have an active aperture of appropriately 2mm. This decreases the number of resolvable points, but also reduces the fly-back time. This results in a very short fly-back time, in practice below 1µs. The cylindrical lens effect is of quadratic dependency of the acoustic velocity ($f = v^2/(\lambda\ (\Delta f/\Delta t))$), therefore a higher acoustic speed results nonlinear in a longer focal length of the cylindrical lens effect, and therefore less beam distortions. This allows for scanning one line with about 6µs and with up to 160 000 lines/second. We can run the microscope with 1600 images/second with an image size of 100 lines x 125 columns. Because the fly-back time is that short, it affects only about 10-15 pixels on each side of the image. This results in a very useful image size for the investigation of the Calcium-signal on dendrites and spines.

The second advantage is the extremely high scanning angle of 102 mrad, resulting in a large field of view. We need a relatively large field of view when we are searching for a suited cell and patch it. The AOD from CTI (CTI 4150) is characterized by an extremely large scanning angle, more than 100 mrad. This is twice as much as the AODs from AA- Optoelectronic.

The smaller aperture requires the use of a smaller laser beam diameter. This then requires a scan lens with a shorter focal length. I will now explain this relationship: We can measure the absolute magnification of the microscope by placing 1µm fluorescent beads under the microscope, and determine the diameter of the bead in the image plane. For this measurement we just remount the CCD-camera, acquire an image of a fluorescent bead and determine its size in the image by simply counting the number of pixels. By looking at the data sheet of the CCD, we can determine the pixel size and hence conclude to the size of the image of the bead in the image plane. In practice, a 1µm fluorescent bead will generate a spot of ~35 µm diameter on the CCD chip, covering about 6 pixel with a 6µm pixel size (Using a 40x Nikon objective lens and an Olympus tube lens).

We project an illumination spot with the scanner on the image plane. This spot of light must not be larger than the image of a bead of minimum resolution. If it would be larger, this would result in a larger illumination spot at the sample, and would reduce the overall resolution and worse image quality. When I know the absolute magnification, I can determine the maximum focus spot of the illumination beam in the image plane. The size of the illumination spot in the image plane can be

determined with the Abbe-formula $\Delta x = \lambda/(2\ NA)$. The numerical aperture is in this case $NA = d/2f$, with d: laser beam diameter and f the focal length of the scan lens. This results in a spot size of the illumination laser of $\Delta x = \lambda f/d$. A smaller beam diameter thus requires a shorter focal length of the scan lens. But as we have an AOD with a larger scanning angle, this allows for a reduction of the focal length of the scan lens (the focal length of the scan lens is linear related with the field of view).

In conclusion, the smaller beam diameter does not affect the field of view because this can be compensated by a scan lens with shorter focal distance. This then results in a smaller field of view, but this is not critical because the AOD from Crystal Technology are of an extreme large scanning angle (twice as much as the devices from AA-Optoelectronics). A smaller beam diameter also results in a lower number of resolvable points, hence a lower resolution. This is also not problematic, as we use this apparatus for scanning a small field of view with high speed and small image dimension (about 200 x 100 pixel). The smaller beam diameter is also advantageous for the cylindrical lens compensation. A smaller beam passes more through the center of the cylindrical lens, hence we minimize spherical aberrations at this lens. All these properties of the AOD from CTI make it quite useful for 2p-scanning purposes, and additionally the fly-back time is extremely short, about 1µs. This allows for a line scan time of about 6µs, and I can easily reach scanning rates above 1000 images per second.

Thee-dimensional scanning

Extension for three-dimensional raster scan with video-rate

Imaging with frequencies between 300 to 1000 Hz is in-between the standard requirements, as measurements of the membrane potential with voltage-sensitive dyes would require a bit higher frame rate (around 2000Hz), and measurements with calcium-indicators only require an image speed of about video rate. Additionally, as no two-photon microscope with such high frame rates is available until now, we lack suited voltage-sensitive dyes for two-photon excitation. The standard calcium-indicator dyes are of a quite high affinity, hence the half-life of such a calcium-transient is in the range of 200ms for dendrites and 100ms for spines for the calcium indicator Oregon Green (Cornelisse et al., 2007; Schmidt et al., 2003). We do not really need sampling frequencies with up to 1000 Hz for such slow signals. Therefore we made some efforts to use the additional scanning rates to extend the data acquisition to the third dimension.

A short example will demonstrate the possible potential. When we acquire the images with 500 images per second, we could use 50 images for each z-stack. In this way we could acquire 10 volumes within 1 second. This sampling rate would be sufficient for the slow calcium-signal in a dendrite or the soma of a nerve cell. The X-Y image dimensions are about 100 x 70 µm, using a standard 40x objective lens. The depth resolution of such an objective lens is 3.2 µm, hence the required distance between two image planes of the z-stack according to the Nyquist sampling rate is 1,6 µm. This would result in a three-dimensional volume of 100 µm x 70 µm in X-Y and a depth of 80 µm. This sounds very promising and would allow for volumetric imaging of a sufficiently large volume.

The drawbacks are mainly technical. Movements of the objective lens are mainly performed with a positioning device using piezo crystals. These crystals change their length when we apply a voltage potential. There are only three vendors of such devices: Physik Instrumente, Piezo Jena and an American company called Mad City Labs. The objective lens must be highly stable during the

movements and may not tilt. Even the smallest tilts of some µm are visible in the images, as we have a resolution below one µm.

The vibrations or movements of the objective lens are quite fast, above 100 Hz. They are only visible with imaging in the raster-scan mode and with image frequencies above 100 Hz. This artifact is not visible with standard two-photon microscopes with their slow image acquisition rates.

A test of the products of the three vendors displayed a clear ranking: The products of Piezo-Jena are not stable enough and result in image distortions of several µm. They are useless for fast movements of the objective lens. Three-dimensional imaging with video-rate can not be done with these devices. The devices from Physik Instrumente are better, but movements of some µm are still visible in the images. This can be ignored for investigations on large objects like the somata of cells. Such a device can be used for such an application, but the stability is not sufficient for investigations on small objects like dendrites or spines. The devices from Mad City Labs displayed the best stability. They are of acceptable quality for these investigations.

The vibrations are also dependent on the form of the command-signal for the depth-movement. I tried several types of signals: a saw tooth signal with sharp edges, a saw tooth signal with rounded edges, a triangle signal with sharp and rounded edges and a sine-wave. A saw tooth signal is characterized by a relatively constant movement, followed by a fast jump back to the starting position. This fast jump back to the starting position always resulted in vibrations of the microscope, independent whether the command signal is with a sharp edge or with a rounded edge. A triangle wave as command signal results in a constant movement of the objective lens, followed by a fast change of the direction of the movement and then a constant movement in the opposite direction. The vibrations are much less, as the needed power for changing the direction is much less than the power needed for a jump back to the staring position. The best command-signal is a sine-wave, as there the forces for a change of the direction of the movements are lowest, but in this case there is no longer a constant movement of the objective lens. This results in a non-homogeneous spacing of the images of the z-stack, and hence in distortions of the image data. This could be corrected by methods of image processing, but an additional post-processing step would complicate the data analysis.

When using a piezo-positioning device for z-scan, I recommend a triangle wave with rounded edges as command signal for three-dimensional scanning. This avoids image distortions during the time of constant movement, and it does not induce large vibrations.

Scanning in the depth-direction by using an electrical tunable lens

There is one other possibility of a z-scan. When the illumination beam of the back-aperture is of a different divergence, this results in a different working distance. I visualize this in the next figure.

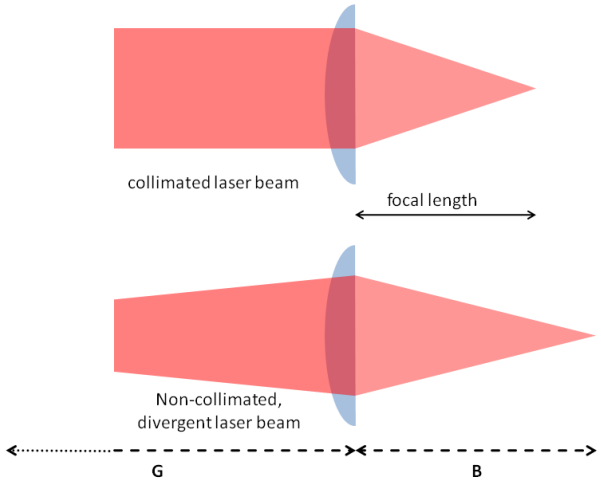

Figure 35. When the illumination beam is collimated, the focus spot is in focal distance from the lens. When the beam is divergent, i.e. it is slightly focused or defocused, the focus spot is located at a different distance from the lens. This can be used for changing the working-distance of the objective lens. When we can control the divergence of the illumination beam, we can control the depth of imaging, and hence can make a scan of the image in the depth-direction without moving any part of the microscope.

There is an interesting new product that allows for a change of the divergence of the beam. It is called a tunable electrical lens from the company Optotune. It consists of two liquids, and the border between the two liquids is of a curved shape. The curvature radius can be changed by current application. The curvature changes according to the amount of current (mA) that flows through the lens. I do not know the exact mechanism, but I think it is a magnetic effect, as the lens is a bit magnetic itself, and the curvature radius is dependent on the amount of current flowing through the lens. I assume one of the liquids is magnetic, and with a change of the magnetic field, one liquid is pressed stronger in one direction, and hence there is a change in the radius of curvature. The lens allows for changing the value of focal distance in the range of 55mm-130mm by the application of current in the range of 0-400mA.

It is easy to change the divergence of the illumination beam with this lens. We just need to place it above the back-aperture of the objective lens. I use a combination of two lenses, to change the divergence to positive and negative values. I visualize the arrangement of the two lenses in the next figure.

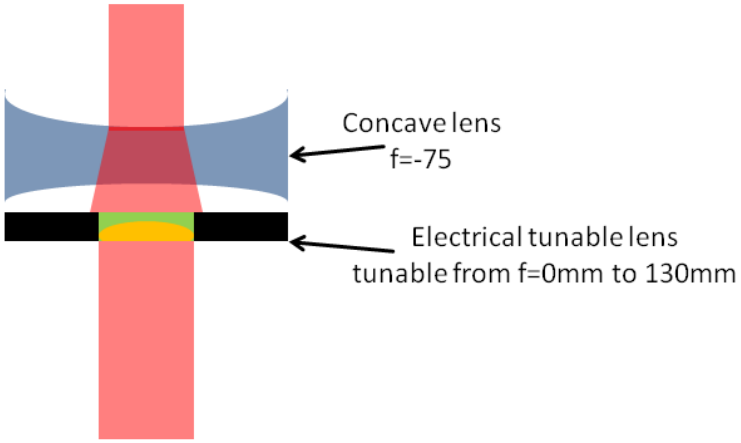

Figure 36, Principle of changing the divergence with an electrical tunable lens. The illumination light passes first through a non-tunable concave lens (f=-75mm). This lens creates a beam-widening. When the electrical lens is set to a focal value of f=75 mm, the divergence from the concave lens is counterbalanced and the beam is collimated again. By changing the focal distance of the electrical lens, I can control the amount of divergence of the illumination beam, and hence the distance of the focal plane from the objective lens.

I placed such a lens system above the objective lens, adjusted the electrical lens to a value of 75mm and started imaging. The first results were very promising. By changing the focal distance of the electric lens, I could change the depth of the focal plane. I was able to vary the depth of the image plane in the range of 100µm. This is a very promising range and would allow for quite a lot of interesting measurements. I did not see a change in the image quality. The signal amplitude was a bit lower, but the spines of pollen grains still looked as long as in the previous imaging apparatus.

The lens should be very fast, according to the data sheet. It should be possible to change the depth of the image plane within less than 10ms, and a continuous scan with a sawtooth-signal should be possible with up to 100Hz. This allows for much higher z-scanning rates than would be achievable with piezo-positioning devices. And these scanning should not induce vibrations at the microscope.

However, there is one drawback. The fluorescent emission would have to pass the electric lens on the way to the photomultiplier that is located at the filter-wheel of the microscope. As the transmission of this additional lens system is not perfect, some photons are absorbed. This results in a lower signal amplitude. A first measurement resulted in a decline in the signal-to-noise ratio of 30-40%. Two-photon microscopy always loses many photons due to scattering, and these photons are not able to reach the detector. (A CCD-chip of a camera can integrate typically about 10 000 photon-generated electrons per pixel, while 2p-imaging detects about 10-100 photons per pixel) An additional decline of the signal amplitude by 40% would severely degrade the signal quality. Therefore, we decided to attach the PMT at a different position. I visualize the setup in the next figure.

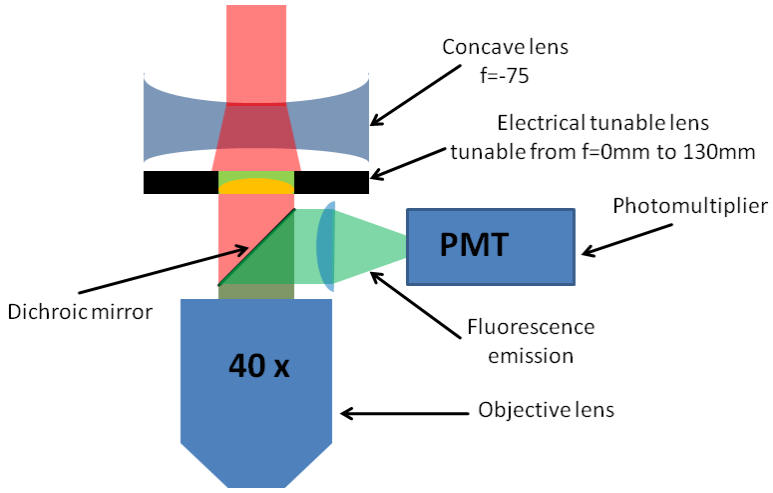

Figure 37. The improved version for inserting the electrical lens for z-scanning. The electric lens was mounted a bit higher, leaving enough space between the objective lens for the dichroic mirror. This layout is advantageous, because the fluorescence emission does not need to pass through the lenses before reaching the detector, hence we avoid absorption losses and can detect more photons. The disadvantage is the larger distance from the back-aperture of the objective lens. When the microscope is not perfectly aligned, the illumination light is approaching the objective not perpendicular, but slightly tilted. In this case we would not fully illuminate the back-aperture of the objective lens. The diameter of the electric lens is 11mm. The diameter of the back-aperture of objective lenses is typically about 8-11mm. This configuration requires a well-aligned beam path, as tilted illumination beams would not fully illuminate the back-aperture of the objective lens.

We insert the dichroic mirror right after the objective lens in this configuration, and prior to the electrical tunable lens system. With this layout, we can capture most of the fluorescence photons and do not suffer from absorption losses by the z-scanning lens system.

This z-scanning system has major advantages. Firstly, placing the dichroic mirror and the PMT directly behind the objective lens should capture more photons, compared to a layout where the PMT is mounted at the filter wheel, quite far away from the back-aperture. Secondly, I do not move the objective lens mechanically, and hence I do not induce any vibrations in the imaging apparatus. These vibrations cause tilts of the objective lens, and hence displacements of the object in the image. These displacements would have to be corrected, and prevent a high image quality at high z-scanning frequencies. Finally, such a system can scan in the depth-direction much faster. A higher scanning speed is the most important advantage. According to the vendor of the electric lens, we should be able to scan the z-direction with up to 100 Hz. A similar z-scanning approach (Gobel and Helmchen, 2007) using a piezo-scanner for z-scans results in z-scan frequencies theoretically up to 20Hz. In practice Göbel used maximally 10 Hz, and most measurements were done at 4Hz. This is an increase of 10-50. This is in agreement with my personal experience with the piezo-devices for z-scanning. The speed of these instruments is very limited. These devices can scan the object with 10Hz, but this is

not sufficient to detect weak signals from small compartments of cells (like dendrites and spines) in noisy image data. A higher image frequency is very helpful, as this allows for the application of image filters to deal with the high noise amplitudes.

The new scanning mode theoretically increases the signal-to-noise ratio about one magnitude and additionally reduces photo-damage

A general problem arises when we scan with such high frequencies: Illumination with a pulsed high-energy two-photon laser results in a lot of bleaching and photo-damage at the illumination spot, much more than in one-photon processes such as confocal microscopy. In out-of-focus regions we have a decrease of photo-damage, but the focus region is illuminated with high intensities and there is more photo-damage than in one-photon microscopy. Scanning a section of the sample 1000 times per second instead of 30 times per second necessarily results in an increased bleaching and photo-damage. Therefore, we must decrease the illumination intensity.

Decreasing the illumination intensity is highly interesting, because it is known that photo-damage is non-linear dependent on the illumination intensity. The generation of fluorescence in 2p microscopy increases with the power of 2 of the illumination intensity, but photo-damage increases with the power of 2.5 (Hopt and Neher, 2001), and bleaching increases with an even higher exponent of 3 (Patterson and Piston, 2000). Therefore, increasing the laser intensity to increase the signal amplitude is only successful to a certain level of laser power. As photo-damage and bleaching increases even faster, measurements are impossible with highest illumination intensity. One way to overcome this problem is increasing the pulse-rate of the laser and a simultaneous reduction of the laser intensity (Ji et al., 2008). The lower laser intensity is equalized by a higher pulse repetition rate with this approach, hence the overall signal amplitude is maintained, but the acquisition procedure is accompanied with less photo-damage.

In principle I do the same as in the publication of Ji and Betzig (Ji et al., 2008). I decrease the laser power and simultaneously increase the number of laser pulses hitting one point of the sample, but I do this by increasing the image frequency, not by an increase of the laser pulse frequency. A measurement of the laser power showed that the AOD-system needs only half of the laser power of the resonance-scanner based 2p-microscope. I will now compare the illumination time and intensity with that other microscope in this lab, a resonant-mirror based two-photon microscope, optimized for 30Hz image frequency and a larger field of view. The absolute increase in photon-gathering time per position of the sample is a bit more complicated, as the new electronics increases the pixel frequency to 20 MHz, a dwell time of 50ns, and we increase the image frequency to 1000 Hz, and decrease the pixel size. The pixel frequency of 20MHz is a factor of 2 faster than at the system based on a frame-grabber and resonant mirror. On the other side, a pixel in the AOD-system is 35 nm large, much smaller than the PSF or the predicted Nyquist sampling rates. Therefore, the fluorescence signal from one point is distributed over several pixels.

It is helpful for the discussion to make new definitions. The natural approach would be a comparison of the pixel dwell time with the photo damage, but dwell time is a bit unlucky definition because it denotes the speed of the internal clock of the electronics, and this is more or less an arbitrary

parameter, not linked to the exposure-time of a point of the sample to the laser beam. Therefore I use the definition called 'dwell-time per PSF'. This denotes the time of illumination of one point of the sample when the focus spot of the laser beam moves over it. A pixel can be up to 10 times smaller than the illumination spot (depending on the zoom factor), and therefore a pixel is 10x longer illuminated than the pixel dwell time. To calculate the 'dwell time per PSF', I need the diameter of the focus spot, and the moving speed of the focus spot in m/s. The diameter (FWHM) of the PSF in two-photon imaging is about $\frac{\lambda}{2 \cdot NA \cdot \sqrt{2}}$. (The Abbe distance between maximum of the Airy-disc and the first minimum is about the same size of the FWHM-diameter (Leischner et al., 2009), and due to the quadratic dependency of the two-photon effect, the focus spot is additionally sharpened by a factor of $\sqrt{2}$. This value is derived by the convolution theorem, stating that a convolution of two functions is equal to a multiplication of the two spectra in Fourier space, therefore the transfer-function of a squared sampling kernel is equal to a convolution of the transfer-function of the non-squared kernel with itself. Convolutions are used in statistics as adding random variables, and the standard-deviation of independent random variables can be added in this way (see page 11 formula (6) in (Leischner et al., 2009)). Therefore, the width (standard-deviation) of the transfer-function increases by a factor of $\sqrt{2}$, resulting in a decrease of the PSF of the same factor. This is more elaborately explained on page 10-12 in the one of my publications (Leischner et al., 2009). Using other resolution criteria like the support of the transfer function would result in an increase in resolution by a factor of 2, but I think $\sqrt{2}$ is a better description.)

The diameter of the PSF is about 0,35 µm (using 800nm and an objective lens with an NA of 0.8). The pixels are about 35nm large, hence the focus spot is illuminating about 10 Pixel simultaneously. I normally scan one line (250 Pixel, 10µm) in 12,5 µs, hence one point of the sample is being illuminated by the focus spot for 0,5µs when the focus spot is moving over it. As the illumination point also spreads over 10 lines in Y-direction, one point is being illuminated 5µs during the acquisition of one image. As I acquire 1000 images per second, I gather fluorescence information from one point of the sample for 5ms during one second imaging time (image parameters 250x80 Pixels x 1000 images per second).

I can now compare this value with the resonant scanner-based 2p-microscope. The resonant scanner acquires images with 31Hz, 482x400 pixel, with a field of view of 120µm x 120µm. We can also use a field of view with twice the size, but then the functional Ca^{2+} signals are of a bad quality. My colleagues mainly use image sizes of 120µm x 120µm here for functional imaging studies. The digitizer is working at 12MHz (some pixels are truncated at the border of the image). We mainly use the same objective lens (Nikon 40x, NA 0.8) as in the new AOD-based 2-photon scanner.

The speed of the focus spot on the sample differs only by a factor of 2. The resonance-scanner moves the focus spot with 120µm/80µs=1.5m/s over the sample (400lines*31Images/s = 12 400 lines/s, resulting in 80µs per line. The real speed is even higher, as the laser is modulated down with a Pockels-cell during the turning point of the resonance mirror), and the AOD-scanner moves the focus spot with 10µm/12.5µs = 0.8m/s (80 lines * 1000 images/s = 80 000 lines/s, resulting in 12.5µs/line). The pixels size in the resonance scanning system is 250nm, much larger than the 35nm of the AOD-based scanner. As the focus spot moves with twice the speed of the AOD-scanner, one point of the sample is only illuminated for 0.25µs during one line-scan. The diameter of the focus spot is only 2-3 pixel in the resonance-scanner. Therefore, one point is only illuminated 3 times during one image acquisition, resulting in 0.75µs illumination time per image. As the acquisition rate is 31 images/s, we

illuminate one point in the field of view for 23.5µs per second imaging time. This is much shorter illumination time than the AOD-based system. The difference is a factor of 210.

As we illuminate one point of the sample 210 times longer with the AOD-based scanning system, we must reduce the illumination intensity. I measured the differences in the illumination intensity in both systems. We use only half of the illumination intensity in the AOD-based scanning system. Therefore, as the two-photon efficiency is of a quadratic dependency, we get only ¼ of the fluorescence. As I illuminate one point of the sample 210 times longer, this results in a theoretical increase of the signal amplitude by a factor of 50. The new microscope acquires 50x more data, and we apply an averaging step to get a smoother signal trace with a better signal-to-noise ratio. The increase of the signal-to-noise ratio by averaging the same signal n-times results in an increased SNR of $\sqrt{n}$, in our case about 7. In brief: the procedure of temporal and spatial oversampling, followed by signal averaging, increases the SNR about one magnitude. This is a huge increase and explains why we can now clearly resolve weak signals from small compartments of cells, like the fluorescence signal from calcium-indicators in spines.

I can increase the signal-to-noise ratio about one magnitude, and this acquisition mode additionally reduces photo-damage. This can be seen as a major breakthrough.

This scanning mode has one more advantage. The focus spot is not placed for a long time on the same position, like in random-access-scan mode, but is moved fast over the sample. One point is illuminated for 0.5µs, corresponding to 40 laser pulses, and then is revisited after 12.5 µs during the next line-scan. This time is long enough for the relaxation of a triplet-state excited fluorophores. The relaxation time of a triplet-state excited fluorophore is about 1µs (Donnert et al., 2007). This short illumination time, combined with a fast revisiting of the same location, allows for an intensive observation of one location without photo-damage.

My colleague Xiaowei Chen summarized the advantages of my microscope from the point of view of an operator of the microscope: When we use a suited magnification for dendritic observations, we can record a signal with this apparatus for minutes, while on the other two-photon microscope based on resonance mirrors, we can normally look at a dendrite for only about 10-15 seconds. This allows for completely different investigation protocols: repeated stimulations, investigations of the spontaneous activity of a dendritic- or a spine-response, and the execution of time-consuming protocols involving the application of pharmacological drugs to block a certain type of ion channel, including the control measurement after wash-out.

Image processing: Correcting the movement artifact

There is one typical artifact that requires some image processing: The objects (cells, dendrites, blood vessels) of the in-vivo movie-observations are moving in an oscillating manner, caused by the pulsing blood flow. Blood vessels change their diameter and are moving according to the heart beat, hence the tissue nearby is also moving. These movements are normally in the range of 1-3 micrometers, hence with a low magnification or a low temporal resolution they are not visible. For observations of large objects, like the somata of pyramidal cells in the brain, they can be ignored, but for investigations on small segments of a cells, like dendrites or dendritic spines, a correction of the movement artifacts is a prerequisite, as these movements are in the range of the size of these structures. Without a correction we can not distinguish if the origin of a change of the fluorescence is caused by a change of the physiological parameter (e.g. the calcium concentration), or if the object simply moved away from the region of interest that marks the small structure like a dendrite or a dentritic spine.

Movements of the objects are a very common artifact during in-vivo imaging with two-photon microscopy, and there is one published method of how they can be corrected (Greenberg and Kerr, 2009). However, their acquisition speed is relatively slow (10 Hz) and the image quality is very good, caused by a really long pixel dwell time (~10 µs). They then focus more on the computational speed of the correction algorithm. In contrast, we have high speed image data (1000 images per second, normally downsampled to about 100 images per second) with a much worse image quality, caused by pixel dwell times about 2 magnitudes faster (50 ns, downsampled data has a pixel dwell time of about 0,5µs). Our data requires special techniques that can deal with a high noise amplitude and hence the low signal-to-noise ratio.

To correct these movements, I apply several steps in sequence: An initial filtering step to reduce the noise, based on methods of mathematical morphology and suited for extreme high noise levels, an adaptive background subtraction step, a threshold selection method and finally we compute the binary correlation. It is specially tailored to work on images of extreme bad quality. In-vivo observations can be of various characteristic concerning background intensity, signal-to-noise-ratio and image content. When we stain multiple cells with the multi-cell bolus loading technique with a membrane-permeable dye (Stosiek et al., 2003), the background-fluorescence is relatively high and non-homogeneous. This leads to a relatively low contrast, but allows for examination of several cells simultaneously. Another loading technique is to patch an individual cell and fill it with a high-concentration of calcium dye. This results in high-contrast images with almost no background, and allows for the observation of calcium concentration in small compartments of a cell like a dendritic spine. Such small and fine structures in the images require a modification of the correction algorithm. Our method here is easily adaptable to these different image characteristics. It requires only a few parameters, and the optimum values can be determined very easily and are mainly dependent on the size of the object in pixel. This makes the application of this method very easy and does not require a lot of training.

Image processing:

The algorithm can be divided into four steps: Noise Reduction, Background subtraction, threshold selection and computation of the correlation. We mainly focused on methods for noise reduction, as our images are characterized by an especially low signal-to-noise ratio, and this is the crucial step for our images. When the noise is reduced, we can apply standard registration procedures to find the

new position and correct it. Without a special noise reduction, a correlation would find a position where the noise correlates best with noise-free image, but not a correlation with the content of the image.

Noise reduction:

Noise reduction is normally done by linear smoothing: The new pixel values are calculated by averaging the neighboring pixels, or in an improved step by weighting the pixels according to their distance to the central pixel. If the weighting curve is of a Gaussian bell shape, this procedure is called Gaussian linear smoothing. This is the most common method for noise reduction.

This method is well investigated and works quite fine as long as the noise is not too high and the objects are relatively large. The disadvantage of this method is that it is not edge-preserving. A sharp edge is necessarily being smoothed. How much of an edge is smoothed is defined by the size of the filter element (defining the number of pixels that contribute to the calculation of the new pixel value) and the shape of the Gaussian function in the filter. If the objects in the image are large in comparison to the filter element and do not have sharp edges, this smoothing method is the method of choice.

The noise amplitude also predefines the size of the filter element. If the noise amplitude is high, a larger number of pixels are needed to calculate a good average value, hence we need a larger filter element. With a larger filter element, we necessarily smooth a sharp edge over a longer distance. The images in figure 38A and 39A are both noisy, but figure 38A allows the use of larger filter elements, as the details are larger and it is not so necessary to preserve their edges.

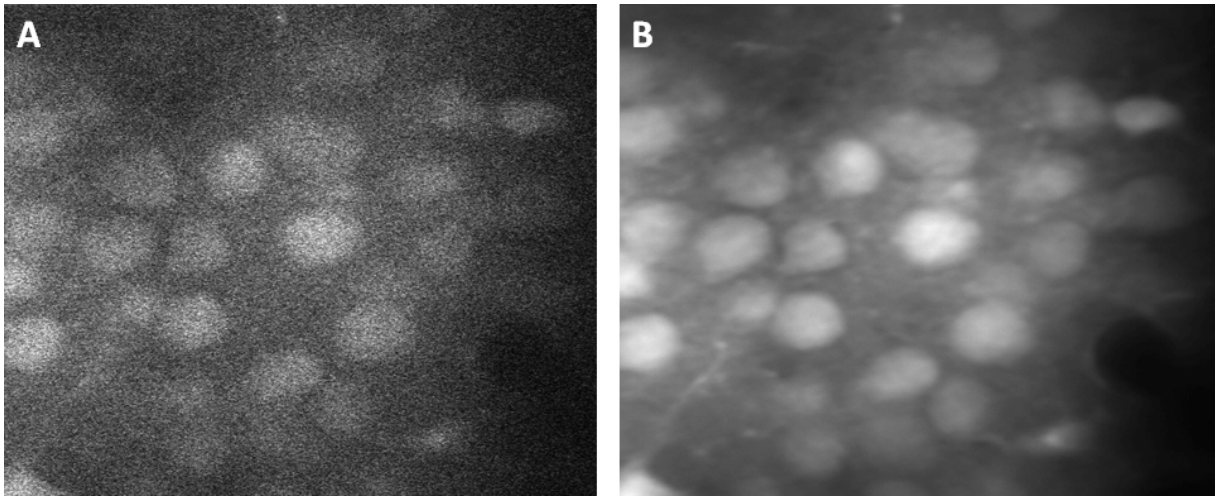

Figure 38: (A) single image from the video-rate two-photon observation form visual cortex, (B) average of ~1000 images from the video data from the left. The cells were stained with the bolus-loading technique (Stosiek et al., 2003). This staining technique results in a quite high background signal. The somas of cells of layer 2/3 are clearly visible. The images were acquired with a resonance-mirror based two-photon scanning microscope.

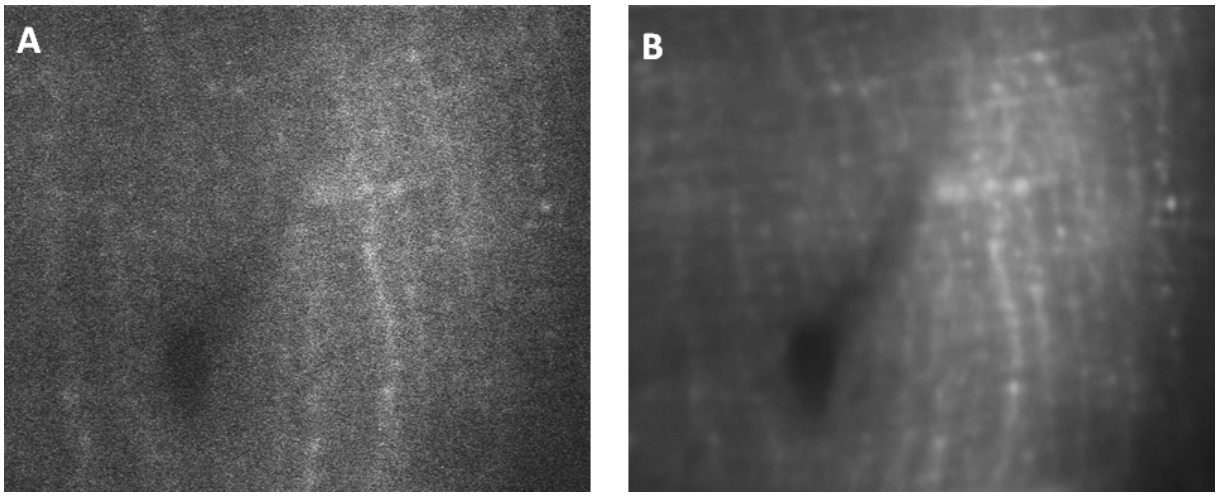

Figure 39: (A) single image of the Purkinje cells dendrites of the cerebellum, stained with the bolus-loading technique. The dendrites are oriented perpendicular to the image plane (B) Average of about 1000 images. One frame of the video data is very noisy, with a much higher noise amplitude than in most imaging application. Such images require a special treatment for noise reduction. These images were acquired with an AOD-based two-photon microscope, a system designed and assembled by my colleague Yuri Kovalchuk.

Recently a lot of research was done to refine the smoothing operations and to remove the noise from corrupted images (Astola and Kuosmanen, 1997; Winkler et al., 1998). Among these studies, two-step processes are especially remarkable. These two-step processes use the first step to decide whether a pixel value is corrupted by noise, and in a second step a noise-free pixel value is estimated(Chan et al., 2005; Nikolova, 2004). These methods have an improved edge preserving property and can deal with higher noise amplitudes and lower SNR. There are a number of parameters that allow for a better optimization of the smoothing results. However, these many parameters make the overall procedure a bit complex, and it is difficult to find the optimum values. As the signal- and noise amplitudes are also varying between measurements (depending on the imaging depth and the preparation quality), we would also have to find new parameters and the whole procedure must be optimized again. Therefore, these methods are not well suited for practical work. I decided to use methods of mathematical morphology (Peters, 1995; Soille, 2003), in particular the rolling ball algorithm(Sternberg, 1983, 1986). The main advantage of these methods is that they only need one parameter, the size of the structuring element. This parameter predefines the size of objects that should be smoothed completely. When this parameter is very small, smaller than the objects in the image, the algorithm reliably smoothes the noise but preserves other details. In contrast to linear smoothing, these methods can also handle highest noise amplitudes. Additionally these methods are fast, robust and edge-preserving.

The rolling ball algorithm is composed of iterative ‘Openings’ and ‘Closings’(Peters, 1995; Sternberg, 1983, 1986). As a ‘Closing’ followed by an ‘Opening’ is sometimes not the same like an ‘Opening’ followed by a ‘Closing’, we performed the operation in both ways and averaged the two results(Peters, 1995). The size of the structuring element was selected in a way to have it smaller than the size of the details in the image. In this way we only reduce the noise, and not the content of the image. If the structuring element is larger than the details, the details itself will be seen as noise

and will be smoothed out. As we only want to reduce the noise initially, the size of the structuring element can be small, e.g. a diameter of 3 to 5 pixels is sufficient. The noise of our photo-multiplier tube is white, e.g. there is no lateral correlation of the noise values. This allows the use of a small structuring element.

The rolling ball algorithm is edge-preserving. This can be a disadvantage as noise can displace the edge. In fig.2 for example the parallel structure is not clearly preserved and the edges are not straight. This can be avoided by using a moderate Gaussian linear smoothing step after the initial rolling ball algorithm.

Adaptive background subtraction by morphological object selection

We have a non-homogenous background when we stain the cells with a membrane-permeable dye using the bulk-loading technique to load cells (Stosiek et al., 2003). This can complicate the threshold selection. A non-homogeneous background can be corrected easily with another morphological filter, called the Top-Hat filter(Gonzalez et al., 2003). This filter selects details according to its lateral size. Everything larger than the preselected diameter is considered background and will be removed. This is a very useful property, as we can select for structures of a certain lateral size. This allows for selecting dendrites or somata of pyramidal cells, as they are of a homogeneous size throughout the image.

Image thresholding to generate binary images for the registration

I did not use a static grey-value for the threshold selection. I used a routine that automatically sets the threshold to a value that a given percent of the brightest pixels are selected. This percentage can be selected very easily and depends on the content of the images, if the objects are rather large or small or if they are relatively isolated or densely distributed throughout the image. Such a selection is easier than selecting the threshold value according to a grey value. Additionally, the absolute intensity value can vary during the measurement due to bleaching or tissue degradation caused by photodamage. This automated threshold selection also compensates bleaching processes. Additionally, we do not have to deal with absolute grey values, and it is easier to select the right value.

The threshold selection was also done to increase speed and reduce the complexity for the next step, the computation of the correlation to find the lateral displacement of the content of the image.

Binary correlation

To calculate the displacement in the next step, we need a reference image, displaying the objects at the average positions. We can get this reference image by simply averaging all images of the video data. This reference image then passes through the same procedures (noise reduction, smoothing, background subtraction) like each single image and results in a binary reference image. This assures that the content in the image is also of the same size, as background rejection in step 3 also rejects objects of the wrong size as background.

I can find the displacement by a simple correlation of the preprocessed reference image with the preprocessed single image. In the computation, I multiply the binary reference image with the binary single image pixel-wise and sum over all pixels. I just computed all possible displacements and selected the global maximum of the correlation. This is relatively slow and it is sure that this step can be accelerated by using an efficient algorithm for finding the optimum position (Greenberg and Kerr, 2009). However, the method is by far too slow to compute it for a live display. It always has to be

done offline. In this case there is not a big need to speed up the algorithm. The correction takes several minutes to hours, and could be accelerated by parallelization.

The previous thresholding step was also inserted to reduce the complexity. As I acquire the images in 16 bit format (65536 gray values), a pixel-wise multiplication of two images and summation over all pixels (image size about 500 x 500 pixels) could end up in large numbers. To avoid possible problems I just applied the thresholding step to avoid large numbers and computed a binary correlation.

Discussion:

In brain research we want to record nerve cell activity from different locations simultaneously. Measurements from deep layers of the brain are normally characterized by a low signal-to-noise ratio and additionally corrupted by movement artifacts caused by the blood flow. We present here a method to correct these movements from images with a low SNR and only small objects present in the images. It is composed of the steps noise reduction, object selection by adaptive background subtraction, threshold selection and computation of the binary correlation.

Our method needs only a few parameters, and these parameters need not to be modified for different noise amplitudes or after the sample bleached. These parameters are easy to estimate, as they mainly depend on the size of the structures of interest (in pixels) and the percentage of pixels that are occupied by the structure. Our algorithm is based on methods of mathematical morphology and is very robust. These methods can deal with highest noise amplitudes, are edge-preserving and relatively fast. Additional information like the heart beat recording is not required. It extracts all information from the given images.

This algorithm is optimized for images of bad quality with a low SNR. Only a few parameters need to be selected: the size of the structuring element for the rolling ball image cleaning (must be smaller than the structure of interest), the size of the linear smoothing mask (quite small to make the edges straight), the size of the structuring element for the TopHat filter (must be larger than the size of the structures of interest), and the percentage of brightest pixels for the threshold selection (can be easily estimated by looking at the images and trying some values). These parameters are easy to find.

The quality and correctness of the result can be evaluated by plotting the displacement versus time (fig. 3). If the oscillations are homogeneous and do not contain any outliers, the results can be considered as correct. Irregularities from the harmonic oscillations are clearly visible when we display a graph showing the displacement versus the frame number. This is a good method to control the result of the correction algorithm.

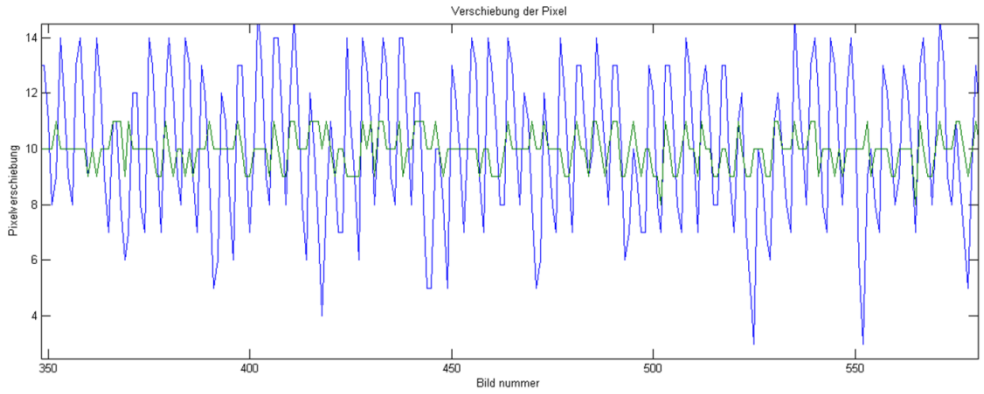

Figure 40: Diagram showing the displacement versus the time: The blue line shows the X-displacement, while the green trace shows the Y-displacement. The images were acquired with 30Hz. The frequency of the oscillation is about 400 per minute, and this is in agreement of the heart beat of a mouse. This diagram is a good check whether the prefilter-procedures and the registration provide good results or not. Sometimes the data is too noisy and the prefilter-procedure can not recover the position of the objects. In such a case, the algorithm can not detect the movement, and the upper graph does not show a harmonic oscillation.

We completely ignore the computational workload and time needed to perform the computation in this work. We compute all possible displacements and select the optimum values. The algorithm is a relatively slow algorithm, but this method can be highly parallelized for increasing the speed. The computational time for a correction of high-speed image data was below 2 minutes (image size is 200x100 pixels, 3000 images, corresponding to an observation of 30 seconds with 100 images per second, using a computer with two Intel Xenon X5560 processors (2.8GHz) and 28GB memory). If we recorded a promising measurement, we started the correction and were able to evaluate the corrected data stack a short time later. As the correction for each image can be computed in parallel, there is a large potential for speed improvements.

Correcting this movement artifact is important for investigations of physiological signals in small compartments of cells like dendrites or dendritic spines. It is still an open question how a complex dendrite integrates several inputs, puts them into relation and computes the output. In order to measure the contribution of single spines simultaneously, an optical measurement is the method of choice. When movements are visible, a correction of these movements is a prerequisite to investigate the contribution of a single spine to the overall response of a cell, and how a cell integrates the variety of inputs from multiple spines.

A two-dimensional correction is not always sufficient, as the oscillations could also be directed in the depth-direction. When we use an objective lenses with moderate magnification (~40x), this is not critical, as the depth resolution is normally much worse than the xy resolution. For example, an objective lens (Olympus 40x) with a numerical aperture of 0.8 has a depth resolution is about 3,3 µm (calculated by the formula $2\ \lambda\ n/NA^2$(Leischner et al., 2009)), compared to 0,5 µm xy resolution. For measurements with these objective lenses, a movement correction for z-movements is normally not necessary. This resolution is sufficient for measurements in dendrites, but measurements in single spines are critical. A better resolution would be advantageous for spine observations. Objective

lenses with acceptable working distances are available with numerical apertures up to 1. This would result in depth-resolutions of about 2 microns. In this case a three-dimensional correction of the movement artifact would be necessary. This would then require the acquisition of three-dimensional data. There are some approaches as to how three-dimensional data can be acquired (Gobel et al., 2007; Reddy and Saggau, 2005).

Chapter 4: Measurements

The newly developed AOD-based two-photon microscope was used for several measurements. We tested different brain regions, e.g. the cortex (visual and auditory area) and the cerebellum, and different staining procedures, e. g. patch-clamp with a dye-filled electrode, electroporation (Potter et al., 1984) or multi-cell bolus loading (Stosiek et al., 2003), staining multiple cells in the same area simultaneously. Many of these experiments were just early tests for the image quality, image depth, and for the lateral and temporal resolution. We sometimes immediately modified the apparatus, and then the old results were no longer of interest. Presenting all measurements we once did is not the focus of this technical PhD thesis. This thesis describes the layout and development of a fast-scanning two-photon microscope. I will only describe the main measurements with the final apparatus. This latest version of the scanning system has been used for about one year for systematic measurements. It consists of one scanning AOD (fast line-scan) and a galvanic mirror for image scan, together with an identical AOD for chromatic compensation, and a cylindrical lens compensation optics.

We did a lot of other tests with this apparatus. Some experiments were in a very early stage, including tests with voltage-sensitive dyes (the microscope can acquire images with up to 2000 images per second, and such a temporal resolution allows for direct measurements of the membrane potential), and activation of channelrhodopsin in virally transfected cells in the cortex. These experiments are technically very difficult, especially the sample preparation. If I would present such data here, I would also have to give a lot of background information on the dye or the transgenic modifications of the biological organism. This would again exceed the focus of this PhD thesis. I will therefore just present the two systematic measurements: one investigation from Horst Henning on Purkinje-cell properties, measured in an acute slice-preparation of the cerebellum, and one in vivo investigation from Xiaowei Chen on the spine-activity of dendrites of the auditory cortex after auditory stimulation.

The measurement of the Calcium-signal in spines of Purkinje cells in an acute slice preparation

First we used the new measurement apparatus for investigations of mGluR1 mediated Ca^{2+} signaling in spines and dendrites of cerebellar Purkinje-cells. The measurements were performed in an acute slice preparation by my colleague Horst Henning. Besides the highly interesting phenomena of Ca^{2+} entry through TRPC3 and mGluR1 receptors, these experiments were a good test for the image quality of the microscope, first because dendritic spines of Purkinje cells are smaller than spines of pyramidal cells in the cortex and therefore especially difficult to resolve. Second, a slice preparation is much easier than an in-vivo preparation, and an experienced researcher will get good results in most of the experiments. Lastly, Purkinje-cells are characterized by a large cell body, and therefore they are especially easy to patch.

Horst Henning investigated the mGluR1 and TRPC3 mediated Ca^{2+} signaling in spines and dendrites by activation of the parallel-fiber to Purkinje cell synapse. He did this by placing a stimulation electrode on top of the slice, and imaged a dendritic area most likely innervated by the stimulated parallel fibers. He made systematic measurements in acute slices from TRPC3 wt and TRPC3 -/- mice. By using the newly designed apparatus, Horst Henning was able to investigate the contribution of the

Ca^{2+} influx through TRPC3 channels to the kinetics of the total mGluR1 mediated Ca^{2+} signal with high temporal resolution.

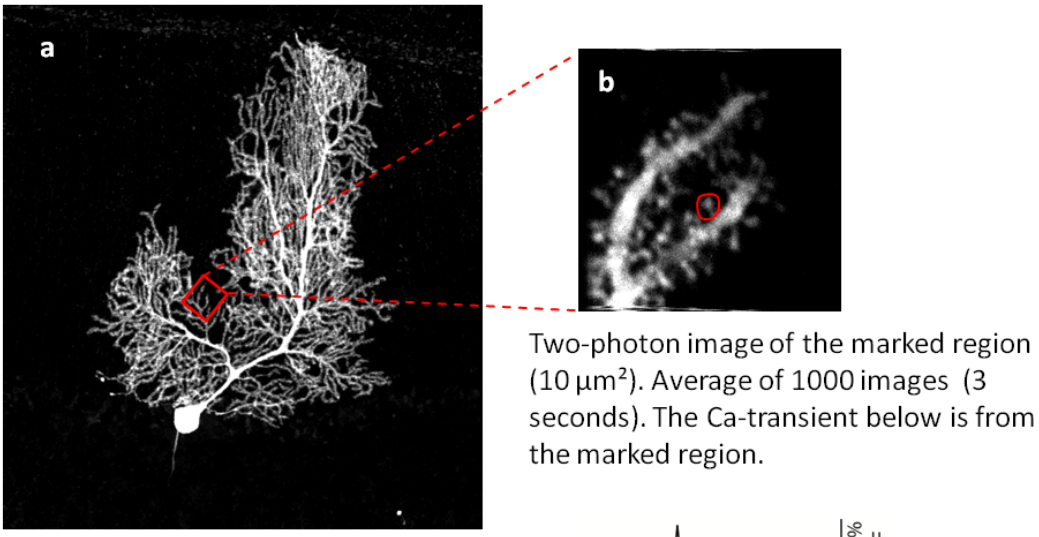

Figure 41: Measurement of Ca^{2+} signals with high temporal resolution: The Purkinje-cell was filled with the patch-pipette containing the Ca^{2+} indicator dye Oregon Green. Horst Henning then focused on a small section of the dendrite, and recorded the area with a high frame rate (typically 320 images per second). The high-speed image data was then sampled down to 32 images per second, and analyzed. The down-sampled image data is of high image quality and allows for a detection of the Ca^{2+} signals in dendritic spines in a single trial, and does not require an averaging of several repeated measurements with the same stimulation protocol.

The high temporal resolution is a major advantage. Previous measurements with a lower sensitivity used several stimulations, and averaged the signals from several single-trial measurements to get the noise-free average signal. Such an averaging-procedure smoothes the rise-time of the Ca^{2+}transients, as the Ca^{2+} transients appear with a delay of approximately 200ms, with a variation of up to +- 50 ms. This variation is present under identical conditions, and is due to the signal transmission through the parallel fiber and the pre-synaptic vesicle-release. A high-sensitivity measurement with high temporal resolution allows for a precise investigation of the time-course of the Ca^{2+} entry into the dendritic spine.

The precise measurement of the calcium kinetics is of high interest, because different processes require a different time-course of the calcium concentration. Although synaptic potentiation and depression are both triggered by changes in the calcium concentration, they likely require very different concentration profiles (Cornelisse et al., 2007; Lisman et al., 2002). LTP is reliably triggered

by sharp increases in calcium with high magnitude, whereas LTD presumably requires a prolonged modest increase in calcium (Cummings et al., 1996; Koester and Sakmann, 1998a; Yang et al., 1999)

In-vivo measurements of spine-activity in the auditory cortex

My colleague Xiaowei Chen used the new microscope for measurements of Ca^{2+} fluctuations in dendrites and spines of the auditory cortex in vivo. The measurements in deeper layers in-vivo are of a much worse image quality, with a lower signal-to-noise ratio. Therefore he used different acquisition parameters than Horst Henning for his measurements in acute slices (see previous paragraph). Horst acquired images with 320 frames per second, as image quality is quite good in the upper layers of the slice, and he gained a good signal quality with this 'moderate' image frequency. Xiaowei Chen measured in deeper layers of the mouse brain, and less photons were coming back from these deep brain regions, and hence the signal had a lower amplitude, and therefore a worse signal-to-noise ratio. To improve the signal quality, Xiaowei Chen used imaging parameters with a threefold increased image frequency, and acquired images with 1000 images/s. As he scans the same region three times more often, he could gather three-times more fluorescence signal. In the high-speed imaging modality, the images are about 3x smaller (250 x 80 Pixel vs. 250 x 250 Pixel). This high-speed image data allows for the application of smoothing methods with stronger parameters, and therefore a higher noise reduction. Altogether, the signal quality of the fluorescence traces of spines are about the same with both imaging parameters, and Xiaowei got similar results like Horst.

Xiaowei Chen performed the whole experiment. He prepared the mouse, and used the 'shadow patching' procedure (Kitamura et al., 2007) to find a suited cell, patch it and fill it with the fluorescent Ca^{2+} indicator. The dye diffused into the cell, and after approximately 20 minutes, the dendrites of the cell were homogeneously stained, and we could start the measurement. Xiaowei searched for a dendrite with horizontal orientation and many visible spines. Then he changed to the high-image rate and high-zoom parameters (200 x 100 Pixel, 1000 images per second, field of view of 5 x 10 µm), and started the measurement. He could continuously measure fluctuations of the Ca^{2+} concentration for about 5 minutes before first signs of cell damage become apparent. Such cell damage is visible by an increase of the fluorescence of the dendrite, most likely caused by a damaged cell membrane and Ca^{2+} entry into the cell. When the cell background becomes bright, the changes in fluorescence become hardly measurable. Technically, we always display $\Delta F/F$ (the ratio of the change of the fluorescence over the average background fluorescence of the same ROI). When the background fluorescence F becomes large, $\Delta F/F$ necessarily becomes small, and therefore we can not get a $\Delta F/F$ signal in the range of 1-3. We need at least a $\Delta F/F$ value of 1 to detect Ca^{2+} transients.

Xiaowei could execute long stimulation protocols within 5 minutes, until first signs of photo-damage become apparent. He placed a speaker next to the ear of the mouse, played several acoustic frequencies and mapped the response of the spines and dendrites in the observed area. He could measure the spectral response function of an individual spine over a wide range of acoustic frequencies.

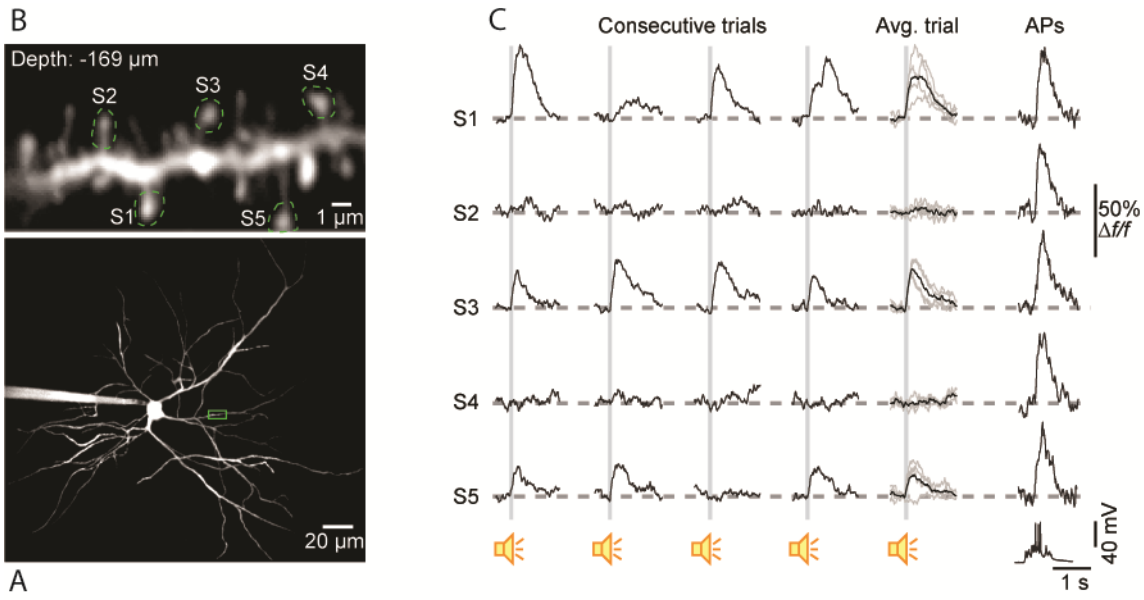

Figure 42: Measurement of the spine response during auditory stimulation. A: overview of the measured cell. We focused on the marked region and imaged that part with high frequency. B: high-resolution image of the observed part of the dendrite. We imaged this part of the cell with 1000 images/second. C: Ca^{2+} transients of the spines marked in B after stimulation with broadband noise of 0dB attenuation for 100ms. The left 5 trials were all subthreshold stimuli, and did not result in an action-potential firing of the cell. The right column shows the Ca^{2+} transients in the spines caused by a back-propagating action potential.

Chapter 5: Discussion:

This PhD thesis describes the development of a high-speed two-photon microscope with image rates up to 1000 images per second. The speed is increased by replacing one mirror-based scanner with an acousto-optical deflector. Replacing a mirror by an acousto-optical deflector is not straightforward as AODs generate several artifacts, namely the chromatic dispersion and the cylindrical lens effect, but these artifacts can be compensated quite well. When all artifacts are compensated, images from the newly developed microscope are of a similar quality and resolution, like the images from comparable mirror-based two-photon microscopes. Measurements with this new apparatus showed a dramatic increase in sensitivity and additionally a decrease of photo damage, allowing for measurements of several minutes duration.

The sensitivity is increased mainly by a temporal and spatial oversampling. The calcium signal is very slow, with fastest decay time in spines of 90ms (Cornelisse et al., 2007), and an imaging speed of 1000 images per second is a temporal oversampling by a factor of about 30. The lateral oversampling is in the same range, as one pixel covers about 40nm of the sample with a higher zoom factor configuration. This is a 5 fold oversampling in X- and in Y-direction, hence the lateral oversampling is about 25 fold. Altogether, this results in an oversampling of up to three magnitudes. This increases the signal-to-noise ratio dramatically, and allows for an additional reduction of the illumination intensity to reduce photo damage. This is a surprisingly simple method to resolve the very weak and noisy calcium signal from tiny dendritic spines. All comparable measurements lacked the full two-dimensional image information (Grewe et al., 2010; Koester and Sakmann, 1998b; Nagayama et al., 2007; Reddy et al., 2008; Reddy and Saggau, 2005) and therefore are unsuited for in vivo observations, as in vivo measurements are normally corrupted by tissue movements of different amplitudes due to the pulsing blood flow. A detection of tissue movements is necessary to estimate the fidelity of the fluorescence traces, and this requires the two-dimensional image information. Data from line-scan or random-access point scan sampling procedures do not allow for the detection of tissue movements. In case of movements, point- or line-scan will gather very noisy data, but the origin of the noise could also be something else, like tissue degradation, bleeding, or simply a problem of the perfusion system.

Although this fast full-frame two-photon imaging modality was especially developed for the needs of in vivo imaging, investigations on slices or cultured cells will also benefit from it. My colleague Horst Henning conducted several acute slice experiments successfully, and he was impressed about the possibility to resolve the calcium-transient in a single trial. Comparable measurements needed an averaging of several stimulations (Cornelisse et al., 2007; Hildebrand et al., 2009) or were done in a slice (Kovalchuk et al., 2000) with much easier optical conditions than an in vivo measurement.

There are a number of other applications for high-speed two-photon imaging. A highly interesting application in the area of brain research is the measurement of the membrane potential of nerve cells in the brain using voltage-sensitive dyes. We made several attempts, but these measurements are quite difficult and there are no established membrane dyes for two-photon excitation. An action potential occurs within 2-3 ms, and therefore the changes of the membrane potential are quite fast. The acquisition speed of this microscope is sufficient for measurements of such fast processes. I made a configuration for image acquisition with up to 1600 images per second, and the galvanic mirror was still operated in the one-dimensional scan mode using a saw tooth control signal. The

galvanic mirror could also be operated in a bidirectional scan mode, using a triangle control signal. This would double the frame rate, reaching 3200 images/second. However, the images would be very small in terms of the number of pixel. 2000 images per second result in an image size of 100 x 100 pixel, and when we combine such an image size with lateral oversampling, we can not map a large section of a dendrite.

Although two-photon microscopy is a 20 year old technique, there are still a number of substantial improvements in recent years. Ji et al. demonstrated a reduction of photo damage by an increase of the laser pulse frequency(Ji et al., 2008). This principle could be combined with this fast scanner, allowing for an additional reduction of photo damage. Another improvement could be the use of a different two-photon laser. There is an interesting new laser from the company IdestaQE with an extreme short pulse width of about 10fs. Reducing the pulse duration results in a higher peak intensity and hence a higher two-photon efficiency. However, a combination of this laser with AOD scanning will be highly challenging, as that new laser has a spectral width of 300nm and I don't know if the chromatic compensation for AODs will still work with such a wide frequency range. Additionally, we need to prechirp the laser beam with extreme values (about 20 000 fs^2), as the laser has to pass two AOD crystals of the material TeO_2, which induce an especially large group-velocity dispersion. A vendor of prechiprer-devices is the company APE in Berlin. I contacted them and asked them whether a prechirping for such extreme values is still possible. They made a fast estimation and told me that they could modify their devices to reach a pulse width of about 15fs. Unfortunately, such a laser with such short pulses is only available with an output power below 1W. I currently use a 3W laser, but only 20-30% of the maximum laser power, so the lower laser power of the new laser would still be useful for measurements in the upper part of the cortex. I do not know if the chromatic compensation for such a broad spectral width is still feasible, but a reduction of the pulse duration by a factor of 6 would be a big improvement. The overall increase would be quite high, as the two-photon efficiency increases in a quadratic dependency with the illumination intensity, therefore a pulse reduction by a factor of 6 should result in an increase of two-photon efficiency of a factor of $6^2=36$.

We did not make systematic measurements of the imaging depth. We measured in a depth of about 200 microns below the brain surface, but only used 20-30% of the maximum laser power. I am convinced that we can image in deeper layers, because we can still increase the laser power for a better illumination there. Additionally, we can change to a higher frame rate, increasing the image quality after temporal down sampling. Once, we were even able to trace an axon of an OGB-labeled Purkinje-cell for some distance through the granular layer of the cerebellum. This was not possible with other microscopes, and therefore this newly developed microscope already showed some advantages in terms of penetration depth.

This fast scanning configuration could be combined with other scanning techniques of microscopy. STED-microscopy (Stimulated Emission Depletion) (Hein et al., 2008; Nägerl et al., 2008; Willig et al., 2007; Willig et al., 2006) could especially benefit from a reduction of photo damage by using a low-power temporal oversampling. The STED technique allows for the acquisition of images with an increased resolution (down to 50nm), but it is also accompanied by an increased bleaching. Although I think that a combination of STED-microscopy with AOD-scanning is possible, I am not sure if a low-power temporal oversampling would result in a reduction of photo damage. STED microscopy implements an additional kind of illumination, the stimulated emission light, and the intensity of this light can not be reduced. It is fixed to the desired lateral resolution. If the stimulated emission light

generates additional photo damage, a low-power temporal oversampling will not reduce photo damage. Only in the other case when photo damage is solely due to the excitation process, a low-power temporal oversampling would decrease the photo damage. The STED-technique has already been combined with two-photon excitation (Ding et al., 2009; Moneron and Hell, 2009), allowing for the acquisition of images in deeper layers (100 microns depth(Ding et al., 2009)) of biological tissue, and avoiding the need of a descanned detection. STED microscopy needs a descanned detection (Westphal et al., 2007) or is only applicable for thin objects with no out-of-focus fluorescence, as STED-microscopy is not a suited method to remove out-of-focus fluorescence. The stimulated emission process requires high light intensities, and this is only present in the donut-shaped focus spot in the focal plane, not in far out-of-focus regions. I think a combination of two-photon STED microscopy with fast optical AOD-based scanning could increase the quality of a measurement.

In a nutshell, there are still a number of substantial improvements possible, but it is questionable if such modifications would result in an improvement of the imaging depth. The imaging depth is the main criterion for in vivo microscopy, as this allows for measurements at different cell types that were not accessible before. This technique was developed with the focus on measurement on dendrites and spines. A large portion of dendrites from cells from deep layers is located in upper parts of the cortex, and is therefore still accessible with this apparatus. The setup in the current configuration with a standard two-photon laser proved to be useful for a lot such biological measurements. It is best suited for the characterization of dendritic input to different cell types, like interneurons and pyramidal cells from different layers of the cortex of an intact brain. As there is a manifold of cell types in the cortex, in a manifold of different brain regions, this microscope will open the way for manifolds of investigations and characterizations for a better understanding of the intact brain in healthy and diseased conditions.

Chapter 6: Summary

Two-photon microscopy is a technique to acquire images in deep layers of biological tissue (0.5-1mm depth), but it is a relatively slow technique (~30 images per second), mainly because mirrors are used for the scan process. This thesis describes the development of a fast two-photon microscope (more than 1000 images/second), using acousto-optical deflectors as scanning devices. In the end, the image quality and high-sensitivity of measurements with this newly developed microscope is demonstrated, showing the capability of resolving calcium transients in individual dendritic spines in vitro and in vivo.

Acousto-optical deflectors are about 10 times faster than revolving mirrors, but they use a different physical principle for beam steering. Instead of a reflection on a flat mirror surface, the diffraction patter of an optical grating is used. The optical grating is created by an acoustic wave, propagating through a transparent crystal, and a change of the acoustic frequency results in a different grating constant, resulting in a different deflection angle of first-order light. This deflection principle is accompanied with several beam distortions. First, laser light of a different wavelength is deflected in a different angle, resulting in a chromatic dispersion when AODs are used in combination with a two-photon laser with a relatively broad spectral range. I review all the existing publications concerning a compensation of this effect and select the best suited one. Second, an AOD creates a beam distortion similar to a cylindrical lens when it is used for a fast linear scan through a certain angle range. I analyze this effect, investigate the consequence for the image quality, develop a compensation scheme and optimize the compensation parameters.

These developments result in a fast two-photon scanning microscope, allowing for a scanning speed of 1000 images per second and more. The higher frame rate theoretically gathers 50 times more fluorescence signal, and hence increases the signal-to-noise ratio 7-fold, about one magnitude, also depending on the imaging parameters like the image size and the frame rate. This allows for high-sensitivity measurements of calcium transients in individual spines. I demonstrate this with two measurements from colleagues using the newly developed microscope, one of an acute cerebellar slice preparation of Purkinje-cells, and one of an in vivo preparation of cells of the auditory cortex.

A lot of biological projects using two-photon microscopy can benefit from such a development of a high-speed and high-sensitivity microscope. The increased sensitivity allows for a detection of weak and noisy signals, or it allows for a reduction of the illumination power, leading to lower photo damage. The high frame rate allows for the detection of fast biological processes, like changes of the membrane potential and the detection of action-potentials with suited voltage-sensitive dyes.

Chapter 7: Publications

I published a number of papers during the time I spend at the institute of neuroscience, but most of them describe work that was done in my previous lab, in the research group 'Bioimaging' from Hans-Ulrich Dodt in the Max Planck Institute of Psychiatry in Munich. I spent altogether about 2.5 years there, first doing my master thesis and graduating in theoretical physics, and then one additional year finishing some research projects. The publication process of the main paper(Dodt et al., 2007) of the research took some time. This also delayed the publication of my secondary publications, describing some technical parts of that imaging technique. Therefore all publications from that institute appeared during my work at the Institute of Neuroscience, during my graduate work on my PhD project. However, although the content of my papers was exclusively done in the MPI of psychiatry, my PhD education helped a lot during the publication procedure, especially the lecture on scientific paper writing, and the highly stimulating new environment with the many new colleagues, giving many suggestions during the procedure of writing the papers. I therefore mention these publications also as a result of my PhD-education.

H.-U. Dodt, U. Leischner, et al., Nature Methods 2007, Ultramicroscopy: three-dimensional visualization of neuronal networks in the whole mouse brain

This paper is the main publication from the MPI of Psychiatry, describing a novel three-dimensional imaging technique to image large tissue samples of formalin-fixed animals, mainly mice. Biological samples (e. g. entire brains) are highly opaque, and images can be acquired normally only from the surface region. This prevents a three-dimensional investigation of the branching pattern of nerve cells in the brain. There is an old publication of a histological procedure (Spalteholz, 1911) how biological samples can be made transparent, by exchanging the water of the sample with certain liquids of different refractive index. Applying this procedure results in a completely transparent sample (e.g. an excised mouse brain), and allows for optical imaging in deep layers inside the tissue.

As we are now able to look deep into the sample, a normal bright-field illumination would generate a lot of background signal and out-of-focus blur. Therefore, we modified the illumination technique to a light-sheet illumination, performed with cylindrical lenses and illuminating the field of view from the side, perpendicular to the direction of observation. This illumination technique illuminates only the focus region, hence no background signal is generated and the images are characterized of a high contrast and low background. By illuminating different positions of the sample, we can gather three-dimensional image data from the whole sample with µm-resolution. We presented several high-resolution images, showing the potential of this novel imaging technique on different sample sizes, e.g. entire mouse embryos of more than one cm, entire *Drosophila Melanogaster* of some mm, and high magnification images of hippocampus samples showing even dendritic spines.

My job during that project was to maintain the optics, the laser and the software, so altogether 'keeping the technical parts of the lab running', and also enabling my colleagues from biology to image their samples. As I had was most experienced in the fine adjustment of the optics, I acquired the image data from all high-resolution samples presented in the figures of that paper. This central position resulted in the second position in the author list.

W. Wein, M. Blume, U. Leischner, et al., MICCAI 2007, Quality-Based Registration and Reconstruction of Optical Tomography Volumes

This paper resulted from a collaboration with the group of Prof. Navab from the chair of medical computer science from the TU-München. They did some three-dimensional image reconstruction for us.

The publication explains an easy image improvement technique by making use of several image acquisitions. We make the biological samples transparent with the 'Spalteholz-procedure'(Spalteholz, 1911) to a large extent, but this transparency is not perfect and image quality still deteriorates deeper inside the sample. The image quality can be quite bad at the bottom of the sample, as we have to look through the whole sample for imaging this location. We could easily avoid this bad image quality by simply turning the sample around, and acquire another image stack of the same sample. As we turned the sample, we can now acquire the previously badly imaged parts from the ground with high image quality, as they are now located in the upper section of the image stack. Now we have two image stacks of the same sample, and have to align and merge them to form one image stack with high-quality.

Technically, this paper describes image procedures for alignment of two 3d image stacks, 3d-rotations, image quality measurements and the generation of one high-quality image stack from two image stacks with a heterogeneous image quality. The technical problems were mainly data handling (one image stack can be larger than 1GB), and a precise alignment, as there are no clear edges in images of bad image quality. My contribution was the generation of the test data, discussing the results when the project evolved, and I made some changes in the illumination for an additional increase of the image quality. This illumination change resulted in more image stacks with a more heterogeneous image quality. When we merge these additional image stacks to one final result, we could achieve even higher image quality.

This was a project from computer science, and the main challenge was data handling of large data sets, performing rotations in 3D, and resampling. I did not have a central position. I just generated the image data.

U. Leischner, et al., PLoS ONE 2009, Resolution of Ultramicroscopy and Field of View Analysis

This paper investigates the depth-resolution and the field of view of the modified illumination technique. We illuminate only the focal plane from the side, perpendicular to the direction of observation. Therefore, the illumination is no longer linked to the imaging lens system, like in confocal microscopy. We can now modify the illumination parameters independently, like the used cylindrical lens or the slit apertures. The thinner the illumination beam, the better the depth-resolution, and this influences also the lateral extension of the thin illumination beam and therefore the useful field of view for this illumination technique.

The paper consists mainly of work from my master thesis on theoretical physics. It is a calculation of cross-sections of the illumination beam at different positions, a measurement of the cross-sections, and the application of resolution criteria. It also considers the description of resolution in Fourier space. I was first- and corresponding author, as I made all the work and also developed the numerical simulations.

U. Leischner, et al. PLoS ONE 2010, Formalin-Induced Fluorescence Reveals Cell Shape and Morphology in Biological Tissue Samples

When I acquired images with cellular resolution and high magnification, I often saw an interesting effect: The background-fluorescence is non-homogeneous, and extra-cellular areas are brighter than intra-cellular areas. This effect can be used to display cells in three dimensions. This technique requires only formalin as fixative, and hence is an easy method for visualizing cells in tissue samples of wild-type animals. Histological or transgenic labeling techniques are not necessary, only a perfusion with formalin. This simplifies the pre-treatment of the sample enormously.

However, the image data is normally corrupted by shadows in the illumination beam, resulting in a non-homogeneous illumination, visible as stripes in the image. These artifacts are very prominent, and need to be corrected before we can use these images. I developed some image reconstruction techniques to remove these stripes. The publication contains a detailed explanation of this method.

I think this publication is my most important one from that lab. It will have the most impact for biomedical research, as it simplifies the sample pre-treatment enormously. This publication is a good example for the work of a physicist in a biological laboratory: I can build a special microscopical apparatus that can acquire images of a special quality under certain conditions, and for special investigations. There are very often investigations that require a modification of a standard microscope: An investigation sometimes requires certain image dimensions, a special modification of the illumination or some image post-processing. Very often there is no commercial microscope available for these special investigations. Although these small technical modifications are not very difficult for a physicist, they require knowledge of the experiments and the imaging conditions. This requires knowledge of all parts of the science. This is the classical description of the work of a physicist: They are needed for work where the different areas of science merge.

Appendix:

Calculation of the chromatic dispersion of a prism

I first used prism as compensation elements to correct the chromatic dispersion of AODs in the early versions of the two-photon microscopes with AOD scanners. Prisms are very cheap, and easy to use for first tests. For the adjustment of the prism I needed to know the value of chromatic dispersion, dependent of the rotation angle. This value also varies with different wavelength and glass types. Here I present the derivation of the formula describing the chromatic dispersion, dependent on the wave-length and the rotation angle of the prism.

In the first step I have to find out, how the refractive index is dependent on the wavelength. I looked for data of glass of SF11 type in the internet data base of Messes Griot (http://www.mellesgriot.com/products/optics/mp_3_1.htm). Plotting the wavelength versus the refractive index results in the following diagram.

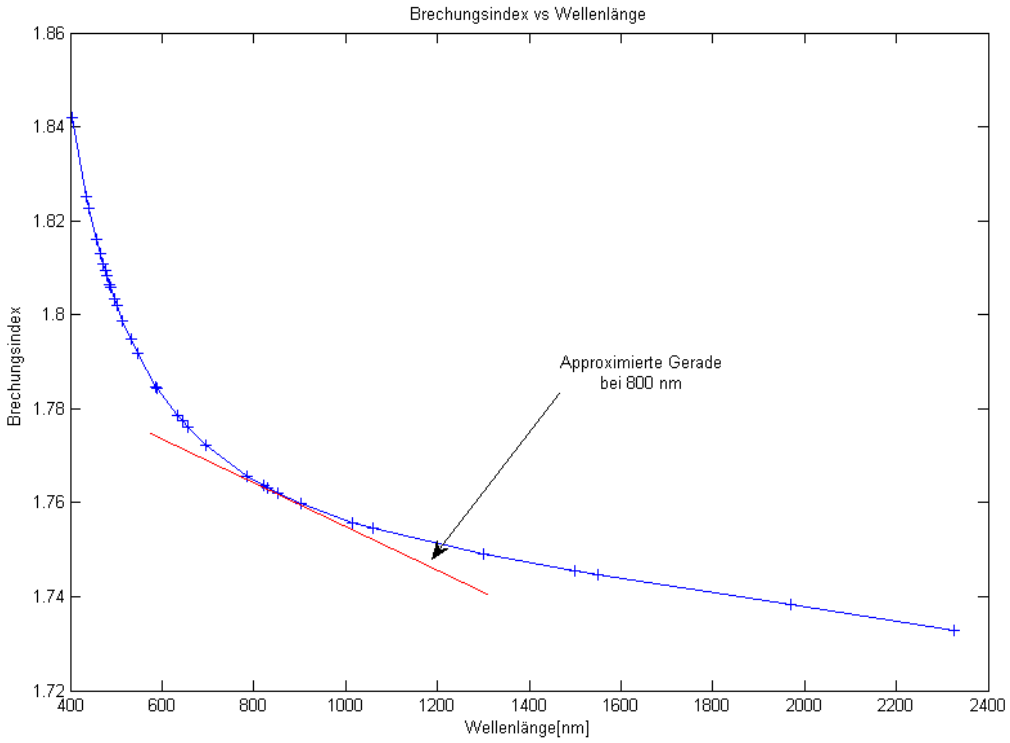

Figure A1: The refractive index versus the wavelength of SF11 glass

I used two data points around 800nm to calculate the slope of the function around 800nm. The result is:

$$n(\lambda) = 1.8102697 - 5.685714.10^{-5}[\frac{1}{nm}] \cdot \lambda$$

Hence, the dispersion is negative. I used the law of Snellius to determine the dependence of the chromatic dispersion from the wavelength.

$$n_1(\lambda)\sin(\alpha_1) = n_2(\lambda)\sin(x_1)$$

I use these denotations in the following derivations:

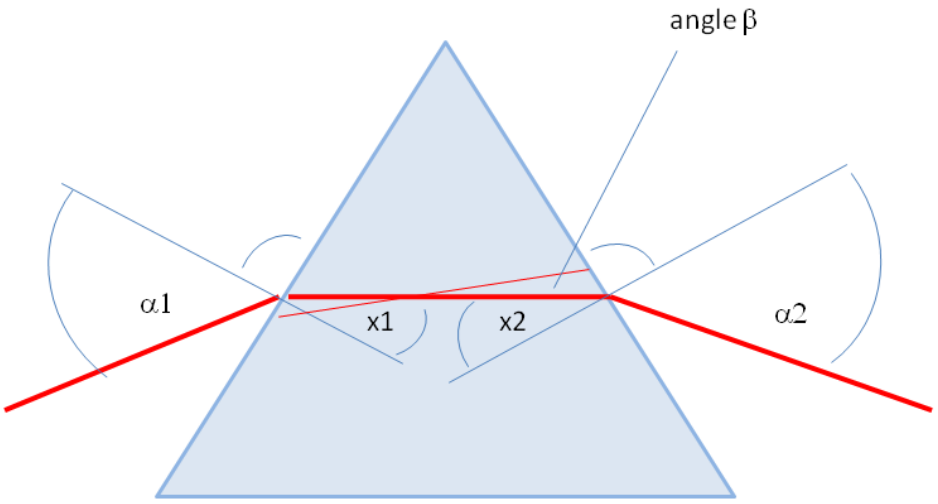

Figure A2: The naming of the different angles involved in the computation

The chromatic dispersion, caused by the entry of the laser beam into the prism, is:

$$x_1 = \arcsin(\frac{n_1}{n_2} \cdot \sin(\alpha_1))$$

$$n_1(\lambda) = 1; Refractive\ index\ of\ air$$

$$n_2(\lambda) = 1.8 - 5.6 \cdot 10^{-5}[\frac{1}{nm}] \cdot \lambda$$

$$\frac{dn_2}{d\lambda} = -5.6 \cdot 10^{-5}[\frac{1}{nm}]$$

The formula for the derivation of the ArcSine function is:

$$\frac{d}{dx}\arcsin(f(x)) = \frac{f'(x)}{\sqrt{1-f(x)^2}}$$

Hence, the formula for the chromatic dispersion, dependent on the entry angle is α_1:

$$\frac{dx_1}{d\lambda} = \frac{\frac{\sin(\alpha_1)\cdot(-1)}{n(\lambda)^2}\cdot(-5.6\cdot 10^{-5})}{\sqrt{1-(\frac{\sin(\alpha_1)}{n(\lambda)})^2}}$$

I get the following formula when the beam exits the prism:

$$n_2(\lambda)\sin(x_2) = n_1\sin(\alpha_2) = \sin(\alpha_2)$$
$$\alpha_2 = \arcsin(n_2(\lambda)\cdot\sin(x_2))$$
$$\frac{d\alpha_2}{d\lambda} = \frac{\sin(x_2)\frac{dn_2}{d\lambda}}{\sqrt{(1-n_2^2(\lambda)\cdot\sin^2(x_2))}}$$

We have to consider that the chromatic dispersion is one time positive and one time negative. But: the angle $\alpha 1$ and x1 are also once positive and once negative. Therefore, the absolute dispersion is of the same sign in both cases.

I can calculate the chromatic dispersion of the entry into the prism and the exit of the prism and can compare both values. I calculated the values for different angles using a short computer program. This resulted in the following diagrams:

The chromatic dispersion at the entry of the prism:

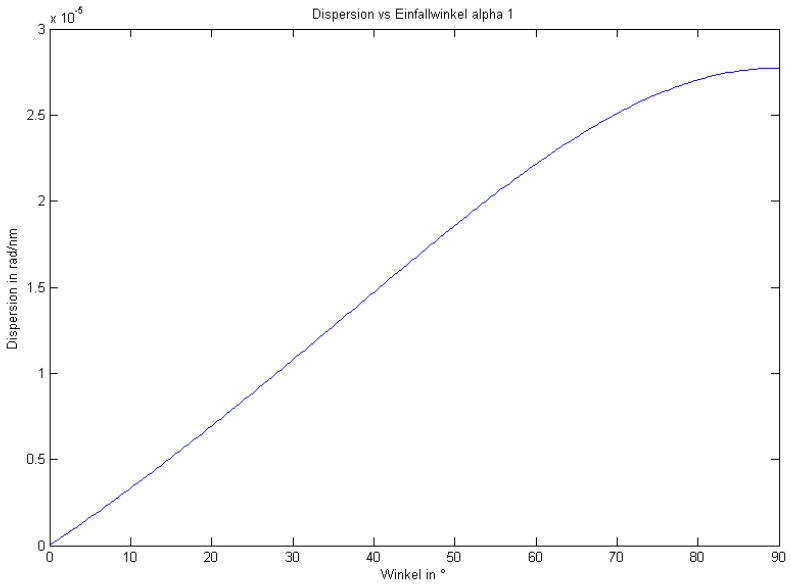

Figure A3: the chromatic dispersion versus the entrance angle of a prism

We have to note: The scale of the Y-Axis is 10^{-5}

The relation at the exit of the prism is as follows:

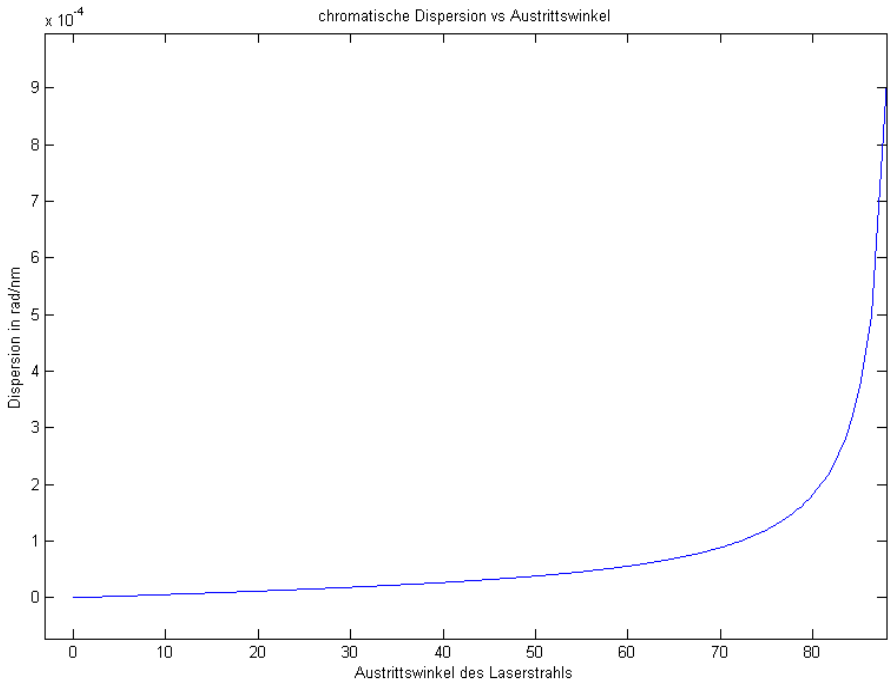

Figure A4: The chromatic dispersion when the beam exits the prism

The scale of the Y-Axis is 10^{-4}

We can finally state, that the chromatic dispersion is an effect that appears mainly at the exit of the prism. It is about 10 times larger there than at the entry of the prism. We get the highest dispersion values when the laser beam exits the prism with a high incident angle, as close to parallel to the prism surface.

We can just add the chromatic dispersion from the entry of the prism with the chromatic dispersion from the exit of the prism, because both values are of the same sign. We can also ignore the chromatic dispersion caused by the entry of the prism, because this value is more than 10 times smaller than the dispersion from the exit of the prism.

The values of the chromatic dispersion are between 0.1 to 0.4 mrad/nm in practical applications. In theory the values can be infinitely high when the laser beam exits the prism with an angle infinitely close to 90 degree, but practical values are up to 0.4 mrad/nm.

The chromatic dispersion of an AOD:

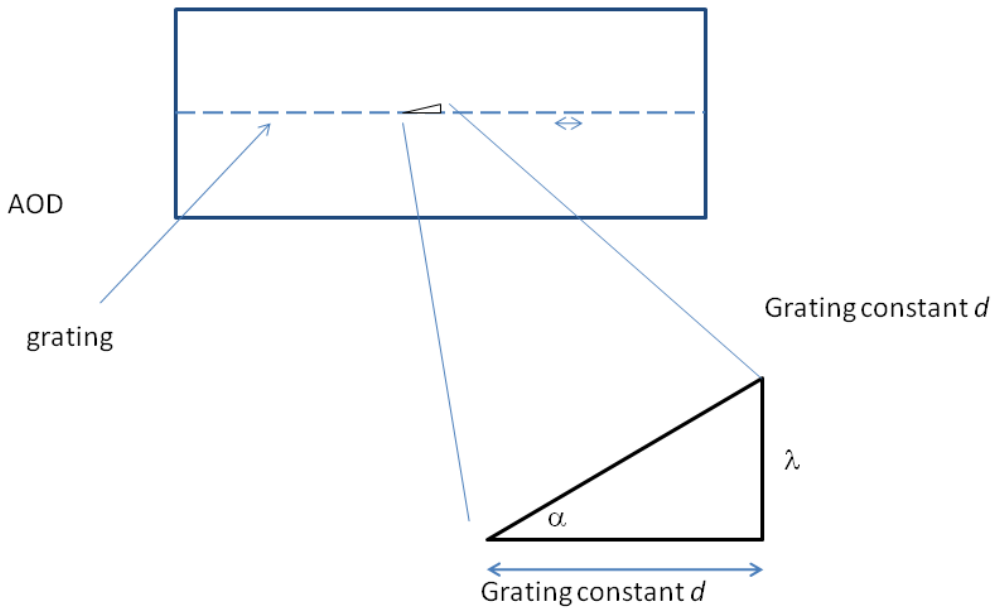

Figure A5: visualization of the grating constants and other parameters

We get the following formulae:

$$\tan(\alpha) = \lambda/d \approx \sin(\alpha) \approx \alpha$$

$$\frac{d\alpha}{d\lambda} = \frac{1}{d}$$

The formula for the grating-constant:

$$\frac{x}{t} = v \Rightarrow x = v \cdot t = \frac{v}{F}$$

F is the frequency of the acoustic wave in the AOD, (F~ 150MHz)

v is the acoustic speed of the TeO2 crystal (=620m/s)

$$x = \frac{620\frac{m}{s}}{150 \cdot 10^6 \frac{1}{s}} \simeq 4.3\mu m$$

$$\frac{1}{d} = \frac{1}{4.3\mu\text{m}} = \frac{1}{4300nm} = 0.24\frac{10^{-3}}{nm} = 0.24\frac{mrad}{nm}$$

I have to look in figure A4 for the exit angle, that creates a chromatic dispersion of 0.24mrad/nm. The value was about 84°, therefore I have to align the prism in a way that the beam exits the prism in this angle. I directed the beam then on the scanning AODs.

This is a fast approximation with small angle approach ($\sin(\alpha) = \tan(\alpha) = \alpha$). This approximation is acceptable, because with the values $\lambda = 0.8\ \mu\text{m}$ and $\text{d} = 4.3\mu\text{m}$, we get a deflection angle of $\alpha = 11°$. The chromatic dispersion of the AOD and the prism are in the same range. Hence, a SF11 prism is suited for a compensation of the chromatic dispersion of the AOD. This was proved by the first apparatus, making images of good quality.

For practical reasons we need to find out the direction of the chromatic dispersion, to place it in the right way for compensation the dispersion of the AOD. This is visualized in the following diagram.

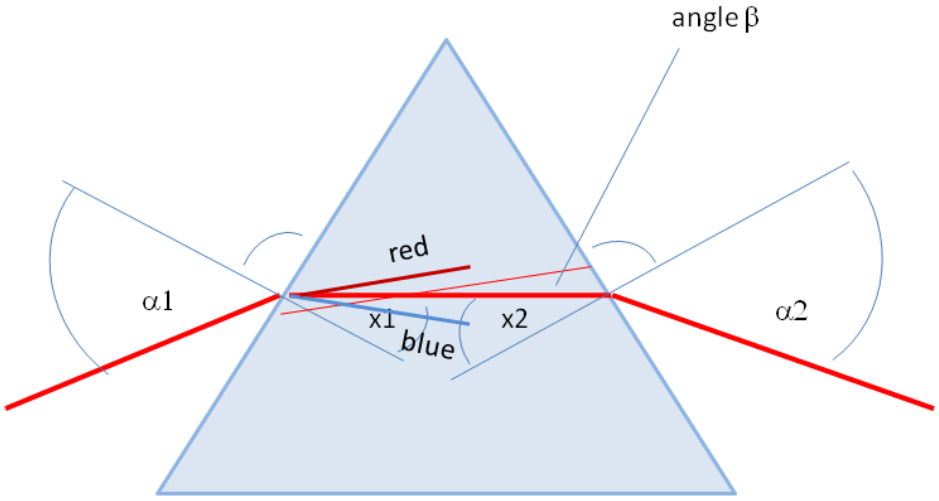

$$n_1 \sin(\alpha_1) = \sin(\alpha_1) = n_2(\lambda)\sin(x_1)$$
$$therefore, as(\sin(\alpha_1) = const.)$$
$$n_2(\lambda) smaller \Rightarrow \sin(x_1) \cong x_1 \quad larger$$

Figure A6: The direction (sign) of the chromatic dispersion at the entrance of the prism

When the beam exits the prism, we get the following relation:

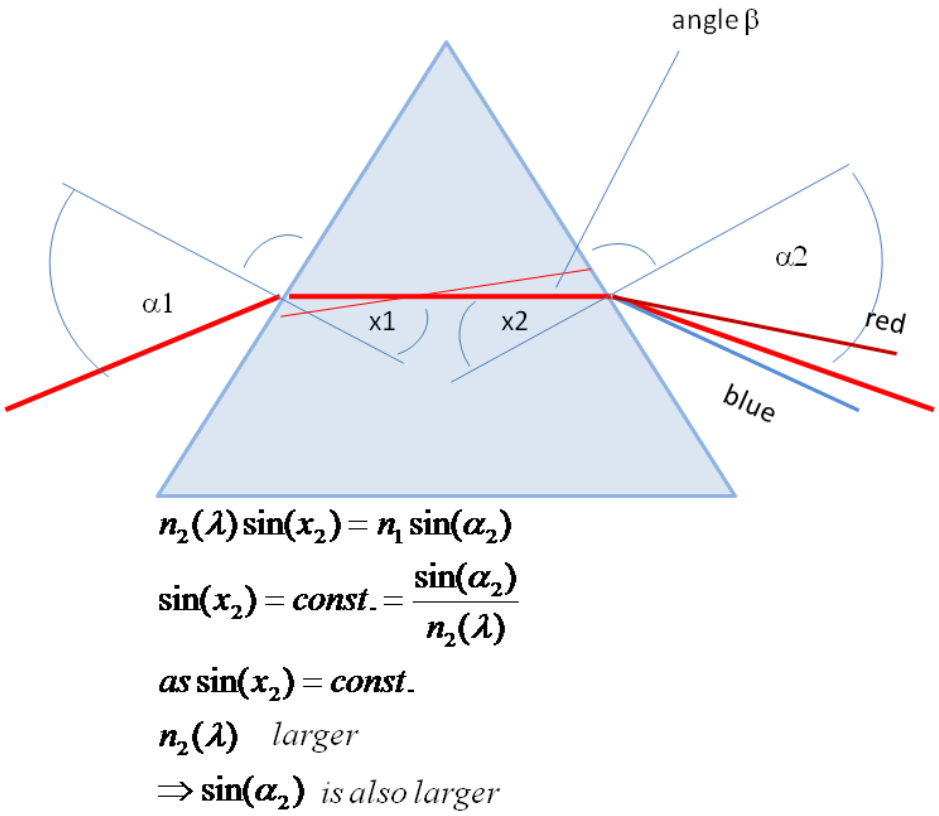

Figure A7: The direction of the chromatic dispersion at the exit of the prism

As already derived, the chromatic dispersions are in the same direction. We can ignore the chromatic dispersion from the entrance of the prism because the values are a factor of about 10 times smaller than at the exit of the prism. It is just important to note that light with a smaller wavelength exits the prism with a higher angle. This is in contrast to the properties of an AOD, where light with a shorter wavelength exits the AOD with a smaller angle.

Abbreviations and technical terms:

2p two-photon

CTI Crystal Technology Inc., this is the name of a vendor of acousto-optical deflectors.

GFP Green Fluorescent Protein

wt wide type, this means in most cases 'non-transgenic'

PSF

Point spread function. This denotes the three-dimensional function that displays the intensity of the focus spot. The mathematical model for mapping of biological tissue is a convolution of the object with the illumination spot. The PSF is equal to the convolution kernel in this model, and hence predefines the size of a point in the image after such a mapping procedure.

Transfer function:

The Fourier-transformation of the PSF. This function is of interest, as the convolution theorem states that a convolution can be calculated by multiplying the Fourier-transformations of both function. Therefore, the transfer-function of the convolution kernel directly indicates what frequencies are being transferred by the convolution operation. This indicates the resolution and the bandwidth.

Image plane:

The location of a microscope, where normally the detector chip would be located. The image from the sample under the microscope would be mapped sharply at this location.

Collimated laser beam:

A laser beam that is not focused or defocused, hence all rays of light in all positions of the laser beam are parallel. In theory, an ideally collimated laser beam is in principal not possible, as the natural divergence is defined by λ/d (d: laser beam diameter, λ: wave length of the laser light), and would require a laser beam with infinite diameter. In practice, we talk about a collimated laser beam when the laser beam diameter d is large enough compared to the wave length, e.g. 5mm beam diameter at 800nm wavelength.

Saw tooth signal:

A signal that looks like a saw-tooth. It is a periodic signal, a line with constant slope, that periodically jumps back to the initial position.

GVD, group velocity dispersion:

The refractive index of most materials is dependent on the wavelength. Therefore, the speed of light varies dependent on the wavelength, and a pulsed laser that consists of several wavelength-components is broadened. In glass, red light travels faster than blue light, and therefore the red components of a laser pulse run in advance of the shorter wavelength components. This broadening is called the group velocity dispersion.

Raster scanning:

Raster scanning denotes the scan pattern to acquire two-dimensional image data with rectangular image size. This is in contrast to random-access scanning, used to target single points and measure the fluorescence intensity from these points with high frequency by jumping between these points, or a line-scan patter, that only scans along one line of the sample. The advantage of a raster scan is that we still get image information, hence we can detect movements of the sample or a swelling of the dendrite due to photo-damage. Photo-damage results in characteristic cell shape alterations, mainly a swelling of the dendrite, and in an increase of the fluorescence of the dendrite, due to an increased Ca^{2+} entry.

Fly-Back time

When we operate an optical element for beam deflection in the line-scan mode, we scan one line until the end, jump back to the beginning and restart the line-scanning procedure again. The time to jump back from one end to the beginning is denoted the 'Fly-Back time'.

Chromatic dispersion:

We talk about chromatic dispersion when different wavelength components of a laser beam propagate in a different direction. This variation of the propagation angle is normally linear, and we use the unit [mrad/nm] for a quantification of the amount of chromatic dispersion.

Upstream/downstream:

I use this term in optics according to the use in genetics, where it describes the relative position to the origin. Upstream denotes 'closer to the laser' along the optical path, while 'downstream' denotes 'closer to the sample' along the optical path.

AOD:

Acousto-optic deflector. This device is build up of a transparent crystal, and an acoustic wave generator, generating an acoustic wave traveling through the crystal. This acoustic wave generates an optical grating, and hence a laser beam can be diffracted by this optical grating. As we can modify the frequency of the acoustic wave very fast, we can modify the diffraction pattern with high speed. Therefore, these devices allow for a beam deflection with high-speed (in the range of some µs), and are much faster than scanning mirrors.

AOM

Acousto-optical modulator. This device is in principle identical to an AOD, but it misses the capability to vary the acoustic frequency. Only the amplitude of the acoustic wave can be modified, hence it allows only for a modification of the amplitude of the diffracted beam, not of the diffraction angle. Such a device can only modulate the beam intensity within µs. They are used for fast modulation of the intensity of a laser beam.

SNR

Signal-to-noise ratio. The value is calculated by dividing the signal amplitude by the noise amplitude. The signal amplitude is defined as difference of the highest signal value and the lowest signal value.

The noise amplitude is defined by the standard-deviation of the difference of the noisy signal from a noise-free signal. In the practical example of a 2d signal of an image, we first generate a noise-free image by averaging a large number of images, and then calculate the difference of the noise-free image and one noisy image. We then compute the standard-deviation of this pixel difference, and this is the noise amplitude. In practice, these values are between 1.5 and 20 in 2p imaging.

PMT

Photo-multiplier-tube. These devices are able to detect lowest numbers of photons, like it is needed in two-photon imaging. A photon is generating a free electron by photo-effect, and this free electron is amplified by an electrical acceleration and targeted on a subsequent dynode, generating additional free electrons with photo-effect. Several amplification-steps can provide an amplification in the range 10 000 without inducing noise. These devices are able to detect single photons.

Digitizing

This names the procedure of transferring the analog value of voltage on the measurement board to the digital number, representing the value of the applied voltage.

Bandwidth

The bandwidth is a value that characterizes the precision of a measurement device. In case of a temporal measurement of fluorescence signals, it denotes the highest measurable frequency that can be detected by the digitizer.

References

Amos, W.B. (1995). Appendix I: Optical Units. In Handbook of Biological Confocal Microscoy, J.B. Pawley, ed.

Astola, J., and Kuosmanen, P. (1997). Fundamentals of nonlinear digital filtering (CRC Press).

Bi, K., Zeng, S., Xue, S., Sun, J., Lv, X., Li, D., and Luo, Q. (2006). Position of the prism in a dispersion-compensated acousto-optic deflector for multiphoton imaging. Applied optics *45*, 8560-8565.

Boyd, R. (2008). Nonlinear optics (Academic Pr).

Brevet, P., and Girault, H. (1996). Second harmonic generation at liquid/liquid interfaces. In Liquid-liquid interfaces, Theory and Methods, A. Volkov, and D.W. Deamer, eds. (CRC Press), pp. 103-137.

Brimrose (2011) Introduction to A-O Deflectors/Scanners http://www.brimrose.com/pdfandwordfiles/aodefl.pdf 2011

Chan, R., Ho, C., and Nikolova, M. (2005). Salt-and-pepper noise removal by median-type noise detectors and detail-preserving regularization. IEEE Transactions on Image Processing *14*, 1479-1485.

Chia-Lung, H., Rachel, G., Ye, P., and Demetri, P. (2009). Barium titanate nanoparticles used as second harmonic radiation imaging probes for cell imaging. In Advanced Microscopy Techniques (Optical Society of America), p. 7367_7360D.

Cornelisse, L., van Elburg, R., Meredith, R., Yuste, R., and Mansvelder, H. (2007). High speed two-photon imaging of calcium dynamics in dendritic spines: consequences for spine calcium kinetics and buffer capacity. PLoS ONE *2*, 1073.

Cummings, J., Mulkey, R., Nicoll, R., and Malenka, R. (1996). Ca2+ signaling requirements for long-term depression in the hippocampus. Neuron *16*, 825-833.

Denk, W., Strickler, J., and Webb, W. (1990). Two-photon laser scanning fluorescence microscopy. Science *248*, 73-76.

Ding, J.B., Takasaki, K.T., and Sabatini, B.L. (2009). Supraresolution imaging in brain slices using stimulated-emission depletion two-photon laser scanning microscopy. Neuron *63*, 429-437.

Dodt, H.-U., Leischner, U., Schierloh, A., Jahrling, N., Mauch, C.P., Deininger, K., Deussing, J.M., Eder, M., Zieglgansberger, W., and Becker, K. (2007). Ultramicroscopy: three-dimensional visualization of neuronal networks in the whole mouse brain. Nat Methods *4*, 331-336.

Donnert, G., Eggeling, C., and Hell, S. (2007). Major signal increase in fluorescence microscopy through dark-state relaxation. Nature Methods *4*, 81-86.

Draaijer, A., and Houpt, P. (1988). A standard video-rate confocal laser-scanning reflection and fluorescence microscope. Scanning *10*, 139-145.

Gerig, J., and Montague, H. (1964). A simple optical filter for chirp radar. Proceedings of the IEEE *52*, 1753-1753.

Gobel, W., and Helmchen, F. (2007). New angles on neuronal dendrites in vivo. Journal of neurophysiology *98*, 3770.

Gobel, W., Kampa, B., and Helmchen, F. (2007). Imaging cellular network dynamics in three dimensions using fast 3D laser scanning. Nature Methods *4*, 73-80.

Gonzalez, R., Woods, R., and Eddins, S. (2003). Digital image processing using MATLAB (Prentice-Hall, Inc. Upper Saddle River, NJ, USA).

Gottlieb, M., Ireland, C., and Ley, J. (1983). Electro-optic and acousto-optic scanning and deflection.

Greenberg, D., and Kerr, J. (2009). Automated correction of fast motion artifacts for two-photon imaging of awake animals. Journal of Neuroscience Methods *176*, 1-15.

Grewe, B., and Helmchen, F. (2009). Optical probing of neuronal ensemble activity. Current Opinion in Neurobiology.

Grewe, B., Langer, D., Kasper, H., Kampa, B., and Helmchen, F. (2010). High-speed in vivo calcium imaging reveals neuronal network activity with near-millisecond precision. Nature Methods *7*, 399-405.

Hein, B., Willig, K.I., and Hell, S.W. (2008). Stimulated emission depletion (STED) nanoscopy of a fluorescent protein-labeled organelle inside a living cell. Proceedings of the National Academy of Sciences *105*, 14271.

Hildebrand, M.E., Isope, P., Miyazaki, T., Nakaya, T., Garcia, E., Feltz, A., Schneider, T., Hescheler, J., Kano, M., and Sakimura, K. (2009). Functional coupling between mGluR1 and Cav3. 1 T-type calcium channels contributes to parallel fiber-induced fast calcium signaling within Purkinje cell dendritic spines. Journal of Neuroscience *29*, 9668.

Hopt, A., and Neher, E. (2001). Highly nonlinear photodamage in two-photon fluorescence microscopy. Biophysical journal *80*, 2029-2036.

Houpt, P., and Draaijer, A. (1989). Confocal laser scanning microscope. (Google Patents).

Hsieh, C., Grange, R., Pu, Y., and Psaltis, D. (2009). Bioconjugation of barium titanate nanocrystals with immunoglobulin G antibody for second harmonic radiation imaging probes. Biomaterials.

Ji, N., Magee, J., and Betzig, E. (2008). High-speed, low-photodamage nonlinear imaging using passive pulse splitters. Nature Methods *5*, 197-202.

Keller, H. (1995). Objective lenses for confocal microscopy. In Biological confocal microscopy, J.B. Pawley, ed., pp. 111-126.

Kitamura, K., Judkewitz, B., Kano, M., Denk, W., and Häusser, M. (2007). Targeted patch-clamp recordings and single-cell electroporation of unlabeled neurons in vivo. Nature Methods *5*, 61-67.

Koester, H., and Sakmann, B. (1998a). Calcium dynamics in single spines during coincident pre-and postsynaptic activity depend on relative timing of back-propagating action potentials and subthreshold excitatory postsynaptic potentials. Proceedings of the National Academy of Sciences of the United States of America *95*, 9596.

Koester, H.J., and Sakmann, B. (1998b). Calcium dynamics in single spines during coincident pre-and postsynaptic activity depend on relative timing of back-propagating action potentials and

subthreshold excitatory postsynaptic potentials. Proceedings of the National Academy of Sciences of the United States of America *95*, 9596.

Kovalchuk, Y., Eilers, J., Lisman, J., and Konnerth, A. (2000). NMDA receptor-mediated subthreshold Ca2+ signals in spines of hippocampal neurons. Journal of Neuroscience *20*, 1791.

Larson, D., Zipfel, W., Williams, R., Clark, S., Bruchez, M., Wise, F., and Webb, W. (2003). Water-soluble quantum dots for multiphoton fluorescence imaging in vivo. Science *300*, 1434.

Lechleiter, J., Lin, D., and Sieneart, I. (2002). Multi-photon laser scanning microscopy using an acoustic optical deflector. Biophysical journal *83*, 2292-2299.

Leischner, U., Schierloh, A., Zieglgänsberger, W., and Dodt, H. (2010). Formalin-Induced Fluorescence Reveals Cell Shape and Morphology in Biological Tissue Samples. PLoS ONE *5*.

Leischner, U., Zieglgänsberger, W., and Dodt, H.-U. (2009). Resolution of Ultramicroscopy and Field of View Analysis. PLoS ONE *4(6)*, 1-14.

Lisman, J., Schulman, H., and Cline, H. (2002). The molecular basis of CaMKII function in synaptic and behavioural memory. Nature Reviews Neuroscience *3*, 175-190.

Lv, X., Zhan, C., Zeng, S., Chen, W., and Luo, Q. (2006). Construction of multiphoton laser scanning microscope based on dual-axis acousto-optic deflector. Review of Scientific Instruments *77*, 046101.

Min, W., Lu, S., Chong, S., Roy, R., Holtom, G., and Xie, X. (2009). Imaging chromophores with undetectable fluorescence by stimulated emission microscopy. Nature *461*, 1105-1109.

Minsky, M. (1961). Microscopy apparatus. (United States, Marvin, Minsky).

Moneron, G., and Hell, S.W. (2009). Two-photon excitation STED microscopy. Optics Express *17*, 14567-14573.

Nagayama, S., Zeng, S., Xiong, W., Fletcher, M.L., Masurkar, A.V., Davis, D.J., Pieribone, V.A., and Chen, W.R. (2007). In vivo simultaneous tracing and Ca2+ imaging of local neuronal circuits. Neuron *53*, 789-803.

Nägerl, U.V., Willig, K.I., Hein, B., Hell, S.W., and Bonhoeffer, T. (2008). Live-cell imaging of dendritic spines by STED microscopy. Proceedings of the National Academy of Sciences *105*, 18982.

Nikolova, M. (2004). A variational approach to remove outliers and impulse noise. Journal of Mathematical Imaging and Vision *20*, 99-120.

Ntziachristos, V. (2010). Going deeper than microscopy: the optical imaging frontier in biology. Nature Methods *7*, 603-614.

Otsu, Y., Bormuth, V., Wong, J., Mathieu, B., Dugué, G., Feltz, A., and Dieudonné, S. (2008). Optical monitoring of neuronal activity at high frame rate with a digital random-access multiphoton (RAMP) microscope. Journal of Neuroscience Methods *173*, 259-270.

Patterson, G., and Piston, D. (2000). Photobleaching in two-photon excitation microscopy. Biophysical journal *78*, 2159-2162.

Peterka, D., Takahashi, H., and Yuste, R. (2011). Imaging Voltage in Neurons. Neuron *69*, 9-21.

Peters, R. (1995). A new algorithm for image noise reduction using mathematical morphology. IEEE Transactions on Image Processing *4*.

Potter, H., Weir, L., and Leder, P. (1984). Enhancer-dependent expression of human kappa immunoglobulin genes introduced into mouse pre-B lymphocytes by electroporation. Proceedings of the National Academy of Sciences of the United States of America *81*, 7161.

Reddy, G., Kelleher, K., Fink, R., and Saggau, P. (2008). Three-dimensional random access multiphoton microscopy for functional imaging of neuronal activity. Nature neuroscience *11*, 713-720.

Reddy, G., and Saggau, P. (2005). Fast three-dimensional laser scanning scheme using acousto-optic deflectors. Journal of Biomedical Optics *10*, 064038.

Roorda, R., Hohl, T., Toledo-Crow, R., and Miesenbock, G. (2004). Video-rate nonlinear microscopy of neuronal membrane dynamics with genetically encoded probes. Journal of neurophysiology *92*, 609.

Salome, R., Kremer, Y., Dieudonne, S., Léger, J., Krichevsky, O., Wyart, C., Chatenay, D., and Bourdieu, L. (2006). Ultrafast random-access scanning in two-photon microscopy using acousto-optic deflectors. Journal of Neuroscience Methods *154*, 161-174.

Schmidt, H., Stiefel, K., Racay, P., Schwaller, B., and Eilers, J. (2003). Mutational analysis of dendritic Ca2+ kinetics in rodent Purkinje cells: role of parvalbumin and calbindin D28k. The Journal of physiology *551*, 13.

Shen, Y.R. (1989). Surface second harmonic generation: a new technique for surface studies. Annu. Rev. Phys. Chem. *40*.

Soille, P. (2003). Morphological image analysis: principles and applications (Springer-Verlag New York, Inc. Secaucus, NJ, USA).

Spalteholz, W. (1911). Über das Durchsichtigmachen von menschlichen und tierischen Präparaten (Leipzig: S. Hirzel).

Sternberg, S.R. (1983). Biomedical Image Processing. Computer, 22-34.

Sternberg, S.R. (1986). Grayscale Morphology. Comput Vision Graph *35*, 333-355.

Stosiek, C., Garaschuk, O., Holthoff, K., and Konnerth, A. (2003). In vivo two-photon calcium imaging of neuronal networks. Proceedings of the National Academy of Sciences *100*, 7319-7324.

Trebino, R., DeLong, K., Fittinghoff, D., Sweetser, J., Krumbügel, M., Richman, B., and Kane, D. (1997). Measuring ultrashort laser pulses in the time-frequency domain using frequency-resolved optical gating. Review of Scientific Instruments *68*, 3277.

Vucinic , D., and Sejnowski, T. (2007). A compact multiphoton 3D imaging system for recording fast neuronal activity. PloS one *2*.

Westphal, V., Lauterbach, M., Di Nicola, A., and Hell, S. (2007). Dynamic far-field fluorescence nanoscopy. New Journal of Physics *9*, 435.

Willig, K.I., Harke, B., Medda, R., and Hell, S.W. (2007). STED microscopy with continuous wave beams. Nature Methods *4*, 915-918.

Willig, K.I., Rizzoli, S.O., Westphal, V., Jahn, R., and Hell, S.W. (2006). STED microscopy reveals that synaptotagmin remains clustered after synaptic vesicle exocytosis. Nature *440*, 935-939.

Winkler, G., Aurich, V., Hahn, K., Martin, A., and Rodenacker, K. (1998). Noise reduction in images: some recent edge-preserving methods (Citeseer).

Yang, S., Tang, Y., and Zucker, R. (1999). Selective induction of LTP and LTD by postsynaptic [Ca2+] i elevation. Journal of neurophysiology *81*, 781.

Zeng, S., Bi, K., Xue, S., Liu, Y., Lv, X., and Luo, Q. (2007). Acousto-optic modulator system for femtosecond laser pulses. Review of Scientific Instruments *78*, 015103.

Zeng, S., Lv, X., Zhan, C., Chen, W., Xiong, W., Jacques, S., and Luo, Q. (2006). Simultaneous compensation for spatial and temporal dispersion of acousto-optical deflectors for two-dimensional scanning with a single prism. Optics letters *31*, 1091-1093.

Acknowledgements:

Special thanks to all lab members, who all supported me during my work. Especially I want to mention Yuri Kovalchuk and Bruno Pichler, who introduced me to the principles of two-photon scanning systems and the technical constrains for *in-vivo* imaging. Many thanks to Horst Henning and Xiaowei Chen, who carefully used my newly developed prototype for their measurements. They showed the usability and the advantages of the new imaging system. I was very happy about their experimental skills of patch-clamp technique *in-vivo* and *in-vitro*, and for the acquisition of such high-quality data.

I also want to thank my colleagues Andreas Fohr for his support during the software development, Werner Zeitz and Bernd Prößner for their assistance during the installation of the electronic peripheral devices, and Felix and Dietmar Beyer for the design and manufacturing of custom-made mechanical adapters.

At this place, I also want to thank my supervisor of my master thesis Hans-Ulrich Dodt for the introduction in the field of optical measurements in brain research. I especially appreciated his support during the publication process of two pending papers from the lab in the Max Planck Institute of Psychiatry.

Thanks to my mentors Thomas Misgeld and Dieter Braun for their support and advice.

And finally special thanks to my supervisor Arthur Konnerth for giving me the opportunity to make my work in a highly interesting research area of brain research, and for selecting a highly promising research project. All kind of biomedical research with two-photon microscopy can benefit from an increase of imaging speed, or the reduction of photo-damage when this microscope is used in the low-power-temporal-oversampling mode. With my background of physics and optics, I would have never seen the potential of such a project.